Published for SISSA by Springer

Received: *September 17, 2017*
Revised: *November 16, 2017*
Accepted: *December 3, 2017*
Published: *December 14, 2017*

Gauge-independent renormalization of the N2HDM

Marcel Krause,[a] **David López-Val,**[a] **Margarete Mühlleitner**[a] **and Rui Santos**[b,c,d]

[a] *Institute for Theoretical Physics, Karlsruher Institute of Technology, Wolfgang-Gaede Str. 1, 76131 Karlsruhe, Germany*
[b] *ISEL — Instituto Superior de Engenharia de Lisboa, Instituto Politécnico de Lisboa, Rua Conselheiro Emídio Navarro 1, 1959-007 Lisboa, Portugal*
[c] *Centro de Física Teórica e Computacional, Faculdade de Ciências, Universidade de Lisboa, Campo Grande, Edifício C8, 1749-016 Lisboa, Portugal*
[d] *LIP, Departamento de Física, Universidade do Minho, Campus de Gualtar, 4710-057 Braga, Portugal*

E-mail: marcel.krause@kit.edu, david.val@kit.edu, margarete.muehlleitner@kit.edu, rasantos@fc.ul.pt

Abstract: The Next-to-Minimal 2-Higgs-Doublet Model (N2HDM) is an interesting benchmark model for a Higgs sector consisting of two complex doublet and one real singlet fields. Like the Next-to-Minimal Supersymmetric extension (NMSSM) it features light Higgs bosons that could have escaped discovery due to their singlet admixture. Thereby, the model allows for various different Higgs-to-Higgs decay modes. Contrary to the NMSSM, however, the model is not subject to supersymmetric relations restraining its allowed parameter space and its phenomenology. For the correct determination of the allowed parameter space, the correct interpretation of the LHC Higgs data and the possible distinction of beyond-the-Standard Model Higgs sectors higher order corrections to the Higgs boson observables are crucial. This requires not only their computation but also the development of a suitable renormalization scheme. In this paper we have worked out the renormalization of the complete N2HDM and provide a scheme for the gauge-independent renormalization of the mixing angles. We discuss the renormalization of the $\mathbb{Z}_2$ soft breaking parameter m_{12}^2 and the singlet vacuum expectation value v_S. Both enter the Higgs self-couplings relevant for Higgs-to-Higgs decays. We apply our renormalization scheme to different sample processes such as Higgs decays into Z bosons and decays into a lighter Higgs pair. Our results show that the corrections may be sizable and have to be taken into account for reliable predictions.

Keywords: Beyond Standard Model, Higgs Physics

ArXiv ePrint: 1708.01578

https://doi.org/10.1007/JHEP12(2017)077

JHEP12(2017)077

Contents

JHEP12(2017)077

1 Introduction

Even after the discovery of the Higgs boson by the LHC experiments ATLAS [1] and CMS [2] there remain many open questions that cannot be solved within the Standard Model (SM). This calls for New Physics (NP) extensions, which feature predominantly extended Higgs sectors. The precise investigation of the Higgs sector has become an important tool in the search for NP, in particular since its direct manifestation through the discovery of new non-SM particles remains elusive. Among the beyond-the-SM (BSM) Higgs sectors those with singlet and doublet extensions are particularly attractive as they are at the same time rather simple and compatible with custodial symmetry. The 2-Higgs-doublet model (2HDM) [3–5] is interesting due to its relation to supersymmetry and has been extensively studied and considered as a possible benchmark model in experimental analyses. It features 5 physical Higgs bosons, 2 CP-even and 1 CP-odd neutral states and a charged Higgs pair. The next-to-minimal 2HDM (N2HDM) is obtained upon extension of the 2HDM by a real singlet field with a $\mathbb{Z}_2$ parity symmetry. It contains in its symmetric phase a viable Dark Matter (DM) candidate. The N2HDM has been the subject of numerous investigations, both in its symmetric [6–20] and in its broken phase [21–23]. The Higgs sector of the latter consists after electroweak symmetry breaking (EWSB) of 3 neutral CP-even scalars, 1 pseudoscalar and a charged Higgs pair. With the Higgs mass eigenstates being superpositions of the singlet and doublet fields the N2HDM entails an interesting phenomenology, namely the possibility of a light Higgs boson, which is not in conflict with the experimental Higgs data in case of a sufficiently large singlet admixture so that its couplings to SM particles are suppressed. The enlarged Higgs sector together with the possibility of light Higgs states allows for cascade Higgs-to-Higgs decays that provide alternative production channels for the heavier Higgs bosons and also give access to the trilinear Higgs self-couplings. Their measurement provides important insights in the understanding of the Higgs mechanism [24–26].

Obviously, any NP extension has to comply with the relevant theoretical and experimental constraints. Thus, also the N2HDM has to provide at least one Higgs boson with a mass of 125 GeV compatible with the LHC data on the discovered Higgs resonance [27]. The additional Higgs bosons must not violate the LHC exclusion limits. The compatibility with the electroweak (EW) precision data has to be guaranteed as well as the compatibility with B-physics and low-energy constraints. As mentioned, a $\mathbb{Z}_2$-symmetric realization of the N2HDM is in addition attractive as it provides a potential DM candidate. In that case, compliance with DM observables provides additional constraints on the parameter space of the model. From the theoretical point of view, the N2HDM Higgs potential has to be bounded from below, its vacuum has to be the global minimum and perturbative unitarity has to be respected. In [22], part of our group investigated the N2HDM in great detail with respect to these constraints. The allowed parameter space was determined and the phenomenological implications were investigated. In the course of this work the model was implemented in `HDECAY` [28, 29]. The generated code, `N2HDECAY`,[1] computes the N2HDM Higgs decay widths and branching ratios including the state-of-the-art higher order QCD

[1] `N2HDECAY` can be obtained from https://www.itp.kit.edu/∼maggie/N2HDECAY/.

JHEP12(2017)077

corrections and off-shell decays. The model was furthermore included in `ScannerS` [30, 31] along with the theoretical conditions and the available experimental constraints, which then allowed to perform extensive parameter scans for the model. In [23], the work was extended and we compared the N2HDM to other NP extensions with the aim to work out observables that can be used to distinguish between various well-motivated BSM Higgs sectors by using collider data.

Since the discovered Higgs bosons behaves very SM-like [32–35], the search for NP in the Higgs sector requires on the theoretical side precise predictions for parameters and observables including higher-order (HO) corrections. In the framework of the 2HDM, some of the authors of this work provided an important basis for the computation of HO corrections in the 2HDM by working out a manifestly gauge-independent renormalization of the two 2HDM mixing angles α and β, which is also numerically stable and process independent [36]. These angles, which diagonalise the neutral CP-even and the neutral CP-odd or charged Higgs sectors, respectively, enter all Higgs couplings so that they are relevant for Higgs boson phenomenology. We completed the renormalization of the 2HDM Higgs sector in [37] by investigating Higgs-to-Higgs decays at EW next-to-leading order (NLO). Subsequent works [38–40] on the 2HDM renormalization applied different approaches and renormalization conditions, confirming our findings where they overlapped.[2] The renormalization of the N2HDM is more involved due to the additional mixing angles and the additional vacuum expectation value related to the singlet field in the broken phase. One of our authors worked on the renormalization of the SM extended by a real singlet field, cf. [42]. In this paper, we combine our expertise gained in the renormalization of the 2HDM and the singlet-extended SM and provide the complete renormalization of the N2HDM. The renormalization of the mixing angles α_i $(i = 1, 2, 3)$ of the neutral sector and the angle β of the CP-odd/charged sector is manifestly gauge independent as well as process independent. Where not parametrically enhanced, it is furthermore numerically stable with respect to missing higher order corrections. We will demonstrate this in the numerical analysis where we explicitly compute the NLO EW corrections to sample Higgs decays. We also use the occasion and clarify in this paper the notion of the alternative tadpole approach with regard to the renormalization framework applied to achieve a manifestly gauge-independent renormalization of the mixing angles. With this paper we provide another important step in the program of precise predictions for BSM Higgs sector parameters and observables including higher order corrections, an indispensable requisite for the correct interpretation of the experimental results.

The paper is organised as follows: in section 2 we introduce our model, set our notation and provide the relevant couplings. Starting with section 3, we describe the renormalization of the model. In section 4 we explain the way we treat the tadpoles in our renormalization procedure, before we give in section 5 the renormalization conditions. Section 6 is dedicated to the computation of the one-loop EW sample decay widths. In section 7 we present our numerical analysis before we conclude in section 8. A detailed description of the phenomenological benchmarks used in our analysis is presented in appendix A. The paper is accompanied by the extensive appendix B presenting the details of the computation of the pinched self-energies in the N2HDM.

[2] For the renormalization of non-minimal Higgs sectors, see also [41].

JHEP12(2017)077

2 Model setup

The N2HDM is obtained from the CP-conserving (or real) 2HDM with a softly broken $\mathbb{Z}_2$ symmetry upon extension by a real singlet field Φ_S with a discrete symmetry, under which $\Phi_S \to -\Phi_S$. The kinetic term of the two $\mathrm{SU}(2)_L$ Higgs doublets Φ_1 and Φ_2 and the singlet field Φ_S is given by

$$\mathcal{L}_{\mathrm{kin}} = (D_\mu \Phi_1)^\dagger (D^\mu \Phi_1) + (D_\mu \Phi_2)^\dagger (D^\mu \Phi_2) + \frac{1}{2} (\partial_\mu \Phi_S)^2 \,, \tag{2.1}$$

in terms of the covariant derivative

$$D_\mu = \partial_\mu + \frac{i}{2} g \sum_{a=1}^{3} \tau^a W_\mu^a + \frac{i}{2} g' B_\mu \,, \tag{2.2}$$

where τ^a denote the Pauli matrices, W_μ^a and B_μ the $\mathrm{SU}(2)_L$ and $\mathrm{U}(1)_Y$ gauge bosons, respectively, and g and g' the corresponding gauge couplings. The scalar potential built from the two $\mathrm{SU}(2)_L$ Higgs doublets and the scalar singlet can be written as

$$\begin{aligned} V = {} & m_{11}^2 |\Phi_1|^2 + m_{22}^2 |\Phi_2|^2 - m_{12}^2 (\Phi_1^\dagger \Phi_2 + \text{h.c.}) + \frac{\lambda_1}{2} (\Phi_1^\dagger \Phi_1)^2 + \frac{\lambda_2}{2} (\Phi_2^\dagger \Phi_2)^2 \\ & + \lambda_3 (\Phi_1^\dagger \Phi_1)(\Phi_2^\dagger \Phi_2) + \lambda_4 (\Phi_1^\dagger \Phi_2)(\Phi_2^\dagger \Phi_1) + \frac{\lambda_5}{2} [(\Phi_1^\dagger \Phi_2)^2 + \text{h.c.}] \\ & + \frac{1}{2} m_S^2 \Phi_S^2 + \frac{\lambda_6}{8} \Phi_S^4 + \frac{\lambda_7}{2} (\Phi_1^\dagger \Phi_1) \Phi_S^2 + \frac{\lambda_8}{2} (\Phi_2^\dagger \Phi_2) \Phi_S^2 \,. \end{aligned} \tag{2.3}$$

The first two lines correspond to the 2HDM part of the N2HDM, and the last line contains the contribution of the singlet field Φ_S. The potential is based on two $\mathbb{Z}_2$ symmetries, where the first one is the trivial generalization of the usual 2HDM $\mathbb{Z}_2$ symmetry to the N2HDM,

$$\Phi_1 \to \Phi_1 \,, \quad \Phi_2 \to -\Phi_2 \,, \quad \Phi_S \to \Phi_S \,. \tag{2.4}$$

It is softly broken by the term involving m_{12}^2. Its extension to the Yukawa sector ensures the absence of tree-level Flavour Changing Neutral Currents (FCNC). The second $\mathbb{Z}_2$ symmetry on the other hand, under which

$$\Phi_1 \to \Phi_1 \,, \quad \Phi_2 \to \Phi_2 \,, \quad \Phi_S \to -\Phi_S \,, \tag{2.5}$$

is not explicitly broken. After EWSB the neutral components of the Higgs fields develop vacuum expectation values (VEVs), which are real in the CP-conserving case. Expanding the elementary field excitations around the doublet VEVs v_1 and v_2 and the singlet VEV v_S, we may write

$$\Phi_1 = \begin{pmatrix} \phi_1^+ \\ \frac{1}{\sqrt{2}}(v_1 + \rho_1 + i\eta_1) \end{pmatrix}, \quad \Phi_2 = \begin{pmatrix} \phi_2^+ \\ \frac{1}{\sqrt{2}}(v_2 + \rho_2 + i\eta_2) \end{pmatrix}, \quad \Phi_S = v_S + \rho_S \,, \tag{2.6}$$

where the field content of the model is parametrized in terms of the charged complex fields ϕ_i^+ $(i = 1, 2)$, the real neutral CP-even fields $\rho_1, \rho_2, \rho_3 \equiv \rho_S$ and the CP-odd fields η_i. The minimisation conditions of the Higgs potential,

$$\left\langle \frac{\partial V}{\partial \Phi_1} \right\rangle = \left\langle \frac{\partial V}{\partial \Phi_2} \right\rangle = \left\langle \frac{\partial V}{\partial \Phi_S} \right\rangle = 0 \,, \tag{2.7}$$

JHEP12(2017)077

where the brackets denote the vacuum state, require the terms linear in the Higgs fields, the tree-level Higgs tadpole parameters T_i ($i = 1, 2, 3$), to vanish in the vacuum. Equation (2.7) leads to the three minimum conditions

$$\frac{1}{v_1}\left\langle \frac{\partial V}{\partial \Phi_1} \right\rangle \equiv \frac{T_1}{v_1} = -\frac{v_2}{v_1} m_{12}^2 + m_{11}^2 + \frac{1}{2}(v_1^2 \lambda_1 + v_2^2 \lambda_{345} + v_S^2 \lambda_7) = 0 \tag{2.8}$$

$$\frac{1}{v_2}\left\langle \frac{\partial V}{\partial \Phi_2} \right\rangle \equiv \frac{T_2}{v_2} = -\frac{v_1}{v_2} m_{12}^2 + m_{22}^2 + \frac{1}{2}(v_1^2 \lambda_{345} + v_2^2 \lambda_2 + v_S^2 \lambda_8) = 0 \tag{2.9}$$

$$\frac{1}{v_S}\left\langle \frac{\partial V}{\partial \Phi_S} \right\rangle \equiv \frac{T_3}{v_S} = m_S^2 + \frac{1}{2}(v_1^2 \lambda_7 + v_2^2 \lambda_8 + v_S^2 \lambda_6) = 0\,, \tag{2.10}$$

with

$$\lambda_{345} \equiv \lambda_3 + \lambda_4 + \lambda_5\,. \tag{2.11}$$

At lowest order, the three tadpole conditions can be used to trade the mass terms m_{11}^2, m_{22}^2 and m_S^2 in favor of the other parameters of the potential. However, non-vanishing tadpole contributions are relevant at higher orders and must be included in the renormalization procedure, this being the reason why we shall retain them in our notation. The mass matrices of the Higgs fields in the gauge basis are obtained from the second derivatives with respect to these fields after replacing the doublet and singlet fields in the Higgs potential by the parametrisations (2.6). Due to charge and CP conservation the 7×7 mass matrix decomposes into three blocks. These are given by 2×2 matrices for the charged and the CP-odd fields, respectively, and a 3×3 matrix for the CP-even states. The former two are identical to the 2HDM case and read

$$M_\eta^2 = \left(\frac{m_{12}^2}{v_1 v_2} - \lambda_5\right)\begin{pmatrix} v_2^2 & -v_1 v_2 \\ -v_1 v_2 & v_1^2 \end{pmatrix} + \begin{pmatrix} \frac{T_1}{v_1} & 0 \\ 0 & \frac{T_2}{v_2} \end{pmatrix} \tag{2.12}$$

$$M_{\phi^\pm}^2 = \left(\frac{m_{12}^2}{v_1 v_2} - \frac{\lambda_4 + \lambda_5}{2}\right)\begin{pmatrix} v_2^2 & -v_1 v_2 \\ -v_1 v_2 & v_1^2 \end{pmatrix} + \begin{pmatrix} \frac{T_1}{v_1} & 0 \\ 0 & \frac{T_2}{v_2} \end{pmatrix}, \tag{2.13}$$

where we have kept explicitly the dependence on the tadpole parameters. They can be diagonalised as

$$D_\eta^2 = R(\beta) M_\eta^2 R^T(\beta) \tag{2.14}$$

$$D_{\phi^\pm}^2 = R(\beta) M_{\phi^\pm}^2 R^T(\beta)\,, \tag{2.15}$$

with the rotation matrix

$$R(\beta) = \begin{pmatrix} c_\beta & s_\beta \\ -s_\beta & c_\beta \end{pmatrix}, \tag{2.16}$$

where we have introduced the abbreviations $\sin x \equiv s_x$ and $\cos x \equiv c_x$. This yields the neutral CP-odd mass eigenstates, G^0 and A, and the charged mass eigenstates, $G^\pm$ and $H^\pm$, respectively. The would-be Goldstone bosons G^0 and $G^\pm$ are massless. Due to the additional real singlet field, the CP-even neutral sector differs from the 2HDM, now featuring

JHEP12(2017)077

a 3×3 mass matrix. In the basis (ρ_1, ρ_2, ρ_3) it can be cast into the form

$$M_\rho^2 = \begin{pmatrix} \lambda_1 c_\beta^2 v^2 + t_\beta m_{12}^2 & \lambda_{345} c_\beta s_\beta v^2 - m_{12}^2 & \lambda_7 c_\beta v v_S \\ \lambda_{345} c_\beta s_\beta v^2 - m_{12}^2 & \lambda_2 s_\beta^2 v^2 + m_{12}^2 / t_\beta & \lambda_8 s_\beta v v_S \\ \lambda_7 c_\beta v v_S & \lambda_8 s_\beta v v_S & \lambda_6 v_S^2 \end{pmatrix} + \begin{pmatrix} \frac{T_1}{v_1} & 0 & 0 \\ 0 & \frac{T_2}{v_2} & 0 \\ 0 & 0 & \frac{T_3}{v_S} \end{pmatrix}, \tag{2.17}$$

where t_β stands for the ratio

$$t_\beta = \frac{v_2}{v_1} \tag{2.18}$$

and v is defined as

$$v^2 = v_1^2 + v_2^2 \,, \tag{2.19}$$

with $v \approx 246\,\text{GeV}$ denoting the SM VEV. We have furthermore used eqs. (2.8)–(2.10) to trade the mass parameters m_{11}^2, m_{22}^2 and m_S^2 for v, t_β and v_S. The neutral mass matrix (2.17) is diagonalised by the rotation matrix $R(\alpha_i)$, which can be parametrized in terms of three mixing angles α_1 to α_3 as

$$R(\alpha_i) = \begin{pmatrix} c_{\alpha_1} c_{\alpha_2} & s_{\alpha_1} c_{\alpha_2} & s_{\alpha_2} \\ -(c_{\alpha_1} s_{\alpha_2} s_{\alpha_3} + s_{\alpha_1} c_{\alpha_3}) & c_{\alpha_1} c_{\alpha_3} - s_{\alpha_1} s_{\alpha_2} s_{\alpha_3} & c_{\alpha_2} s_{\alpha_3} \\ -c_{\alpha_1} s_{\alpha_2} c_{\alpha_3} + s_{\alpha_1} s_{\alpha_3} & -(c_{\alpha_1} s_{\alpha_3} + s_{\alpha_1} s_{\alpha_2} c_{\alpha_3}) & c_{\alpha_2} c_{\alpha_3} \end{pmatrix}. \tag{2.20}$$

Without loss of generality the angles can be chosen in the range

$$-\frac{\pi}{2} \leq \alpha_{1,2,3} < \frac{\pi}{2} \,. \tag{2.21}$$

The mass eigenstates H_1, H_2 and H_3 are obtained from the gauge basis (ρ_1, ρ_2, ρ_3) as

$$\begin{pmatrix} H_1 \\ H_2 \\ H_3 \end{pmatrix} = R \begin{pmatrix} \rho_1 \\ \rho_2 \\ \rho_3 \end{pmatrix}, \tag{2.22}$$

and the diagonal mass matrix D_ρ^2 is given by

$$D_\rho^2 = R(\alpha_i) M_\rho^2 R^T(\alpha_i) \equiv \text{diag}(m_{H_1}^2, m_{H_2}^2, m_{H_3}^2) \,. \tag{2.23}$$

We use the convention where the mass eigenstates are ordered by ascending mass as

$$m_{H_1} < m_{H_2} < m_{H_3} \,. \tag{2.24}$$

The full set of the N2HDM parameters is given by the parameters of the N2HDM potential eq. (2.3), the VEVs and the free parameters of the SM:

$$\lambda_1, \ldots, \lambda_8 \,, \quad m_{11}^2 \,, \quad m_{22}^2 \,, \quad m_S^2 \,, \quad m_{12}^2 \,, \quad v_1 \,, \quad v_2 \,, \quad v_S \,, \quad g \,, \quad g' \,, \quad y_\Psi \,, \tag{2.25}$$

where y_Ψ denotes the Yukawa couplings. The dimension-two mass terms $m_{11}^2, m_{22}^2, m_S^2$ are fixed by the minimum conditions of the potential (2.8)–(2.10), while the remaining quantities correspond to the free input parameters in the gauge basis of the N2HDM. For the

JHEP12(2017)077

	κ_{H_iVV}
H_1	$c_{\alpha_2}c_{\beta-\alpha_1}$
H_2	$-c_{\beta-\alpha_1}s_{\alpha_2}s_{\alpha_3} + c_{\alpha_3}s_{\beta-\alpha_1}$
H_3	$-c_{\alpha_3}c_{\beta-\alpha_1}s_{\alpha_2} - s_{\alpha_3}s_{\beta-\alpha_1}$

Table 1. Neutral CP-even Higgs H_i couplings to the massive gauge bosons $V = W, Z$.

renormalization of the model it is convenient to relate as many parameters as possible to physical parameters, like for example masses and the electric charge. This allows then to apply physical conditions in the renormalization of the respective parameters. Furthermore, the minimum conditions can be used to trade m_{11}^2, m_{22}^2 and m_S^2 for the tadpole parameters $T_{1,2,3}$. Denoting by m_Ψ the fermion masses, by m_W and m_Z the W and Z boson masses, respectively, and by e the electric charge, the 'physical' set of N2HDM parameters is given by

$$m_{H_{1,2,3}},\ m_A,\ m_{H^\pm},\ \alpha_1\ ,\ \alpha_2\ ,\ \alpha_3\ ,\ T_1,\ T_2,\ T_3,\ m_{12}^2,\ v_S,\ t_\beta,\ e,\ m_W,\ m_Z,\ m_\Psi. \tag{2.26}$$

We will specify in the following sections how these parameters get renormalized in our way of treating the tadpoles. Note also that later in our renormalization procedure we will express v_S through a physical quantity that depends on it, given by a Higgs-to-Higgs decay width.

For the computation of the electroweak corrections to the Higgs decays we need the Higgs couplings, which we briefly summarize here. Since the singlet field ρ_3 does not couple directly to the SM particles, any change in the tree-level Higgs couplings with respect to the 2HDM is due to the mixing of the three neutral fields ρ_i $(i = 1, 2, 3)$. This means that any coupling not involving the CP-even neutral Higgs bosons remains unchanged compared to the 2HDM and can be found e.g. in [5]. Introducing the Feynman rules for the coupling of the Higgs fields H_i to the massive gauge bosons $V \equiv W, Z$ via

$$i\, g_{\mu\nu}\, \kappa_{H_iVV}\, g_{H^{\rm SM}VV}\, H_i\, V^\mu\, V^\nu\,, \tag{2.27}$$

where $g_{H^{\rm SM}VV}$ denotes the SM Higgs coupling factor, we obtain the effective couplings

$$\kappa_{H_iVV} = c_\beta R_{i1} + s_\beta R_{i2}\,. \tag{2.28}$$

The SM coupling in terms of the gauge boson masses m_W and m_Z, the $\mathrm{SU}(2)_L$ gauge coupling g and the Weinberg angle θ_W, is given by

$$g_{HVV}^{\rm SM} = \begin{cases} g m_W & \text{for } V = W \\ g m_Z/\cos\theta_W & \text{for } V = Z \end{cases}\,. \tag{2.29}$$

In table 1 we list the effective couplings after replacing the R_{ij} by their parametrisation in terms of the mixing angles.

JHEP12(2017)077

	u-type	d-type	leptons
type I	Φ_2	Φ_2	Φ_2
type II	Φ_2	Φ_1	Φ_1
lepton-specific	Φ_2	Φ_2	Φ_1
flipped	Φ_2	Φ_1	Φ_2

Table 2. The four Yukawa types of the $\mathbb{Z}_2$-symmetric 2HDM defined by the Higgs doublet that couples to each kind of fermion.

	u-type	d-type	leptons
type I	$\frac{R_{i2}}{s_\beta}$	$\frac{R_{i2}}{s_\beta}$	$\frac{R_{i2}}{s_\beta}$
type II	$\frac{R_{i2}}{s_\beta}$	$\frac{R_{i1}}{c_\beta}$	$\frac{R_{i1}}{c_\beta}$
lepton-specific	$\frac{R_{i2}}{s_\beta}$	$\frac{R_{i2}}{s_\beta}$	$\frac{R_{i1}}{c_\beta}$
flipped	$\frac{R_{i2}}{s_\beta}$	$\frac{R_{i1}}{c_\beta}$	$\frac{R_{i2}}{s_\beta}$

Table 3. Coupling coefficients κ_{H_iff} of the Yukawa couplings of the N2HDM Higgs bosons H_i as defined in eq. (2.30).

In the Yukawa sector there exist four types of coupling structures after extending the $\mathbb{Z}_2$ symmetry (2.4) to the Yukawa sector to avoid tree-level FCNCs. They are the same as in the 2HDM and summarized in table 2. The CP-even H_i Yukawa couplings can be derived from the N2HDM Yukawa Lagrangian

$$\mathcal{L}_Y = -\sum_{i=1}^{3} \frac{m_f}{v} \kappa_{H_iff} \bar{\psi}_f \psi_f H_i \,. \tag{2.30}$$

The effective coupling factors κ_{H_iff} in terms of the mixing matrix elements R_{ij} and the mixing angle β are provided in table 3. Replacing the R_{ij} by their parametrisation in terms of the α_i results in the effective coupling expressions given for type I and II in table 4.

For the H_i couplings to the Z boson and the pseudoscalar A or the Goldstone G^0 the Feynman rules read

$$\lambda_\mu(H_iZA) = \frac{\sqrt{g^2+g'^2}}{2}(p_{H_i} - p_A)_\mu \tilde{\kappa}_{H_iVH} \,, \tag{2.31}$$

$$\lambda_\mu(H_iZG^0) = \frac{\sqrt{g^2+g'^2}}{2}(p_{H_i} - p_{G^0})_\mu \kappa_{H_iVV} \,, \tag{2.32}$$

where p_A, p_{G^0} and p_{H_i} are the incoming four-momenta of the pseudoscalar, the Goldstone boson and the H_i, respectively. The tilde over the coupling factor for the pseudoscalar indicates that it is not an effective coupling in the sense introduced above, as it is not normalized to a corresponding SM coupling, since there is no SM counterpart. The Feynman rules for the H_i couplings to the charged pairs $W^\mp$ and $H^\pm$ or $G^\pm$ read

$$\lambda_\mu(H_iW^\mp H^\pm) = \pm\frac{ig}{2}(p_{H_i} - p_{H^\pm})_\mu \tilde{\kappa}_{H_iVH} \,, \tag{2.33}$$

$$\lambda_\mu(H_iW^\mp G^\pm) = \pm\frac{ig}{2}(p_{H_i} - p_{G^\pm})_\mu \kappa_{H_iVV} \,, \tag{2.34}$$

JHEP12(2017)077

Type I			
$\kappa_{H_i ff}$	u	d	l
H_1	$(c_{\alpha_2} s_{\alpha_1})/s_\beta$	$(c_{\alpha_2} s_{\alpha_1})/s_\beta$	$(c_{\alpha_2} s_{\alpha_1})/s_\beta$
H_2	$(c_{\alpha_1} c_{\alpha_3} - s_{\alpha_1} s_{\alpha_2} s_{\alpha_3})/s_\beta$	$(c_{\alpha_1} c_{\alpha_3} - s_{\alpha_1} s_{\alpha_2} s_{\alpha_3})/s_\beta$	$(c_{\alpha_1} c_{\alpha_3} - s_{\alpha_1} s_{\alpha_2} s_{\alpha_3})/s_\beta$
H_3	$-(c_{\alpha_1} s_{\alpha_3} + c_{\alpha_3} s_{\alpha_1} s_{\alpha_2})/s_\beta$	$-(c_{\alpha_1} s_{\alpha_3} + c_{\alpha_3} s_{\alpha_1} s_{\alpha_2})/s_\beta$	$-(c_{\alpha_1} s_{\alpha_3} + c_{\alpha_3} s_{\alpha_1} s_{\alpha_2})/s_\beta$
Type II			
$\kappa_{H_i ff}$	u	d	l
H_1	$(c_{\alpha_2} s_{\alpha_1})/s_\beta$	$(c_{\alpha_1} c_{\alpha_2})/c_\beta$	$(c_{\alpha_1} c_{\alpha_2})/c_\beta$
H_2	$(c_{\alpha_1} c_{\alpha_3} - s_{\alpha_1} s_{\alpha_2} s_{\alpha_3})/s_\beta$	$-(c_{\alpha_3} s_{\alpha_1} + c_{\alpha_1} s_{\alpha_2} s_{\alpha_3})/c_\beta$	$-(c_{\alpha_3} s_{\alpha_1} + c_{\alpha_1} s_{\alpha_2} s_{\alpha_3})/c_\beta$
H_3	$-(c_{\alpha_1} s_{\alpha_3} + c_{\alpha_3} s_{\alpha_1} s_{\alpha_2})/s_\beta$	$(s_{\alpha_1} s_{\alpha_3} - c_{\alpha_1} c_{\alpha_3} s_{\alpha_2})/c_\beta$	$(s_{\alpha_1} s_{\alpha_3} - c_{\alpha_1} c_{\alpha_3} s_{\alpha_2})/c_\beta$

Table 4. The effective Yukawa couplings $\kappa_{H_i ff}$ of the N2HDM Higgs bosons H_i, as defined in eq. (2.30), in type I and type II.

	$\tilde{\kappa}_{H_i VH}$
H_1	$-c_{\alpha_2} s_{\beta-\alpha_1}$
H_2	$s_{\beta-\alpha_1} s_{\alpha_2} s_{\alpha_3} + c_{\alpha_3} c_{\beta-\alpha_1}$
H_3	$c_{\alpha_3} s_{\beta-\alpha_1} s_{\alpha_2} - s_{\alpha_3} c_{\beta-\alpha_1}$

Table 5. The coupling factors $\tilde{\kappa}_{H_i VH}$ as defined in the Feynman rules eqs. (2.31) and (2.33) for the H_i couplings to a pair of Higgs and gauge bosons.

where $p_{H^\pm}$ and $p_{G^\pm}$ denote the four-momenta of $H^\pm$ and $G^\pm$ and again all momenta are taken as incoming. The coupling factors $\tilde{\kappa}_{H_i VH}$ are listed in table 5.

The trilinear Higgs self-couplings needed for the Higgs decays into a pair of lighter Higgs bosons are quite lengthy. For their explicit form, we refer the reader to the appendix of ref. [22].

Note finally, that by letting $\alpha_1 \to \alpha + \pi/2$ and $\alpha_{2,3} \to 0$, we obtain the limit of a 2HDM with an additional decoupled singlet. By the shift $\pi/2$ the usual 2HDM convention is matched, and α diagonalises the 2×2 mass matrix in the CP-even Higgs sector yielding the two CP-even mass eigenstates h and H, respectively, with $m_h \leq m_H$ by convention. Hence,

$$\text{N2HDM} \;\to\; \text{2HDM} \quad \Longleftrightarrow \quad \begin{cases} \alpha_1 \to \alpha + \frac{\pi}{2} \\ \alpha_2 \to 0 \\ \alpha_3 \to 0 \end{cases} . \tag{2.35}$$

3 Renormalization

The computation of the EW corrections to the Higgs decays involves ultraviolet (UV) divergences. Decays with external charged particles additionally induce infrared (IR) divergences. The UV divergences are canceled by the renormalization of the parameters and

JHEP12(2017)077

wave functions involved in the process. In the following we will present the renormalization of the N2HDM Higgs sector. For the purpose of this work we must deal with the renormalization of the electroweak and the Higgs sectors. With the main focus being on the renormalization of the N2HDM Higgs sector, in the sample decays presented in the numerical analysis we do not include processes that require the treatment of IR divergences or the renormalization of the fermion sector. Note also that we do not need to renormalize the gauge-fixing Lagrangian since we choose to write it already in terms of renormalized fields and parameters [43–45]. In the renormalization of the N2HDM Higgs sector we closely follow the procedure applied in the 2HDM renormalization of refs. [36, 37]. There, for the first time, a gauge-independent renormalization has been worked out for the 2HDM mixing angles by applying the treatment of the tadpoles of ref. [46], which we call the alternative tadpole scheme, in combination with the pinch technique. The pinch technique allows to unambiguously extract the gauge-parameter independent parts of the decay amplitude and in particular of the angular counterterms. The N2HDM encounters four mixing angles instead of only two in the 2HDM. This leads to more complicated renormalization conditions compared to the 2HDM, as will be shown below. Additionally, the pinched self-energies needed in this renormalization program have to be worked out explicitly for the N2HDM. This has been done here for the first time. Since the formulae are quite lengthy, we defer them to appendix B.2, which is part of appendix B that is dedicated to the detailed presentation of the pinch technique in the N2HDM. We hope our results to be useful for further works on this subject in the future.

For the renormalization we replace the bare parameters p_0, that are involved in the process and participate in the EW interactions, by the renormalized ones, p, and the corresponding counterterms δp,

$$p_0 = p + \delta p\,. \tag{3.1}$$

Denoting generically scalar and vector fields by Ψ, the fields are renormalized through their field renormalization constants Z_Ψ as

$$\Psi_0 = \sqrt{Z_\Psi}\,\Psi\,. \tag{3.2}$$

Note that in case the different field components mix Z_Ψ is a matrix.

Gauge sector. The counterterms to be introduced in the gauge sector are independent of the Higgs sector under investigation. For convenience of the reader and to set our notation, we still repeat the necessary replacements here. The massive gauge boson masses and the electric charge are replaced by[3]

$$m_W^2 \to m_W^2 + \delta m_W^2 \tag{3.3}$$

$$m_Z^2 \to m_Z^2 + \delta m_Z^2 \tag{3.4}$$

$$e \to (1 + \delta Z_e)\, e\,. \tag{3.5}$$

[3]The quantities on the left-hand side are the bare ones, where for convenience we dropped the index '0'. The ones on the right-hand side are the renormalized ones plus the corresponding counterterms.

The gauge boson fields are renormalized by their field renormalization constants δZ,

$$W^{\pm} \to \left(1 + \frac{1}{2}\delta Z_{WW}\right) W^{\pm} \tag{3.6}$$

$$\begin{pmatrix} Z \\ \gamma \end{pmatrix} \to \begin{pmatrix} 1 + \frac{1}{2}\delta Z_{ZZ} & \frac{1}{2}\delta Z_{Z\gamma} \\ \frac{1}{2}\delta Z_{\gamma Z} & 1 + \frac{1}{2}\delta Z_{\gamma\gamma} \end{pmatrix} \begin{pmatrix} Z \\ \gamma \end{pmatrix}. \tag{3.7}$$

Fermion sector. Although not needed in the computation of our sample decay widths in the numerical analysis, for completeness we also include the renormalization of the fermion sector. The counterterms of the fermion masses m_f are defined through

$$m_f \to m_f + \delta m_f \,. \tag{3.8}$$

And the bare left- and right-handed fermion fields

$$f_{L/R} \equiv P_{L/R} f \quad , \quad \text{with} \quad P_{L/R} = (1 \mp \gamma_5)/2 \,, \tag{3.9}$$

are replaced by their corresponding renormalized fields according to

$$f_{L/R} \to \left(1 + \frac{1}{2}\delta Z_f^{L/R}\right) f_{L/R} \,. \tag{3.10}$$

Higgs sector. The renormalization is performed in the mass basis and the mass counterterms are defined through

$$m_\Phi^2 \to m_\Phi^2 + \delta m_\Phi^2 \,. \tag{3.11}$$

The field Φ stands generically for the N2HDM Higgs mass eigenstates, $\Phi \equiv H_1, H_2, H_3, A, H^\pm$. The replacement of the fields by the renormalized ones and their counterterms differs from the 2HDM case only by the fact that the wave function counterterm matrix in the CP-even neutral Higgs sector is now a 3×3 instead of a 2×2 matrix. Hence,

$$\begin{pmatrix} H_1 \\ H_2 \\ H_3 \end{pmatrix} \to \begin{pmatrix} 1 + \frac{1}{2}\delta Z_{H_1H_1} & \frac{1}{2}\delta Z_{H_1H_2} & \frac{1}{2}\delta Z_{H_1H_3} \\ \frac{1}{2}\delta Z_{H_2H_1} & 1 + \frac{1}{2}\delta Z_{H_2H_2} & \frac{1}{2}\delta Z_{H_2H_3} \\ \frac{1}{2}\,\delta Z_{H_3H_1} & \frac{1}{2}\,\delta Z_{H_3H_2} & 1 + \frac{1}{2}\,\delta Z_{H_3H_3} \end{pmatrix} \begin{pmatrix} H_1 \\ H_2 \\ H_3 \end{pmatrix} \tag{3.12}$$

$$\begin{pmatrix} G^0 \\ A \end{pmatrix} \to \begin{pmatrix} 1 + \frac{1}{2}\delta Z_{G^0G^0} & \frac{1}{2}\delta Z_{G^0A} \\ \frac{1}{2}\delta Z_{AG^0} & 1 + \frac{1}{2}\delta Z_{AA} \end{pmatrix} \begin{pmatrix} G^0 \\ A \end{pmatrix} \tag{3.13}$$

$$\begin{pmatrix} G^\pm \\ H^\pm \end{pmatrix} \to \begin{pmatrix} 1 + \frac{1}{2}\delta Z_{G^\pm G^\pm} & \frac{1}{2}\delta Z_{G^\pm H^\pm} \\ \frac{1}{2}\delta Z_{H^\pm G^\pm} & 1 + \frac{1}{2}\delta Z_{H^\pm H^\pm} \end{pmatrix} \begin{pmatrix} G^\pm \\ H^\pm \end{pmatrix}. \tag{3.14}$$

And for the mixing angles we make the replacements

$$\alpha_i \to \alpha_i + \delta\alpha_i \,, \quad i = 1, 2, 3 \tag{3.15}$$

$$\beta \to \beta + \delta\beta \,. \tag{3.16}$$

JHEP12(2017)077

For the soft $\mathbb{Z}_2$-breaking mass parameter m_{12}^2, finally, we replace

$$m_{12}^2 \to m_{12}^2 + \delta m_{12}^2 \,. \tag{3.17}$$

The tadpoles vanish at leading order, but the terms linear in the Higgs fields get loop contributions at higher orders. It must therefore be ensured that the correct vacuum is reproduced also at higher orders. As outlined in the following, there are two different approaches, depending on whether one chooses the tadpoles or the VEVs to be renormalized. The tadpole parameters T_i $(i = 1, 2, 3)$ and the VEVs $v_{1,2,S}$ are correspondingly replaced by

$$T_i \to T_i + \delta T_i \,, \tag{3.18}$$

or alternatively by

$$v_{1,2,S} \to v_{1,2,S} + \delta v_{1,2,S} \,. \tag{3.19}$$

4 Treatment of the tadpoles

The renormalization conditions fix the finite parts of the counterterms. Throughout this paper we will fix the renormalization constants for the masses and fields through on-shell (OS) conditions. Using an OS scheme provides an unambiguous interpretation of the bare parameters in the classical Lagrangian in terms of physically measurable quantities. In ref. [36] it has been shown that the renormalization of the 2HDM mixing angles requires special care. Schemes used in the literature before, which are based on the definition of the counterterms through off-diagonal wave function renormalization constants and a naive treatment of the tadpoles, were shown to lead to gauge-dependent quantities. In order to cure this problem, in [36] for the first time a renormalization scheme has been worked out in which the angular counterterms are explicitly gauge independent. This guarantees the gauge independence of the decay amplitudes also in case the angular counterterms are not defined via a physical scheme as given e.g. by the renormalization through a physical process. The renormalization scheme developed in [36] is based on the combination of the alternative tadpole scheme with the pinch technique. The pinch technique allows for the extraction of the truly gauge-independent parts of the angular counterterms and requires the use of the alternative tadpole scheme.

As alluded to above, we treat the tadpoles in the alternative tadpole scheme in order to be able to define the angular (and also mass) counterterm in a gauge-independent way. While this procedure has been introduced in [36], we take here the occasion to explicitly pin down the differences between the standard and the alternative tadpole scheme. This, in particular, also reveals how these differences reflect in the renormalization of the singlet VEV.

The basic difference between the two schemes is the fact that in the alternative scheme as introduced by Fleischer and Jegerlehner in [46], also referred to by 'FJ' in the following, the VEV is taken as primary input parameter. Accordingly, one introduces an explicit VEV counterterm, along with a renormalization condition for the VEV. Instead, in the standard scheme the tadpole is assumed to be a primary input quantity. Accordingly, one introduces a tadpole counterterm, to be fixed through a renormalization condition applied

JHEP12(2017)077

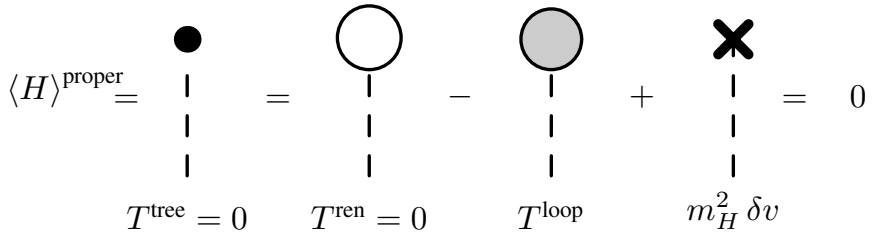

Figure 1. Renormalization condition in the alternative tadpole scheme: with the neutral component Φ^0 of the Higgs doublet Φ defined as $\Phi^0 = (v + H)/\sqrt{2}$, the requirement for the VEV to represent the true minimum of the Higgs potential translates into $\langle H \rangle^{\text{proper}} = 0$ or, equivalently, the renormalized tadpole graph (white blob) to vanish. The proper VEV coincides with the tree-level VEV (fixed by the condition $T^{\text{tree}} = 0$). Together with the condition $T^{\text{ren}} = T^{\text{tree}} = 0$, this relates the tadpole loop diagram (grey blob) at a given loop order to the VEV counterterm.

to the tadpole terms. We call the *proper* VEV the all-order Higgs vacuum expectation value $\langle \Phi \rangle = v/\sqrt{2}$. It represents the true ground state of the theory and is connected to the particle masses and electroweak couplings. At tree level the proper VEV and the bare VEV coincide while at arbitrary loop orders the proper VEV corresponds to the renormalized VEV. In the alternative tadpole scheme the proper VEV coincides with the tree-level VEV and hence is gauge-parameter independent. In this scheme one renormalizes the VEV explicitly and its counterterm δv is fixed by ensuring the proper VEV to be $v/\sqrt{2} = v^{\text{tree}}/\sqrt{2}$ to all orders. This renormalization condition yields $\delta v = T^{\text{loop}}/m_H^2$, where T^{loop} denotes the tadpole parameter at loop level. Notice that this is equivalent to i) identifying the tree-level tadpole with the renormalized tadpole $T^{\text{tree}} = T^{\text{ren}}$; ii) and then setting $T^{\text{ren}} = T^{\text{tree}} = 0$, as required by the minimum conditions on the Higgs potential — cf. figure 1 for a schematic representation. The condition generalises to multi-Higgs sectors, and we will show below in the example of the N2HDM, how the renormalization condition for the VEV counterterm is obtained. In practice, this scheme is equivalent to inserting tadpole graphs explicitly in the calculations. Since at loop level the proper VEV is given by the renormalized one, and in the FJ scheme coincides with the tree-level VEV, we have

$$v^{\text{ren}}|_{\text{FJ}} = v^{\text{tree}} = \left.\frac{2m_W}{g}\right|^{\text{tree}} . \tag{4.1}$$

When a given v-dependent Lagrangian is used at higher orders these tree-level parameters $\{g, m_W\}^{\text{tree}}$ still have to be renormalized, and they are then replaced by their corresponding renormalized parameters as

$$\left.\frac{2m_W}{g}\right|^{\text{tree}} \to \left.\frac{2m_W}{g}\right|_{\text{FJ}}^{\text{ren}} + \underbrace{\left.\frac{2m_W}{g}\left(\frac{\delta m_W^2}{2m_W^2} - \frac{\delta g}{g}\right)\right|_{\text{FJ}}}_{\equiv \Delta v} . \tag{4.2}$$

It is important to note that Δv is a mere label and not a VEV counterterm as such. This makes obvious that δv and Δv are completely unrelated. In particular, they feature a totally different divergence structure. Figure 1 depicts the renormalization condition for

JHEP12(2017)077

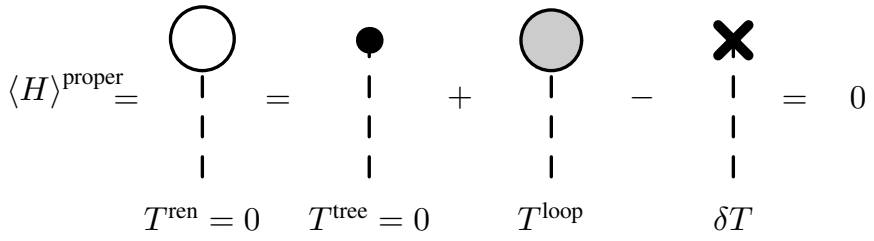

Figure 2. Renormalization condition in the standard tadpole scheme: the requirement of the renormalized tadpole graph (white blob) to vanish together with the tree-level tadpole being zero fixes the tadpole counterterm.

the alternative tadpole scheme. In the standard scheme, on the other hand, the proper VEV is obtained from the minimisation of the gauge-dependent loop-corrected potential and hence is in principle gauge dependent.

An equivalent condition to the one that fixes the VEV counterterm in the FJ scheme is now necessary to determine the tadpole counterterm in the standard scheme. This is achieved by requiring the renormalized tadpole to vanish. Together with the requirement of the tree-level tadpole to be zero, this fixes the tadpole counterterm δT. As repeatedly emphasized, the tadpole counterterm features here explicitly, since the tadpole is an input parameter in the standard scheme, cf. figure 2.

For the singlet VEV v_S a similar distinction, i.e. δv_S versus Δv_S has to be made. When v_S is related to measurable parameters the NLO VEV shift Δv_s denotes the corresponding combination of parameter counterterms, similarly to eq. (4.2). In ref. [47] it was shown that, in an R_ξ gauge, a divergent part for Δv_S in the standard scheme is precluded at one loop if the scalar field obeys a rigid invariance. This is the case for typical singlet-extended Higgs sectors, e.g. the real singlet model [42], and thereby the N2HDM singlet scalar. In all these cases the singlet field is disconnected from the gauge sector and hence invariant under global gauge transformations. The conclusion of ref. [47] relies on the use of the standard scheme, where the renormalized VEV coincides with the loop-corrected one as the renormalized tadpoles are set to zero.[4] However, this no longer applies if the VEVs are renormalized in the alternative tadpole scheme. In this case $\Delta v_S^{\rm FJ}$ becomes indeed a UV-divergent quantity. We can prove it to cancel part of the UV poles that genuinely appear if one-loop amplitudes are computed in the FJ-scheme, when the corresponding tree-level amplitudes are directly sensitive to the singlet VEV v_S. Salient examples are the Higgs-to-Higgs decays, which we discuss in detail in section 6.

[4]Let us also notice that ref. [47] distinguishes two (equivalent) parametrisations for the renormalization transformation of a generic scalar field VEV, $\langle\Phi\rangle = \frac{v}{\sqrt{2}}$:

$$v \to v + \delta v = \sqrt{Z_\Phi}(v + \delta\overline{v})\,, \tag{4.3}$$

where $\sqrt{Z_\Phi}$ is the field renormalization constant of the respective scalar field, whereas $\delta\overline{v}$ quantifies how the VEV itself is shifted differently by higher-order contributions with respect to the field. In our current conventions, $\delta v \to \Delta v$ and $\delta\overline{v} \to \Delta\overline{v}$. The results of ref. [47], together with [42], show that for a gauge-singlet scalar the quantity Δv_s in the standard scheme is UV finite at one loop order.

JHEP12(2017)077

4.1 Alternative tadpole scheme for the N2HDM

In the following, we elaborate in detail the implications of the alternative tadpole scheme. We derive the necessary relations for the N2HDM, highlighting the differences with respect to the 2HDM case, derived in [36]. At tree level the minimum conditions of the N2HDM potential lead to the three relations eqs. (2.8)–(2.10) for the tadpole parameters, or alternatively

$$T_1^{\text{tree}} = 0\,, \quad T_2^{\text{tree}} = 0 \quad \text{and} \quad T_3^{\text{tree}} = 0\,. \tag{4.4}$$

These can be used to replace the parameters m_{11}^2, m_{22}^2 and m_S^2 by the VEVs v_1, v_2 and v_S. Note, however, that at arbitrary loop order, this may only be done *after* the *proper VEVs* are taken into account in the Higgs potential. More precisely, at NLO the VEVs are modified in order to take into account the NLO effects, as

$$v_i^{\text{bare}} = v_i^{\text{ren}} + \delta v_i \overset{\text{FJ}}{=} v_i^{\text{tree}} + \delta v_i\,, \quad i = 1, 2, S\,. \tag{4.5}$$

In the alternative tadpole scheme, δv_1, δv_2 and δv_S correspond to the proper doublet and singlet VEV counterterms in the gauge basis. In turn, v_i^{ren} are the *proper* VEVs, i.e. in the FJ scheme the renormalized VEVs (coinciding with the tree-level VEVs), and hence the VEVs that generate the necessary mass relations for the gauge bosons, fermions and the scalars. The VEVs are called the *proper* VEVs if the gauge-invariant relations presented in figure 1 (for the SM case) are fulfilled at all orders, which means that the VEVs represent the true vacuum state of the theory at all orders in perturbation theory. At NLO, we insert the relations eq. (4.5) into the tadpole relations eqs. (2.8)–(2.10). At NLO, the left-hand side of the equations is given by

$$T_i^{\text{bare}} = \underbrace{T_i^{\text{tree}}}_{=0} + T_i^{\text{loop}} = T_i^{\text{loop}}\,, \quad i \equiv 1, 2, 3\,. \tag{4.6}$$

We then get the NLO expressions for eqs. (2.8)–(2.10),

$$T_1^{\text{loop}} = T_1^{\text{tree}} + \left(m_{12}^2 \frac{v_2^{\text{tree}}}{v_1^{\text{tree}}} + \lambda_1 (v_1^{\text{tree}})^2\right)\delta v_1 + \left(-m_{12}^2 + \lambda_{345} v_1^{\text{tree}} v_2^{\text{tree}}\right)\delta v_2 + \lambda_7 v_1^{\text{tree}} v_S^{\text{tree}}\, \delta v_S \tag{4.7}$$

$$T_2^{\text{loop}} = T_2^{\text{tree}} + \left(-m_{12}^2 + \lambda_{345} v_1^{\text{tree}} v_2^{\text{tree}}\right)\delta v_1 + \left(m_{12}^2 \frac{v_1^{\text{tree}}}{v_2^{\text{tree}}} + \lambda_2 (v_2^{\text{tree}})^2\right)\delta v_2 + \lambda_8 v_2^{\text{tree}} v_S^{\text{tree}}\, \delta v_S \tag{4.8}$$

$$T_3^{\text{loop}} = T_3^{\text{tree}} + \lambda_6 (v_S^{\text{tree}})^2 \delta v_S + \lambda_7 v_1^{\text{tree}} v_S^{\text{tree}} \delta v_1 + \lambda_8 v_2^{\text{tree}} v_S^{\text{tree}} \delta v_2\,. \tag{4.9}$$

Since the NLO effects for the VEVs have been taken into account in form of the counterterms in eq. (4.5), the FJ-renormalized VEVs $v_i^{\text{tree}} = v_i^{\text{ren}}$ now represent the true ground states of the theory, namely those for which $\langle \rho_i \rangle = 0$. The tree-level relations in eq. (4.4) can therefore be applied, and, in so doing, the VEV counterterms δv_1, δv_2 and δv_S are given in terms of the tadpole loops T_1^{loop}, T_2^{loop} and T_3^{loop}. By comparing with the squared

JHEP12(2017)077

mass matrix M_ρ^2 of eq. (2.17) we find analytically

$$\begin{pmatrix} T_1^{\text{loop}} \\ T_2^{\text{loop}} \\ T_3^{\text{loop}} \end{pmatrix} = \begin{pmatrix} m_{12}^2 t_\beta + \lambda_1 (v^{\text{tree}})^2 c_\beta^2 & -m_{12}^2 + \lambda_{345} (v^{\text{tree}})^2 s_\beta c_\beta & \lambda_7 c_\beta v^{\text{tree}} v_S^{\text{tree}} \\ -m_{12}^2 + \lambda_{345} (v^{\text{tree}})^2 s_\beta c_\beta & m_{12}^2/t_\beta + \lambda_2 (v^{\text{tree}})^2 s_\beta^2 & \lambda_8 s_\beta v^{\text{tree}} v_S^{\text{tree}} \\ \lambda_7 c_\beta v^{\text{tree}} v_S^{\text{tree}} & \lambda_8 s_\beta v^{\text{tree}} v_S^{\text{tree}} & \lambda_6 (v_S^{\text{tree}})^2 \end{pmatrix} \begin{pmatrix} \delta v_1 \\ \delta v_2 \\ \delta v_S \end{pmatrix}$$
$$= \mathcal{M}_\rho^2 \Big|_{T_i=0} \begin{pmatrix} \delta v_1 \\ \delta v_2 \\ \delta v_S \end{pmatrix} . \tag{4.10}$$

Rotation to the mass basis yields

$$\begin{pmatrix} \delta v_{H_1} \\ \delta v_{H_2} \\ \delta v_{H_3} \end{pmatrix} = \begin{pmatrix} \frac{T_{H_1}^{\text{loop}}}{m_{H_1}^2} \\ \frac{T_{H_2}^{\text{loop}}}{m_{H_2}^2} \\ \frac{T_{H_3}^{\text{loop}}}{m_{H_3}^2} \end{pmatrix} , \tag{4.11}$$

where $T_{H_i}^{\text{loop}} = R(\alpha_i) T_i^{\text{loop}}$, and hence

$$\begin{pmatrix} \delta v_1 \\ \delta v_2 \\ \delta v_S \end{pmatrix} = R(\alpha_i)^T \begin{pmatrix} \frac{T_{H_1}^{\text{loop}}}{m_{H_1}^2} \\ \frac{T_{H_2}^{\text{loop}}}{m_{H_2}^2} \\ \frac{T_{H_3}^{\text{loop}}}{m_{H_3}^2} \end{pmatrix} . \tag{4.12}$$

The latter identity is helpful in practice, as the calculation of the tadpole diagrams is usually performed in the mass basis, but the VEV shifts are introduced most conveniently in the gauge basis. Rewriting eq. (4.11), the quantities δv_{H_i} can be interpreted as connected tadpole diagrams, containing the Higgs tadpole and its propagator at zero momentum transfer,

$$\delta v_{H_i} = \frac{-i}{m_{H_i}^2} i T_{H_i}^{\text{loop}} = \frac{-i}{m_{H_i}^2} \left(\right. \quad H_i \quad \left. \right) = \left(\quad H_i \quad \right) . \tag{4.13}$$

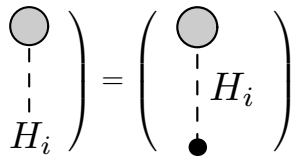

We want to emphasize again that in the alternative tadpole scheme eq. (4.13) defines the counterterms of the vacuum expectation values. In contrast to the standard scheme, no tadpole counterterms are introduced. Tadpole graphs appear through the gauge-invariant condition in figure 1.

Once the leading-order VEVs are promoted to higher orders, namely by inserting eq. (4.5) into a generic VEV-dependent Lagrangian $\mathcal{L}(v_1, v_2, v_S)$, the contribution of the VEV counterterms δv_1, δv_2 and δv_S, as given by eq. (4.12), is equivalent to introducing explicit tadpole graphs in all loop amplitudes. Moreover, all tree-level relations between the VEVs and the weak sector parameters (masses, coupling constants) hold again. In particular, for the doublet VEVs this means with $(v_1^2 + v_2^2 = v^2)$

$$v^{\text{ren}}|_{\text{FJ}} = v^{\text{tree}} = \frac{2 m_W}{g} \Big|^{\text{tree}} \tag{4.14}$$

JHEP12(2017)077

then

$$v_1^{\text{ren}}|_{\text{FJ}} = v_1^{\text{tree}} = \frac{2m_W c_\beta}{g}\Big|^{\text{tree}} \qquad \text{and} \qquad v_2^{\text{ren}}|_{\text{FJ}} = v_2^{\text{tree}} = \frac{2m_W s_\beta}{g}\Big|^{\text{tree}} . \tag{4.15}$$

By applying the renormalization conditions for the VEVs, the tree-level VEVs ensure the true ground state of the potential. Since they are not directly related to a physical observable, we express the FJ-renormalized doublet VEVs in terms of physical tree-level parameters, here m_W, g and the mixing angle β. In higher order calculations, these parameters are then renormalized by choosing physical renormalization conditions.[5] To better illustrate the implications of the alternative tadpole scheme, we consider the scalar-vector-vector vertex between the physical H_1 and a W boson pair. We first define the Feynman rules, needed in the following, by

$$H_1 W^\mu W^\nu \;:\; i g_{H_1 WW}\, g^{\mu\nu} \tag{4.16}$$

$$H_1 H_j W^\mu W^\nu \;:\; i g_{H_1 H_j WW}\, g^{\mu\nu} , \quad j = 1,2,3 . \tag{4.17}$$

The coupling constants for the triple vertex in terms of the mixing angles and the VEVs v_1 and v_2 are

$$\begin{aligned} g_{H_1 WW} &\equiv g^{\text{SM}}_{HWW}\, \kappa_{H_1 WW} \\ &= g m_W c_{\alpha_2} c_{\beta-\alpha_1} = \frac{g^2 v c_{\alpha_2} c_{\beta-\alpha_1}}{2} = \frac{g^2 c_{\alpha_2}}{2}(c_{\alpha_1} v_1 + s_{\alpha_1} v_2) , \end{aligned} \tag{4.18}$$

and for the quartic vertices

$$\begin{aligned} g_{H_1 H_1 WW} &\equiv \kappa_{H_1 H_1 ZZ}\, g^{\text{SM}}_{HWW} = \frac{g^2\, c_{\alpha_2}^2}{2} \\ g_{H_1 H_2 WW} &\equiv \kappa_{H_1 H_2 ZZ}\, g^{\text{SM}}_{HWW} = -\frac{g^2\, c_{\alpha_2} s_{\alpha_2} s_{\alpha_3}}{2} \\ g_{H_1 H_3 WW} &\equiv \kappa_{H_1 H_3 ZZ}\, g^{\text{SM}}_{HWW} = -\frac{g^2\, c_{\alpha_2} s_{\alpha_2} c_{\alpha_3}}{2} . \end{aligned} \tag{4.19}$$

When expressing the couplings in terms of the VEVs, care has to be taken to differentiate between the angle β in the sense of a mixing angle and β in the sense of the ratio of the VEVs. Only the latter is to be replaced by the VEVs that are to be renormalized. The same distinction must be applied for the α_i. Note that in all couplings but the trilinear and quartic Higgs self-couplings the angles α_i have the roles of mixing angles. Only in the Higgs self-couplings, the α_i partly appear in the sense of the ratio of N2HDM potential parameters. Bearing these considerations in mind, we see that the quartic couplings do not receive any δv_i, whereas $g_{H_1 WW}$ contains β as ratio of the VEVs. Instead, the angles

[5] We call the mixing angles *physical* in the sense that they appear in the Higgs couplings and hence enter physical observables.

JHEP12(2017)077

α_1 and α_2 are mixing angles here. At NLO, we therefore have to make the replacement

$$
\begin{aligned}
ig_{H_1WW} &= \frac{ig^2 c_{\alpha_2}}{2}(c_{\alpha_1} v_1^{\text{tree}} + s_{\alpha_1} v_2^{\text{tree}}) + \frac{ig^2 c_{\alpha_2}}{2}(c_{\alpha_1}\delta v_1 + s_{\alpha_1}\delta v_2) \\
&\overset{(4.12)}{=} ig_{H_1WW} + \frac{ig^2 c_{\alpha_2}}{2}\left[c_{\alpha_2}\frac{T_{H_1}^{\text{loop}}}{m_{H_1}^2} - s_{\alpha_2}s_{\alpha_3}\frac{T_{H_2}^{\text{loop}}}{m_{H_2}^2} - s_{\alpha_2}c_{\alpha_3}\frac{T_{H_3}^{\text{loop}}}{m_{H_3}^2}\right] \\
&= ig_{H_1WW} \\
&\quad + ig_{H_1H_1WW}\left(\frac{-i}{m_{H_1}^2}\right) iT_{H_1}^{\text{loop}} + ig_{H_1H_2WW}\left(\frac{-i}{m_{H_2}^2}\right) iT_{H_2}^{\text{loop}} + ig_{H_1H_3WW}\left(\frac{-i}{m_{H_3}^2}\right) iT_{H_3}^{\text{loop}} \\
&= ig_{H_1WW} + \Bigg(\quad + \quad + \quad \Bigg)_{\text{trunc}} \\
&\equiv ig_{H_1WW}^{\text{tad}} \,.
\end{aligned}
\tag{4.20}
$$

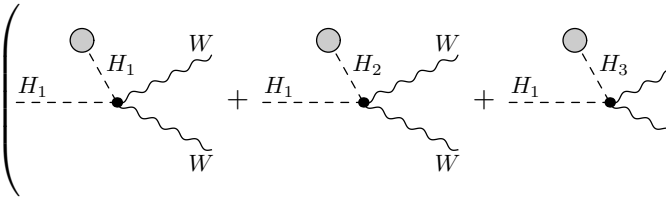

The subscript 'trunc' means that all Lorentz structure of the vector bosons as well as the Lorentz structure of the coupling has been suppressed here for simplicity. The second term in the second line generates, through the VEV counterterms δv_i, the tadpole diagrams contributing to the scalar-vector-vector vertex. On the other hand, as the VEVs in this expression have already been expanded to NLO through $v_i \to v_i^{\text{tree}} + \delta v_i$, we use all tree-level relations, in particular eq. (4.15), to fix the (FJ-renormalized) VEVs v_i^{tree} in terms of the tree-level weak sector parameters and the angle β.[6] At loop level the EW parameters and mixing angles that enter the coupling, here g, m_W, β, α_1 and α_2 have to be renormalized, i.e. we replace them by their renormalized values plus the corresponding counterterms, cf. eq. (3.1). We then get for the vertex of eq. (4.20)

$$
ig_{H_1WW}^{\text{tad}} + igm_W c_{\alpha_2} c_{\beta-\alpha_1}\left[\frac{\delta g}{g} + \frac{\delta m_W^2}{2m_W^2} - t_{\alpha_2}\delta\alpha_2 - t_{\beta-\alpha_1}(\delta\beta - \delta\alpha_1)\right] . \tag{4.21}
$$

The exact form of these counterterms[7] depends on the renormalization conditions, which will be given in the next section.

Our derivation also shows the difference with respect to the 2HDM, namely the last two terms in eq. (4.20) do not arise in the 2HDM. They are due to the additional singlet-doublet mixing and have no counterpart in a pure 2HDM structure (cf. eq. (A.61) of [36]).

As a final remark, let us summarize the key differences with respect to the standard tadpole scheme. In the latter case, VEV counterterms of the form of eq. (4.13) are strictly speaking not introduced. Instead, one introduces renormalized tadpoles and tadpole counterterms, fulfilling the same condition as in figure 1 — that is, $T_i^{\text{ren}} = 0$ with $T_i^{\text{ren}} = T_i^{\text{loop}} - \delta T_i$. In doing so, the VEVs correspond to the ground state of the loop-corrected scalar potential, and the corresponding VEV relations to weak sector parameters

[6] Note, that since we use the tree-level relations, the angle β in the sense of the ratio of the VEVs and in the sense of the mixing angle coincide.

[7] Since the $\text{SU}(2)_L$ coupling is not chosen to be an independent input parameter, it will be given in terms of the counterterms for m_W, m_Z and e.

JHEP12(2017)077

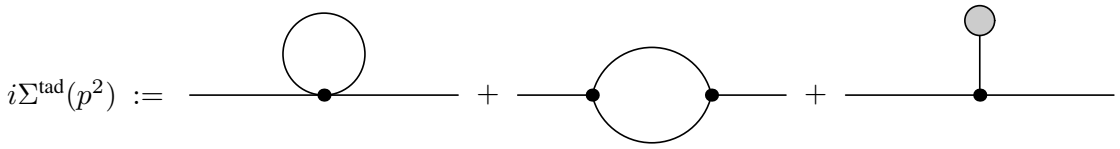

Figure 3. Modified self-energy $i\Sigma^{\text{tad}}(p^2)$ in the alternative tadpole scheme, consisting of all 1 particle-irreducible (PI) self-energy diagrams together with the one-loop tadpole diagrams, indicated by a gray blob.

hold order-by-order. Due to the fact that in the standard tadpole scheme one considers the VEVs from the one-loop corrected potential (in contrast to the alternative scheme, where one considers the tree-level VEVs), VEV diagrams in the self-energies and vertices explicitly vanish and thus need not be taken into account, at the expense of defining mass counterterms which become manifestly gauge dependent.

In practice, the rigorous introduction of the VEV counterterms in the alternative tadpole scheme yields the following rules for its application in the renormalization of a generic process within the N2HDM:

1. Include explicit tadpole contributions in all self-energies used to define the (off-diagonal) wave function renormalization constants[8] and wherever the self-energies appear in the counterterms, such that now $\Sigma^{\text{tad}}(p^2)$ contains the additional tadpole contributions, cf. figure 3.

2. Include explicit tadpole contributions in the virtual vertex corrections, if the tadpole insertions are connected to an existing coupling. This is applicable e.g. to all triple Higgs self-interactions as well as to the Higgs couplings to gauge bosons.

In the alternative tadpole scheme not only the angular counterterms but also the mass counterterms become gauge independent. This has been shown for the electroweak sector in [48]. All counterterms of the electroweak sector have exactly the same structure as in the standard scheme. Only the self-energies Σ have to be replaced by the self-energies Σ^{tad} containing the tadpole contributions. Note however, that there are no tadpole contributions to the transverse photon-Z self-energy $\Sigma^T_{\gamma Z}$ nor to the transverse photon self-energy $\Sigma^T_{\gamma\gamma}$ so that

$$\Sigma^{\text{tad},T}_{\gamma Z/\gamma\gamma} = \Sigma^T_{\gamma Z/\gamma\gamma}\,. \tag{4.22}$$

Having introduced the tadpole scheme, we now list explicitly the counterterms needed in the computation of the electroweak corrections. In particular, we illustrate the renormalization of the N2HDM Higgs sector.

5 Renormalization conditions

With the previous section we are now able to specify the counterterms needed in the renormalization of the N2HDM. Those of the EW and Yukawa sector correspond to the

[8]Diagonal wave function corrections, instead, are constructed from derivatives of the corresponding self-energies with respect to p^2, hence the tadpole-dependent contributions vanish.

JHEP12(2017)077

ones of the SM, while differences obviously arise in the Higgs sector itself. For completeness, all counterterms of the model will be listed, although not all of them will be necessary to study the sample processes discussed in section 7.

5.1 Counterterms of the gauge sector

The gauge bosons are renormalized through OS conditions implying the mass counterterms

$$\delta m_W^2 = \mathrm{Re}\Sigma_{WW}^{\mathrm{tad},T}(m_W^2) \quad \text{and} \quad \delta m_Z^2 = \mathrm{Re}\Sigma_{ZZ}^{\mathrm{tad},T}(m_Z^2)\,, \tag{5.1}$$

where T denotes the transverse part of the self-energy including the tadpole contributions. The wave function renormalization constants that guarantee the correct OS properties are given by

$$\delta Z_{WW} = -\mathrm{Re}\left.\frac{\partial\Sigma_{WW}^T(p^2)}{\partial p^2}\right|_{p^2=m_W^2} \tag{5.2}$$

$$\begin{pmatrix} \delta Z_{ZZ} & \delta Z_{Z\gamma} \\ \delta Z_{\gamma Z} & \delta Z_{\gamma\gamma} \end{pmatrix} = \begin{pmatrix} -\mathrm{Re}\left.\frac{\partial\Sigma_{ZZ}^T(p^2)}{\partial p^2}\right|_{p^2=m_Z^2} & 2\frac{\Sigma_{Z\gamma}^T(0)}{m_Z^2} \\ -2\mathrm{Re}\frac{\Sigma_{Z\gamma}^T(m_Z^2)}{m_Z^2} & -\left.\frac{\partial\Sigma_{\gamma\gamma}^T(p^2)}{\partial p^2}\right|_{p^2=0} \end{pmatrix}. \tag{5.3}$$

Note that in eqs. (5.2) and (5.3) they are the same in the standard and in the alternative tadpole scheme introduced above. The reason is that the tadpoles are independent of the external momentum so that the derivatives of the self-energies do not change. Furthermore, $\Sigma_{\gamma Z}^T$ is identical in both schemes, as alluded to above. For better readability we therefore drop the superscript 'tad' here and wherever possible. For the same reasons the counterterm for the electric charge is invariant with respect to the choice of the tadpole scheme. The electric charge is renormalized to be the full electron-positron photon coupling for OS external particles in the Thomson limit. This implies that all corrections to this vertex vanish OS and for zero momentum transfer. The counterterm for the electric charge in terms of the transverse photon-photon and photon-Z self-energies reads [49]

$$\delta Z_e^{\alpha(0)} = \frac{1}{2}\left.\frac{\partial\Sigma_{\gamma\gamma}^T(k^2)}{\partial k^2}\right|_{k^2=0} + \frac{s_W}{c_W}\frac{\Sigma_{\gamma Z}^T(0)}{m_Z^2}\,. \tag{5.4}$$

The sign in the second term of eq. (5.4) differs from the one in [49] because we have adopted different sign conventions in the covariant derivative of eq. (2.2). In our computation we will use the fine structure constant at the Z boson mass $\alpha(m_Z^2)$ as input. This way the results are independent of large logarithms due to light fermions $f \neq t$. The counterterm δZ_e is therefore modified as [49]

$$\delta Z_e^{\alpha(m_Z^2)} = \delta Z_e^{\alpha(0)} - \frac{1}{2}\Delta\alpha(m_Z^2) \tag{5.5}$$

$$\Delta\alpha(m_Z^2) = \left.\frac{\partial\Sigma_{\gamma\gamma}^T(k^2)}{\partial k^2}\right|_{k^2=0} - \frac{\Sigma_{\gamma\gamma}^T(m_Z^2)}{m_Z^2}\,, \tag{5.6}$$

where the transverse part of the photon self-energy $\Sigma_{\gamma\gamma}^T$ in eq. (5.6) includes only the light fermion contributions. The calculation of the EW one-loop corrected Higgs decay widths

JHEP12(2017)077

also requires the renormalization of the weak coupling g, which can be related to e and the gauge boson masses as

$$g = \frac{e m_Z}{\sqrt{m_Z^2 - m_W^2}} \,. \tag{5.7}$$

Its counterterm can therefore be expressed in terms of the electric charge and gauge boson mass counterterms through

$$\frac{\delta g}{g} = \delta Z_e - \frac{1}{2(1 - m_Z^2/m_W^2)} \left(\frac{\delta m_W^2}{m_W^2} - \frac{\delta m_Z^2}{m_Z^2} \right). \tag{5.8}$$

5.2 Counterterms of the fermion sector

Defining the following structure for the fermion self-energies

$$\Sigma_f(p^2) = \not{p}\Sigma_f^L(p^2)P_L + \not{p}\Sigma_f^R(p^2)P_R + m_f\Sigma_f^{Ls}(p^2)P_L + m_f\Sigma_f^{Rs}(p^2)P_R \tag{5.9}$$

the fermion mass counterterms applying OS conditions are given by

$$\frac{\delta m_f}{m_f} = \frac{1}{2}\mathrm{Re}\left[\Sigma_f^{\mathrm{tad},L}(m_f^2) + \Sigma_f^{\mathrm{tad},R}(m_f^2) + \Sigma_f^{\mathrm{tad},Ls}(m_f^2) + \Sigma_f^{\mathrm{tad},Rs}(m_f^2)\right] . \tag{5.10}$$

The fermion wave function renormalization constants are determined from

$$\begin{aligned} \delta Z_f^{L/R} = &-\mathrm{Re}\Sigma_f^{\mathrm{tad},L/R}(m_f^2) \\ &- m_f^2 \frac{\partial}{\partial p^2}\mathrm{Re}\left(\Sigma_f^{L/R}(p^2) + \Sigma_f^{R/L}(p^2) + \Sigma_f^{L/Rs}(p^2) + \Sigma_f^{R/Ls}(p^2)\right)\Big|_{p^2=m_f^2} . \end{aligned} \tag{5.11}$$

5.3 Higgs field and mass counterterms

The OS conditions for the physical Higgs bosons yield the mass counterterms ($i = 1, 2, 3$)

$$\delta m_{H_i}^2 = \mathrm{Re}[\Sigma_{H_iH_i}^{\mathrm{tad}}(m_{H_i}^2)] \tag{5.12}$$

$$\delta m_A^2 = \mathrm{Re}[\Sigma_{AA}^{\mathrm{tad}}(m_A^2)] \tag{5.13}$$

$$\delta m_{H^\pm}^2 = \mathrm{Re}[\Sigma_{H^\pm H^\pm}^{\mathrm{tad}}(m_{H^\pm}^2)] \,. \tag{5.14}$$

Having absorbed the tadpoles into the self-energies, no tadpole counterterms appear explicitly in the mass counterterms any more, in contrast to the corresponding expressions in the standard tadpole scheme. The OS conditions for the Higgs bosons yield the following wave function renormalization counterterm 3×3 matrix for the CP-even neutral N2HDM scalars,

$$\delta Z_{H_iH_j} = \begin{pmatrix} -\mathrm{Re}\left.\frac{\partial\Sigma_{H_1H_1}(k^2)}{\partial k^2}\right|_{k^2=m_{H_1}^2} & 2\frac{\mathrm{Re}\left[\Sigma_{H_1H_2}^{\mathrm{tad}}(m_{H_2}^2)\right]}{m_{H_1}^2 - m_{H_2}^2} & 2\frac{\mathrm{Re}\left[\Sigma_{H_1H_3}^{\mathrm{tad}}(m_{H_3}^2)\right]}{m_{H_1}^2 - m_{H_3}^2} \\ 2\frac{\mathrm{Re}\left[\Sigma_{H_2H_1}^{\mathrm{tad}}(m_{H_1}^2)\right]}{m_{H_2}^2 - m_{H_1}^2} & -\mathrm{Re}\left.\frac{\partial\Sigma_{H_2H_2}(k^2)}{\partial k^2}\right|_{k^2=m_{H_2}^2} & 2\frac{\mathrm{Re}\left[\Sigma_{H_2H_3}^{\mathrm{tad}}(m_{H_3}^2)\right]}{m_{H_2}^2 - m_{H_3}^2} \\ 2\frac{\mathrm{Re}\left[\Sigma_{H_3H_1}^{\mathrm{tad}}(m_{H_1}^2)\right]}{m_{H_3}^2 - m_{H_1}^2} & 2\frac{\mathrm{Re}\left[\Sigma_{H_3H_2}^{\mathrm{tad}}(m_{H_2}^2)\right]}{m_{H_3}^2 - m_{H_2}^2} & -\mathrm{Re}\left.\frac{\partial\Sigma_{H_3H_3}(k^2)}{\partial k^2}\right|_{k^2=m_{H_3}^2} \end{pmatrix} . \tag{5.15}$$

JHEP12(2017)077

The diagonal entries are obtained as customary by enforcing the poles of the renormalized Higgs two-point Green's functions to have residue 1. The non-diagonal constants follow from demanding that no $H_i \to H_j$ transitions occur between different on-shell fields. For further details we refer the reader to the appendix A.1 of [36].

In the CP-odd and charged sector we have the 2×2 matrices

$$\begin{pmatrix} \delta Z_{G^0G^0} & \delta Z_{G^0A} \\ \delta Z_{AG^0} & \delta Z_{AA} \end{pmatrix} = \begin{pmatrix} -\mathrm{Re}\left.\frac{\partial \Sigma_{G^0G^0}(k^2)}{\partial k^2}\right|_{k^2=0} & -2\frac{\mathrm{Re}\left[\Sigma^{\mathrm{tad}}_{G^0A}(m_A^2)\right]}{m_A^2} \\ 2\frac{\mathrm{Re}\left[\Sigma^{\mathrm{tad}}_{G^0A}(0)\right]}{m_A^2} & -\mathrm{Re}\left.\frac{\partial \Sigma_{AA}(k^2)}{\partial k^2}\right|_{k^2=m_A^2} \end{pmatrix} \tag{5.16}$$

$$\begin{pmatrix} \delta Z_{G^\pm G^\pm} & \delta Z_{G^\pm H^\pm} \\ \delta Z_{H^\pm G^\pm} & \delta Z_{H^\pm H^\pm} \end{pmatrix} = \begin{pmatrix} -\mathrm{Re}\left.\frac{\partial \Sigma_{G^\pm G^\pm}(k^2)}{\partial k^2}\right|_{k^2=0} & -2\frac{\mathrm{Re}\left[\Sigma^{\mathrm{tad}}_{G^\pm H^\pm}(m^2_{H^\pm})\right]}{m^2_{H^\pm}} \\ 2\frac{\mathrm{Re}\left[\Sigma^{\mathrm{tad}}_{G^\pm H^\pm}(0)\right]}{m^2_{H^\pm}} & -\mathrm{Re}\left.\frac{\partial \Sigma_{H^\pm H^\pm}(k^2)}{\partial k^2}\right|_{k^2=m^2_{H^\pm}} \end{pmatrix}. \tag{5.17}$$

5.4 Angular counterterms

As in the 2HDM, we renormalize the mixing angles based on the definition of the counterterms through off-diagonal wave function renormalization constants and combine this with the alternative tadpole approach together with the application of the pinch technique in order to arrive at an unambiguous gauge-independent definition of the mixing angle counterterms. Let us note that a process-dependent renormalization of the mixing angles would also lead to a gauge-independent renormalization, as shown in [36] for the 2HDM case. In the N2HDM the situation becomes more involved as *four* different processes need to be identified to fix all mixing angle counterterms $\delta\alpha_i$ and $\delta\beta$. Moreover, the construction of such a process-dependent scheme is complicated by the fact that the different Higgs decay modes typically rely on more than one mixing angle, implying that the different angular counterterms appear as linear combinations in each individual vertex counterterm. It is therefore imperative to choose a set of processes where the angular counterterm dependences enter as a linearly independent combination, such that they can be fixed unambiguously through linear combinations of the different decay widths. Moreover, all these processes have to be phenomenologically accessible. The process-dependent renormalization of the N2HDM mixing angles is hence rather unpractical from a physical point of view, and we will therefore not consider it any further.

While the expression for the counterterm in the charged and CP-odd sector, $\delta\beta$, in terms of the off-diagonal wave function renormalization constants does not change with respect to the 2HDM, this is not the case for the mixing angle counterterms $\delta\alpha_i$ in the CP-even sector. We therefore present their derivation here. It is based on the idea of making the counterterms $\delta\alpha_i$ (and also $\delta\beta$) appear in the inverse propagator matrix and thereby in the wave function renormalization constants in a way that is consistent with the internal relations of the N2HDM.[9] This can be achieved by performing the renormalization in the

[9]The renormalization of the mixing matrix in the scalar sector of a theory with an arbitrary number of scalars was first discussed in [50].

JHEP12(2017)077

physical basis (H_1, H_2, H_3), but temporarily switching to the gauge basis (ρ_1, ρ_2, ρ_3), and back again. For the CP-even sector of the N2HDM this means,

$$\begin{pmatrix} H_1 \\ H_2 \\ H_3 \end{pmatrix}_{\text{bare}} = R(\alpha_i)\Big|_{\text{bare}} \begin{pmatrix} \rho_1 \\ \rho_2 \\ \rho_3 \end{pmatrix}_{\text{bare}} \quad \rightarrow \quad R(\alpha_i + \delta\,\alpha_i)\,\sqrt{Z_{\rho_i}} \begin{pmatrix} \rho_1 \\ \rho_2 \\ \rho_3 \end{pmatrix}$$
$$= \underbrace{R(\delta\alpha_i)\,R(\alpha_i)\,\sqrt{Z_{\rho_i}}\,R(\alpha_i)^T}_{\sqrt{Z_{H_i}}}\,R(\alpha_i) \begin{pmatrix} \rho_1 \\ \rho_2 \\ \rho_3 \end{pmatrix} = \sqrt{Z_{H_i}} \begin{pmatrix} H_1 \\ H_2 \\ H_3 \end{pmatrix} . \tag{5.18}$$

The field renormalization matrix in the mass basis can be parametrized as

$$\sqrt{Z_{H_i}} = R(\delta\alpha_i) \begin{pmatrix} 1+\frac{\delta Z_{H_1H_1}}{2} & \delta C_{12} & \delta C_{13} \\ \delta C_{21} & 1+\frac{\delta Z_{H_2H_2}}{2} & \delta C_{23} \\ \delta C_{31} & \delta C_{32} & 1+\frac{\delta Z_{H_3H_3}}{2} \end{pmatrix} = \tag{5.19}$$
$$\begin{pmatrix} 1+\frac{\delta Z_{H_1H_1}}{2} & c_{\alpha_2}c_{\alpha_3}\delta\alpha_1+s_{\alpha_3}\delta\alpha_2+\delta C_{12} & c_{\alpha_3}\delta\alpha_2-s_{\alpha_3}c_{\alpha_2}\delta\alpha_1+\delta C_{13} \\ -c_{\alpha_2}c_{\alpha_3}\delta\alpha_1-s_{\alpha_3}\delta\alpha_2+\delta C_{21} & 1+\frac{\delta Z_{H_2H_2}}{2} & \delta\alpha_3+s_{\alpha_2}\delta\alpha_1+\delta C_{23} \\ -c_{\alpha_3}\delta\alpha_2+s_{\alpha_3}c_{\alpha_2}\delta\alpha_1+\delta C_{31} & -\delta\alpha_3-s_{\alpha_2}\delta\alpha_1+\delta C_{32} & 1+\frac{\delta Z_{H_3H_3}}{2} \end{pmatrix},$$

where $\delta C_{ij} = \delta C_{ji}$ in agreement with the fact that $\sqrt{Z_{\rho_i}}$ is a symmetric matrix. By identifying the off-diagonal elements with the off-diagonal wave function renormalization constants $\delta Z_{H_iH_j}/2$ $(i \neq j)$, the three neutral CP-even angular counterterms are obtained as

$$\begin{aligned} \delta\alpha_1 &= \frac{c_{\alpha_3}}{4\,c_{\alpha_2}}\left(\delta Z_{H_1H_2} - \delta Z_{H_2H_1}\right) - \frac{s_{\alpha_3}}{4\,c_{\alpha_2}}\left(\delta Z_{H_1H_3} - \delta Z_{H_3H_1}\right) \\ \delta\alpha_2 &= \frac{c_{\alpha_3}}{4}\left(\delta Z_{H_1H_3} - \delta Z_{H_3H_1}\right) + \frac{s_{\alpha_3}}{4}\left(\delta Z_{H_1H_2} - \delta Z_{H_2H_1}\right) \\ \delta\alpha_3 &= \frac{1}{4}\left(\delta Z_{H_2H_3} - \delta Z_{H_3H_2}\right) + \frac{s_{\alpha_2}}{4c_{\alpha_2}}\left[s_{\alpha_3}\left(\delta Z_{H_1H_3} - \delta Z_{H_3H_1}\right) - c_{\alpha_3}\left(\delta Z_{H_1H_2} - \delta Z_{H_2H_1}\right)\right] , \end{aligned} \tag{5.20}$$

while the auxiliary counterterms δC_{ij} do not play a role in the remainder of the discussion.

The definition of the counterterm $\delta\beta$ can be taken over from the 2HDM. It is derived analogously to the $\delta\alpha_i$, but from the charged and CP-odd Higgs sectors. In this case, there are altogether four off-diagonal wave function constants, while only three free parameters to be fixed. For details, we refer to ref. [36]. There we proposed two different possible counterterm choices for β, one based on the charged and the other on the CP-odd sector. Also here we will apply these two possible choices, given by

$$\delta\beta^{(1)} = \frac{1}{4}(\delta Z_{G^\pm H^\pm} - \delta Z_{H^\pm G^\pm}) \tag{5.21}$$

and

$$\delta\beta^{(2)} = \frac{1}{4}(\delta Z_{G^0A} - \delta Z_{AG^0})\,. \tag{5.22}$$

All wave function renormalization constants appearing in the counterterms eqs. (5.20), (5.21) and (5.22) are renormalized in the OS scheme and given by the corresponding entries

JHEP12(2017)077

in the wave function counterterm matrices eqs. (5.15), (5.16) and (5.17). While the use of the alternative tadpole scheme ensures that the angular counterterms can be expressed in a gauge-independent way, at this stage they still contain a dependence on the gauge-fixing parameter. We therefore combine the virtues of the alternative tadpole scheme with the pinch technique [51–58]. The pinch technique allows us to extract the truly gauge-independent parts of the angular counterterms.

5.4.1 Gauge-independent pinch technique-based angular counterterm schemes

By the application of the pinch technique it is possible to define *pinched* self-energies $\overline{\Sigma}$ which are truly gauge independent. They are built up by the tadpole self-energies evaluated in the Feynman gauge and extra pinched components Σ^{add}, i.e.

$$\overline{\Sigma}(p^2) = \Sigma^{\text{tad}}(p^2)\Big|_{\xi_V=1} + \Sigma^{\text{add}}(p^2)\,, \tag{5.23}$$

where ξ_V stands for the gauge fixing parameters ξ_Z, ξ_W and ξ_γ of the R_ξ gauge. By Σ^{add} we dub the additional (explicitly ξ_V-independent) self-energy contributions obtained via the pinch technique. It is important to notice that, in order to apply the pinch technique, it is necessary to explicitly include all tadpole topologies, i.e. to use the alternative tadpole scheme. In appendix B we present the basic idea of the pinch technique (see also refs. [51–58] for a detailed exposition). We exemplarily show, for the CP-even sector, how to proceed in the derivation of the pinched self-energy. Additionally, we give useful formulae on the gauge dependences of the scalar self-energies and for the application of the pinch technique in the N2HDM.

On-shell tadpole-pinched scheme. The self-energy Σ^{add} in eq. (5.23) is explicitly independent of the gauge fixing parameter ξ_V. By replacing the wave function renormalization constants in the counterterms eqs. (5.20), (5.21) and (5.22) with their OS renormalization definitions given by the corresponding entries in the wave function counterterm matrices eqs. (5.15), (5.16) and (5.17) we arrive, upon expressing these in terms of the pinched self-energies, at the following expressions for the angular counterterms $\delta\alpha_i$,

$$\begin{aligned}
\delta_{\alpha_1} =& \frac{c_{\alpha_3}}{2c_{\alpha_2}} \frac{\text{Re}\left(\left[\Sigma^{\text{tad}}_{H_1H_2}(m^2_{H_2})+\Sigma^{\text{tad}}_{H_2H_1}(m^2_{H_1})\right]_{\xi_V=1}+\Sigma^{\text{add}}_{H_1H_2}(m^2_{H_2})+\Sigma^{\text{add}}_{H_2H_1}(m^2_{H_1})\right)}{m^2_{H_1}-m^2_{H_2}} \\
&- \frac{s_{\alpha_3}}{2c_{\alpha_2}} \frac{\text{Re}\left(\left[\Sigma^{\text{tad}}_{H_1H_3}(m^2_{H_3})+\Sigma^{\text{tad}}_{H_3H_1}(m^2_{H_1})\right]_{\xi_V=1}+\Sigma^{\text{add}}_{H_1H_3}(m^2_{H_3})+\Sigma^{\text{add}}_{H_3H_1}(m^2_{H_1})\right)}{m^2_{H_1}-m^2_{H_3}} \\
\delta_{\alpha_2} =& \frac{c_{\alpha_3}}{2} \frac{\text{Re}\left(\left[\Sigma^{\text{tad}}_{H_1H_3}(m^2_{H_3})+\Sigma^{\text{tad}}_{H_3H_1}(m^2_{H_1})\right]_{\xi_V=1}+\Sigma^{\text{add}}_{H_1H_3}(m^2_{H_3})+\Sigma^{\text{add}}_{H_3H_1}(m^2_{H_1})\right)}{m^2_{H_1}-m^2_{H_3}} \\
&+ \frac{s_{\alpha_3}}{2} \frac{\text{Re}\left(\left[\Sigma^{\text{tad}}_{H_1H_2}(m^2_{H_2})+\Sigma^{\text{tad}}_{H_2H_1}(m^2_{H_1})\right]_{\xi_V=1}+\Sigma^{\text{add}}_{H_1H_2}(m^2_{H_2})+\Sigma^{\text{add}}_{H_2H_1}(m^2_{H_1})\right)}{m^2_{H_1}-m^2_{H_2}} \\
\delta_{\alpha_3} =& \frac{1}{2} \frac{\text{Re}\left[\Sigma^{\text{tad}}_{H_2H_3}(m^2_{H_3})+\Sigma^{\text{tad}}_{H_3H_2}(m^2_{H_2})\right]_{\xi_V=1}+\Sigma^{\text{add}}_{H_2H_3}(m^2_{H_3})+\Sigma^{\text{add}}_{H_3H_2}(m^2_{H_2})}{m^2_{H_2}-m^2_{H_3}} \\
&+ \frac{s_{\alpha_2}}{2c_{\alpha_2}} \left\{ \frac{s_{\alpha_3}\,\text{Re}\left(\left[\Sigma^{\text{tad}}_{H_1H_3}(m^2_{H_3})+\Sigma^{\text{tad}}_{H_3H_1}(m^2_{H_1})\right]_{\xi_V=1}+\Sigma^{\text{add}}_{H_1H_3}(m^2_{H_3})+\Sigma^{\text{add}}_{H_3H_1}(m^2_{H_1})\right)}{m^2_{H_1}-m^2_{H_3}} \right. \\
&\left. - \frac{c_{\alpha_3}\,\text{Re}\left(\left[\Sigma^{\text{tad}}_{H_1H_2}(m^2_{H_2})+\Sigma^{\text{tad}}_{H_2H_1}(m^2_{H_1})\right]_{\xi_V=1}+\Sigma^{\text{add}}_{H_1H_2}(m^2_{H_2})+\Sigma^{\text{add}}_{H_2H_1}(m^2_{H_1})\right)}{m^2_{H_1}-m^2_{H_2}} \right\}.
\end{aligned} \tag{5.24}$$

JHEP12(2017)077

And for the two chosen renormalization prescriptions of $\delta\beta$ we get

$$\delta\beta^{(1)} = -\frac{\mathrm{Re}\left(\left[\Sigma^{\mathrm{tad}}_{G^\pm H^\pm}(0)+\Sigma^{\mathrm{tad}}_{G^\pm H^\pm}(m^2_{H^\pm})\right]_{\xi_V=1}+\Sigma^{\mathrm{add}}_{G^\pm H^\pm}(0)+\Sigma^{\mathrm{add}}_{G^\pm H^\pm}(m^2_{H^\pm})\right)}{2m^2_{H^\pm}} \tag{5.25}$$

$$\delta\beta^{(2)} = -\frac{\mathrm{Re}\left(\left[\Sigma^{\mathrm{tad}}_{G^0 A}(0)+\Sigma^{\mathrm{tad}}_{G^0 A}(m^2_A)\right]_{\xi_V=1}+\Sigma^{\mathrm{add}}_{G^0 A}(0)+\Sigma^{\mathrm{add}}_{G^0 A}(m^2_A)\right)}{2m^2_A}\,. \tag{5.26}$$

With this procedure we have now obtained angular counterterms that are explicitly gauge independent.

The additional contribution $\Sigma^{\mathrm{add}}_{Hh}$ has been given for the MSSM in [59], and the ones for the 2HDM in [36, 40, 60]. We have derived the contributions necessary in the N2HDM, given here for the first time ($i,j=1,2,3$),

$$\begin{aligned}\Sigma^{\mathrm{add}}_{H_iH_j}(p^2) = -\frac{g^2}{32\pi^2 c_W^2}\left(p^2-\frac{m^2_{H_i}+m^2_{H_j}}{2}\right)\Big\{&\mathcal{O}^{(1)}_{H_iH_j}B_0(p^2;m^2_Z,m^2_A)+\mathcal{O}^{(2)}_{H_iH_j}B_0(p^2;m^2_Z,m^2_Z)\\ &+2c_W^2\left[\mathcal{O}^{(1)}_{H_iH_j}B_0(p^2;m^2_W,m^2_{H^\pm})+\mathcal{O}^{(2)}_{H_iH_j}B_0(p^2;m^2_W,m^2_W)\right]\Big\}\end{aligned} \tag{5.27}$$

$$\Sigma^{\mathrm{add}}_{G^0A}(p^2) = \frac{-g^2}{32\pi^2 c_W^2}\left(p^2-\frac{m^2_A}{2}\right)\sum_{i=1}^{3}\mathcal{O}^{(3)}_{H_iH_i}B_0(p^2;m^2_Z,m^2_{H_i}) \tag{5.28}$$

$$\Sigma^{\mathrm{add}}_{G^\pm H^\pm}(p^2) = \frac{-g^2}{16\pi^2}\left(p^2-\frac{m^2_{H^\pm}}{2}\right)\sum_{i=1}^{3}\mathcal{O}^{(3)}_{H_iH_i}B_0(p^2;m^2_W,m^2_{H_i})\,, \tag{5.29}$$

where B_0 is the scalar two-point function [61, 62], while the shorthand notation $\mathcal{O}^{(x)}_{H_iH_j}$ ($x=1,\ldots,4$) stands for different coupling combinations in the Higgs-gauge sector,

$$\begin{aligned}\mathcal{O}^{(1)}_{H_iH_j} &= \tilde{\kappa}_{H_iVH}\times\tilde{\kappa}_{H_jVH}\\ \mathcal{O}^{(2)}_{H_iH_j} &= \kappa_{H_iVV}\times\kappa_{H_jVV}\\ \mathcal{O}^{(3)}_{H_iH_j} &= \kappa_{H_iVV}\times\tilde{\kappa}_{H_jVH}\\ \mathcal{O}^{(4)}_{H_iH_j} &= R_{i1}R_{j1}+R_{i2}R_{j2}\,.\end{aligned} \tag{5.30}$$

We note that in the N2HDM the following sum rules hold,

$$\begin{aligned}&\mathcal{O}^{(1)}_{H_iH_j}+\mathcal{O}^{(2)}_{H_iH_j}=\mathcal{O}^{(4)}_{H_iH_j}\,, && \sum_{i=1}^{3}\mathcal{O}^{(1)}_{H_iH_i}=\sum_{i=1}^{3}\mathcal{O}^{(2)}_{H_iH_i}=1\,,\\ &\sum_{i=1}^{3}\mathcal{O}^{(3)}_{H_iH_i}=0\,, && \sum_{i=1}^{3}\kappa_{H_iVV}\kappa_{H_iff}=1\,.\end{aligned} \tag{5.31}$$

Due to the third sum rule, the additional pinched contributions in eqs. (5.28), (5.29) are UV-finite in the N2HDM. In the 2HDM limit ($\alpha_{2,3}=0$), the combination $\mathcal{O}^{(4)}_{H_iH_j}$ becomes the Kronecker delta $\delta_{H_iH_j}$ and hence, for $i\neq j$, the additional pinched contributions in eq. (5.27) become UV-finite by themselves as well.

In the general N2HDM case instead, $\Sigma^{\mathrm{add}}_{H_1H_2}$, $\Sigma^{\mathrm{add}}_{H_2H_1}$, $\Sigma^{\mathrm{add}}_{H_1H_3}$, $\Sigma^{\mathrm{add}}_{H_3H_1}$, $\Sigma^{\mathrm{add}}_{H_2H_3}$, $\Sigma^{\mathrm{add}}_{H_3H_2}$ contain UV-divergent poles, which nevertheless cancel as they enter the mixing angle counterterms eq. (5.24) via the additive structure $\Sigma^{\mathrm{add}}_{H_iH_j}(m_i^2)+\Sigma^{\mathrm{add}}_{H_jH_i}(m_j^2)$, which is UV-finite.

JHEP12(2017)077

$p_\star$ tadpole-pinched scheme. Along the same lines followed for the 2HDM in ref. [36], we now generalise the $p_\star$ *tadpole-pinched scheme* to the N2HDM Higgs sector. Again, we replace the scalar self-energies within the mixing angle counterterms with the corresponding *pinched* self-energies, $\overline{\Sigma}$, (5.23), which we evaluate this time at the average of the particle momenta squared [63],

$$p^2_{\star,ij} = \frac{m^2_{\Phi_i} + m^2_{\Phi_j}}{2}\,, \tag{5.32}$$

where $(\Phi_i, \Phi_j) = (H_i, H_j)$, $(G^\pm, H^\pm)$ and (G^0, A), respectively. In this way the additional self-energies $\Sigma^{\rm add}$ vanish, and the pinched self-energies are given by the tadpole self-energies $\Sigma^{\rm tad}$ computed in the Feynman gauge, i.e.

$$\overline{\Sigma}(p^2_\star) = \Sigma^{\rm tad}(p^2_\star)\Big|_{\xi_V=1}\,. \tag{5.33}$$

The angular counterterms $\delta\alpha_i$ in eq. (5.20) then read

$$\begin{aligned}
\delta_{\alpha_1} &= \frac{c_{\alpha_3}\,\Sigma^{\rm tad}_{H_1H_2}(p^2_{\star,12})}{c_{\alpha_2}(m^2_{H_1} - m^2_{H_2})} - \frac{s_{\alpha_3}\,\Sigma^{\rm tad}_{H_1H_3}(p^2_{\star,13})}{c_{\alpha_2}(m^2_{H_1} - m^2_{H_3})} \\
\delta_{\alpha_2} &= \frac{c_{\alpha_3}{\rm Re}\,\Sigma^{\rm tad}_{H_1H_3}(p^2_{\star,13})}{m^2_{H_1} - m^2_{H_3}} + \frac{s_{\alpha_3}{\rm Re}\,\Sigma^{\rm tad}_{H_1H_2}(p^2_{\star,12})}{m^2_{H_1} - m^2_{H_2}} \\
\delta_{\alpha_3} &= \frac{{\rm Re}\,\Sigma^{\rm tad}_{H_2H_3}(p^2_{\star,23})}{m^2_{H_3} - m^2_{H_2}} + \frac{s_{\alpha_2}}{c_{\alpha_2}}\left\{\frac{s_{\alpha_3}\,{\rm Re}\,\Sigma^{\rm tad}_{H_1H_3}(p^2_{\star,13})}{m^2_{H_1} - m^2_{H_3}} - \frac{c_{\alpha_3}\,{\rm Re}\,\Sigma^{\rm tad}_{H_1H_2}(p^2_{\star,12})}{m^2_{H_1} - m^2_{H_2}}\right\},
\end{aligned} \tag{5.34}$$

with the different $p_\star$ scales being

$$p^2_{\star,12} = \frac{m^2_{H_1} + m^2_{H_2}}{2}\,, \qquad p^2_{\star,13} = \frac{m^2_{H_1} + m^2_{H_3}}{2}\,, \qquad p^2_{\star,23} = \frac{m^2_{H_2} + m^2_{H_3}}{2}\,. \tag{5.35}$$

For the counterterm $\delta\beta$ we get

$$\delta\beta^{(1)} = -\frac{{\rm Re}\left[\overline{\Sigma}_{G^\pm H^\pm}\left(\frac{m^2_{H^\pm}}{2}\right)\right]}{m^2_{H^\pm}} \tag{5.36}$$

or alternatively

$$\delta\beta^{(2)} = -\frac{{\rm Re}\left[\overline{\Sigma}_{G^0 A}\left(\frac{m^2_A}{2}\right)\right]}{m^2_A}\,. \tag{5.37}$$

5.5 Renormalization of m^2_{12}

The soft $\mathbb{Z}_2$ breaking parameter m^2_{12} enters the Higgs self-couplings. For the computation of higher-order corrections to Higgs-to-Higgs decays it therefore has to be renormalized as well. We may consider two different renormalization schemes.

JHEP12(2017)077

Modified minimal substraction scheme. One possibility is to use a modified $\overline{\text{MS}}$ scheme, cf. [37], where the counterterm δm_{12}^2 is chosen such that it cancels all residual terms of the amplitude that are proportional to

$$\Delta = \frac{1}{\epsilon} - \gamma_E + \ln(4\pi)\,, \tag{5.38}$$

where γ_E denotes the Euler-Mascheroni constant. These terms obviously contain the remaining UV divergences given as poles in ϵ together with additional finite constants that appear universally in all loop integrals. The renormalization of δm_{12}^2 in this scheme is thereby given by

$$\delta m_{12}^2 = \delta m_{12}^2(\Delta)|_{\overline{\text{MS}}}\,. \tag{5.39}$$

The right-hand side of the equation symbolically denotes all terms proportional to Δ that are necessary to cancel the Δ dependence of the remainder of the amplitude.

Process-dependent renormalization. Alternatively, one could resort to a process-dependent scheme, in which case the divergent parts of δm_{12}^2, along with additional finite remainders, are related to a physical on-shell Higgs-to-Higgs decay. While this method provides a physical definition for the counterterm, it relies on having at least one kinematically accessible on-shell Higgs-to-Higgs decay. For a generic Higgs-to-Higgs decay process $H_i \to H_j H_k$, where the final state pair $H_j H_k$ can also be a pair of pseudoscalars, if kinematically allowed, the counterterm δm_{12}^2 is then fixed by imposing as renormalization condition

$$\Gamma^{\text{LO}}(H_i \to H_j H_k) \stackrel{!}{=} \Gamma^{\text{NLO}}(H_i \to H_j H_k)\,. \tag{5.40}$$

Note that δm_{12}^2 is gauge independent in either of the proposed schemes, and also independently on how the tadpole topologies are treated. The key reason is that m_{12}^2 is indeed a genuine parameter of the original N2HDM Higgs potential before EWSB, and hence unlinked to the VEV, this being the source for the potential gauge-parameter dependences that arise at higher orders in certain schemes. In this paper we will apply the $\overline{\text{MS}}$ renormalization scheme.

6 One-loop EW corrected decay widths

Having elaborated in detail the renormalization scheme for the N2HDM, we compute the NLO EW corrections to a selected set of decay widths, in order to illustrate their impact. The chosen decays widths are

$$H_{2/3} \to ZZ \tag{6.1}$$

$$H_{2/3} \to AA \tag{6.2}$$

$$H_3 \to H_2 H_2 \quad \text{and} \quad H_2 \to H_1 H_1\,. \tag{6.3}$$

All processes require the renormalization of the mixing angles. The Higgs-to-Higgs decays demand in addition the renormalization of m_{12}^2. And the Higgs decays into CP-even pairs, eq. (6.3), additionally involve the renormalization of v_S. The chosen processes are structurally different and involve the various mixing angles in different more or less complicated

JHEP12(2017)077

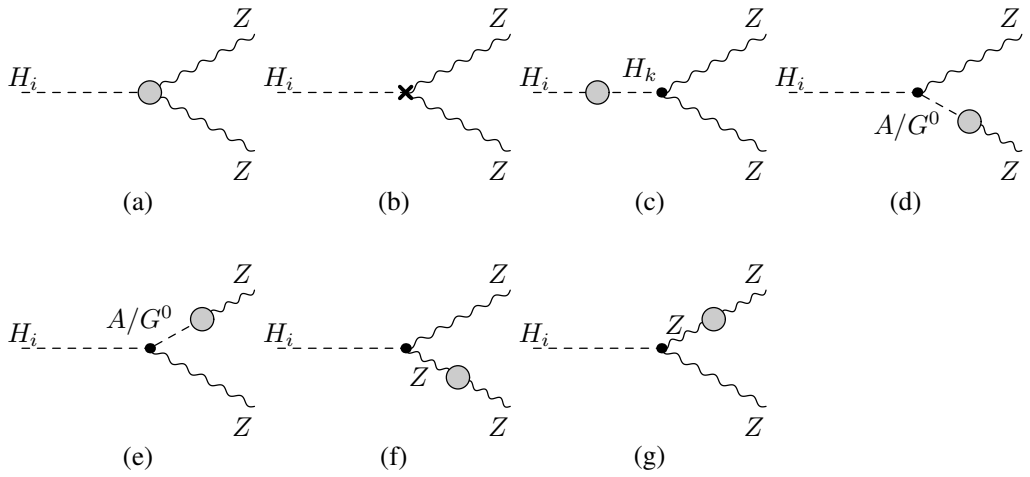

Figure 4. Generic diagrams contributing to the virtual corrections of the decay $H_i \to ZZ$: vertex corrections (a) and corrections to the external legs (c)-(g), where $k = 1, 2, 3$. Diagram (b) displays the vertex counterterm.

combinations, allowing us to study the impact of our renormalization scheme in different situations, and enabling us to study the renormalization of the Higgs potential parameter m_{12}^2 as well as of the singlet VEV v_S. Note finally that all these decays only involve electrically neutral particles, so that we do not encounter any IR divergences in the EW corrections.

6.1 The NLO EW corrected decay $H_i \to ZZ$

The LO decay width for the decay of a CP-even Higgs boson H_i into a pair of Z bosons,

$$H_i \to ZZ\,, \tag{6.4}$$

is given by

$$\Gamma^{\text{LO}}(H_i \to ZZ) = \frac{\alpha \kappa^2_{H_i VV}}{32 s_W^2 m_W^2 m_{H_i}} (m_{H_i}^4 - 4m_{H_i}^2 m_Z^2 + 12 m_Z^4) \sqrt{1 - \frac{4m_Z^2}{m_{H_i}^2}} \tag{6.5}$$

and depends on the mixing angles through the coupling factors

$$\begin{aligned}
\kappa_{H_1 VV} &= R_{11}\, c_\beta + R_{12}\, s_\beta = c_{\alpha_2} c_{\beta-\alpha_1} \\
\kappa_{H_2 VV} &= R_{21}\, c_\beta + R_{22}\, s_\beta = -c_{\beta-\alpha_1} s_{\alpha_2} s_{\alpha_3} + c_{\alpha_3} s_{\beta-\alpha_1} \\
\kappa_{H_3 VV} &= R_{31}\, c_\beta + R_{32}\, s_\beta = -c_{\alpha_3}\, c_{\beta-\alpha_1}\, s_{\alpha_2} - s_{\alpha_3}\, s_{\beta-\alpha_1}\,.
\end{aligned} \tag{6.6}$$

The generic diagrams describing the virtual corrections contributing to the NLO decay width together with the counterterm diagram introduced to cancel the UV divergences are displayed in figure 4. With the decay width involving only neutral particles there are neither IR divergences nor real corrections. The corrections to the external legs in figure 4 (c), (f) and (g) vanish due to the OS renormalization of H_i and Z, respectively, and the mixing contributions (d) and (e) are zero because of the Ward identity satisfied by the OS Z boson. The one-particle irreducible (1PI) diagrams contributing to the vertex corrections originate from the triangle diagrams with scalars, fermions, massive gauge bosons and ghost particles in the loops, depicted in the first three rows of figure 5, and from the diagrams involving four-particle vertices, as given by the last four diagrams of figure 5.

JHEP12(2017)077

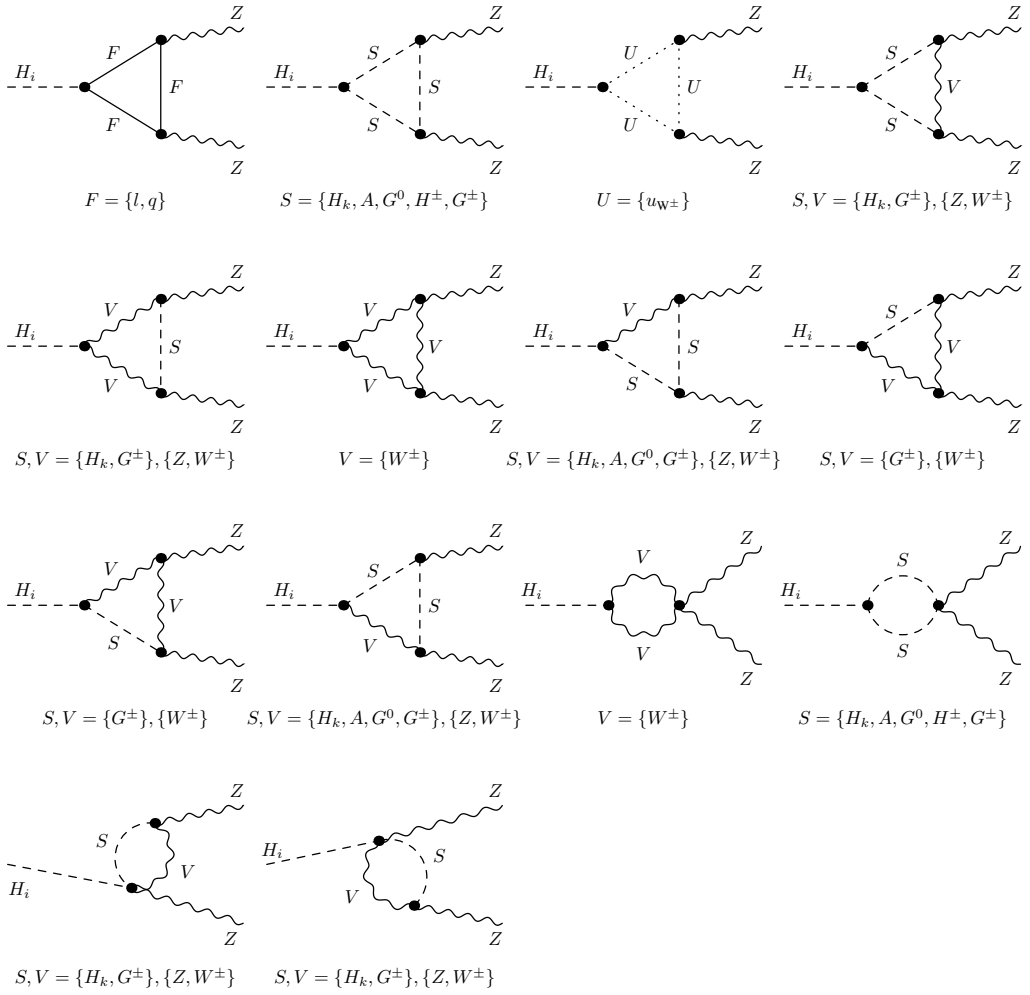

Figure 5. Generic diagrams contributing to the vertex corrections in $H_i \to ZZ$ with fermions F, scalar bosons S, gauge bosons V and ghost particles U in the loops.

To work out the vertex counterterms, the relations

$$s_\varphi \to s_\varphi + c_\varphi\, \delta\varphi \qquad \text{and} \qquad c_\varphi \to c_\varphi - s_\varphi\, \delta\varphi \tag{6.7}$$

are helpful for the derivation of the entries in the rotation matrix counterterm δR obtained from eq. (2.20),

$$\begin{aligned}
\delta R_{11} &= -c_{\alpha_1} s_{\alpha_2}\delta_{\alpha_2} - s_{\alpha_1} c_{\alpha_2}\delta_{\alpha_1} \\
\delta R_{12} &= -s_{\alpha_1} s_{\alpha_2}\delta_{\alpha_2} + c_{\alpha_2} c_{\alpha_1}\delta_{\alpha_1} \\
\delta R_{13} &= c_{\alpha_2}\delta_{\alpha_2} \\
\delta R_{21} &= -c_{\alpha_1} c_{\alpha_3}\delta_{\alpha_1} + s_{\alpha_1} s_{\alpha_3}\delta_{\alpha_3} - c_{\alpha_1}(s_{\alpha_2} c_{\alpha_3}\delta_{\alpha_3} + s_{\alpha_3} c_{\alpha_2}\delta_{\alpha_2}) + s_{\alpha_2} s_{\alpha_3} s_{\alpha_1}\delta_{\alpha_1} \\
\delta R_{22} &= -c_{\alpha_1} s_{\alpha_3}\delta_{\alpha_3} - s_{\alpha_1} c_{\alpha_3}\delta_{\alpha_1} - s_{\alpha_1}(s_{\alpha_2} c_{\alpha_3}\delta_{\alpha_3} + s_{\alpha_3} c_{\alpha_2}\delta_{\alpha_2}) - c_{\alpha_1} s_{\alpha_2} s_{\alpha_3}\delta_{\alpha_1} \\
\delta R_{23} &= -s_{\alpha_2} s_{\alpha_3}\delta_{\alpha_2} + c_{\alpha_2} c_{\alpha_3}\delta_{\alpha_3} \\
\delta R_{31} &= s_{\alpha_1} c_{\alpha_3}\delta_{\alpha_3} + c_{\alpha_1} s_{\alpha_3}\delta_{\alpha_1} - c_{\alpha_1}(c_{\alpha_2} c_{\alpha_3}\delta_{\alpha_2} - s_{\alpha_2} s_{\alpha_3}\delta_{\alpha_3}) + s_{\alpha_1} s_{\alpha_2} c_{\alpha_3}\delta_{\alpha_1} \\
\delta R_{32} &= s_{\alpha_1} s_{\alpha_3}\delta_{\alpha_1} - c_{\alpha_1} c_{\alpha_3}\delta_{\alpha_3} + s_{\alpha_1} s_{\alpha_2} s_{\alpha_3}\delta_{\alpha_3} - c_{\alpha_3}(s_{\alpha_1} c_{\alpha_2}\delta_{\alpha_2} + c_{\alpha_1} s_{\alpha_2}\delta_{\alpha_1}) \\
\delta R_{33} &= -s_{\alpha_2} c_{\alpha_3}\delta_{\alpha_2} - c_{\alpha_2} s_{\alpha_3}\delta_{\alpha_3}\,.
\end{aligned} \tag{6.8}$$

JHEP12(2017)077

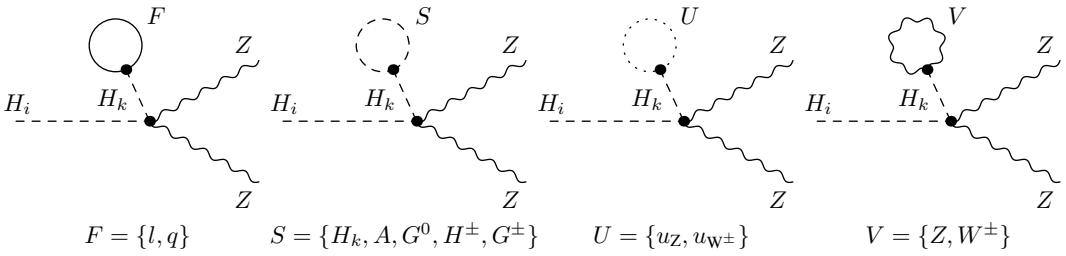

Figure 6. Tadpole contributions to the vertex diagrams to be included in the decay $H_i \to ZZ$ in the alternative tadpole scheme.

The H_iZZ vertex counterterm in terms of the different parameter counterterms and wave function renormalization constants is obtained from the corresponding counterterm Lagrangian

$$\mathcal{L}^{\rm ct}_{H_iZZ} = \left(\frac{g m_Z^2 \kappa_{H_i ff}}{m_W} \left[\frac{\delta m_Z^2}{m_Z^2} - \left(\frac{\delta m_W^2}{2m_W^2} - \frac{\delta g}{g} \right) + \delta Z_{ZZ} + \frac{1}{2} \delta Z_{H_iH_i} + \frac{1}{2} \sum_{j \neq i} \frac{\kappa_{H_jVV}}{\kappa_{H_iVV}} \delta Z_{H_jH_i} \right] \right.$$
$$\left. + \frac{g m_Z^2}{m_W} \left[\delta R_{i1}\, c_\beta + \delta R_{i2}\, s_\beta - (R_{i1}\, s_\beta - R_{i2}\, c_\beta) \delta\beta \right] \right) g^{\mu\nu} H_i Z_\mu Z_\nu \,, \tag{6.9}$$

with the various counterterms given in section 3 and the δR_{ij} defined in eq. (6.8). Since we apply the alternative tadpole scheme, tadpole contributions to the H_iZZ vertex have to be taken into account explicitly in the computation of the decay width. They are shown in figure 6. The formulae for the vertex corrections and counterterms in terms of the scalar one-, two- and three-point functions are quite lengthy so that we do not display them explicitly here.

6.2 The decay $H_i \to AA$ at NLO EW

The LO decay width of the CP-even H_i decay into a pair of CP-odd scalars,

$$H_i \to AA \,, \tag{6.10}$$

reads

$$\Gamma^{\rm LO}(H_i \to AA) = \frac{\alpha \left| \lambda_{H_iAA} \right|^2}{8 s_W^2 \; m_{H_i}} \sqrt{1 - \frac{4m_A^2}{m_{H_i}^2}} \,. \tag{6.11}$$

It is governed by the trilinear coupling

$$g_{H_iAA} = -i \cdot \lambda_{H_iAA} = g \frac{1}{2m_W} \left\{ - M^2 \left[\frac{R_{i1}}{c_\beta} + \frac{R_{i2}}{s_\beta} \right] + m_{H_i}^2 \left[\frac{R_{i1} s_\beta^2}{c_\beta} + \frac{R_{i2}\, c_\beta^2}{s_\beta} \right] \right.$$
$$\left. + 2\, m_A^2 \left[R_{i1} c_\beta + R_{i2} s_\beta \right] \right\} , \tag{6.12}$$

where $M^2 \equiv m_{12}^2/(s_\beta c_\beta)$.

JHEP12(2017)077

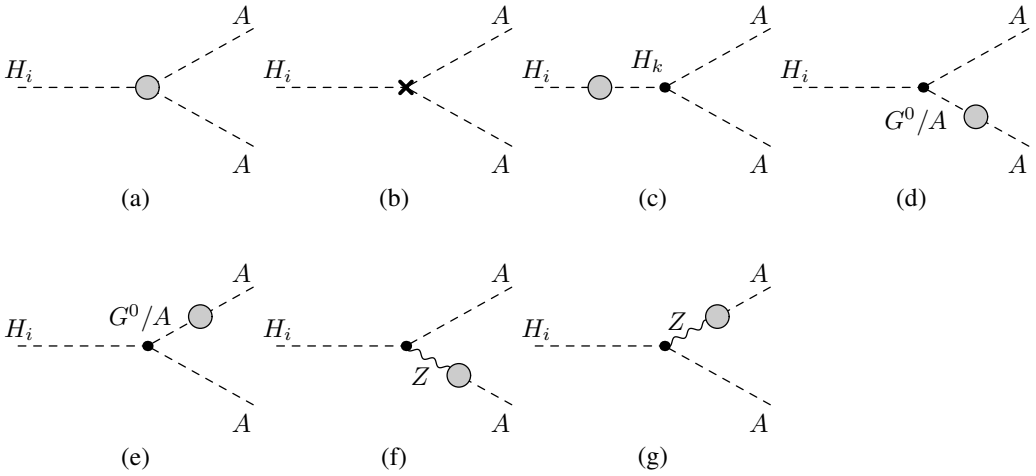

Figure 7. Generic diagrams contributing to the virtual corrections of the decay $H_i \to AA$: vertex corrections (a) and corrections to the external legs (c)-(g). Diagram (b) displays the corresponding vertex counterterm.

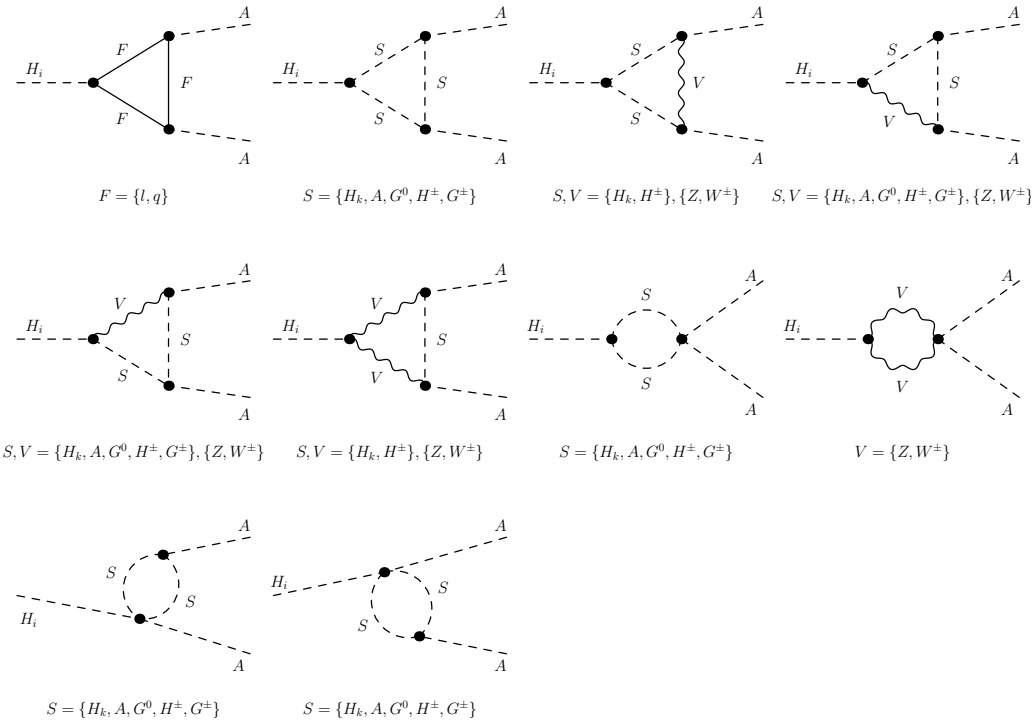

Figure 8. Generic diagrams contributing to the vertex corrections in $H_i \to AA$.

The EW one-loop corrections consist of the virtual corrections and the counterterm contributions ensuring the UV-finiteness of the decay amplitude. Again we do not have to deal with IR divergences nor real corrections. The virtual corrections, consisting of the corrections to the external legs and the pure vertex corrections, are shown in figure 7. The corrections to the external legs in figure 7 (c), (d) and (e) are zero because of the OS renormalization of the external fields, while diagrams (f) and (g) vanish due to a Slavnov-Taylor identity [64]. The 1PI diagrams of the vertex corrections are depicted in figure 8.

JHEP12(2017)077

They are given by the triangle diagrams with fermions, scalars and gauge bosons in the loops and by the diagrams containing four-particle vertices. The counterterm contributions consist of the genuine vertex counterterm $\delta g^{\text{vertex}}_{H_iAA}$ and the counterterm insertions on the external legs $\delta g^{\text{field}}_{H_iAA}$,

$$\delta g_{H_iAA} = \delta\, g^{\text{field}}_{H_iAA} + \delta\, g^{\text{vertex}}_{H_iAA}\,, \tag{6.13}$$

with

$$\delta\, g^{\text{field}}_{H_iAA} = g_{H_iAA}\left[\delta Z_{AA} + \frac{1}{2}\,\delta Z_{H_iH_i} + \frac{1}{2}\sum_{i\neq j}\frac{g_{H_jAA}}{g_{H_iAA}}\,\delta Z_{H_jH_i} + \frac{g_{H_iAG}}{g_{H_iAA}}\,\delta Z_{G^0A}\right] \tag{6.14}$$

and

$$\begin{aligned}
\delta\, g^{\text{vertex}}_{H_iAA} = &-g_{H_iAA}\left(\frac{\delta m_W^2}{2m_W^2} - \frac{\delta g}{g}\right) + \frac{g}{2m_W}\left\{\left(R_{i1}\frac{s_\beta^2}{c_\beta} + R_{i2}\frac{c_\beta^2}{s_\beta}\right)\delta m_{H_i}^2 - \left(\frac{R_{i1}}{c_\beta} + \frac{R_{i2}}{s_\beta}\right)\delta M^2\right.\\
&+2\left[R_{i1}c_\beta + R_{i2}s_\beta\right]\delta m_A^2 - M^2\left(\frac{\delta R_{i1}}{c_\beta} + \frac{\delta R_{i2}}{s_\beta}\right) + m_{H_i}^2\left(\frac{s_\beta^2}{c_\beta}\,\delta R_{i1} + \frac{c_\beta^2}{s_\beta}\,\delta R_{i2}\right)\\
&+2m_A^2\left[c_\beta\delta R_{i1} + s_\beta\delta R_{i2}\right] + M^2\left(R_{i1}\frac{\delta c_\beta}{c_\beta^2} + R_{i2}\frac{\delta s_\beta}{s_\beta^2}\right) + 2m_A^2\left[R_{i1}\delta c_\beta + R_{i2}\,\delta s_\beta\right]\\
&\left.+m_{H_i}^2\left[R_{i1}\,\frac{s_\beta^2}{c_\beta}\left(2\frac{\delta s_\beta}{s_\beta} - \frac{\delta c_\beta}{c_\beta}\right) + R_{i2}\,\frac{c_\beta^2}{s_\beta}\left(2\frac{\delta c_\beta}{c_\beta} - \frac{\delta s_\beta}{s_\beta}\right)\right]\right\},
\end{aligned} \tag{6.15}$$

with the δR_{ij} given in eq. (6.8). Working in the alternative tadpole scheme, we additionally have to take into account the vertices dressed with the tadpoles, displayed in figure 9.

The one-loop correction to the decay is obtained from the interference of the loop-corrected decay amplitude $\mathcal{M}^{\text{1loop}}_{H_iAA}$ with the LO amplitude $\mathcal{M}^{\text{LO}}_{H_iAA}$. The one-loop amplitude combines the virtual viz. vertex corrections $\mathcal{M}^{\text{virt}}_{H_iAA}$ and the counterterm amplitude $\mathcal{M}^{\text{ct}}_{H_iAA} = \delta g_{H_iAA} + \mathcal{M}^{\text{tad}}_{H_iAA}$, with $\mathcal{M}^{\text{tad}}_{H_iAA}$ denoting the vertices with the tadpoles,

$$\mathcal{M}^{\text{1loop}}_{H_iAA} = \mathcal{M}^{\text{virt}}_{H_iAA} + \mathcal{M}^{\text{ct}}_{H_iAA}\,. \tag{6.16}$$

The NLO corrections factorize from the LO amplitude so that the loop-corrected partial width can be cast into the form

$$\begin{aligned}
\Gamma^{\text{NLO}} &= \Gamma^{\text{LO}} + \frac{m_{H_i}}{32\pi}\sqrt{1 - \frac{4m_A^2}{m_{H_i}^2}}\,2\,\text{Re}\left[(\mathcal{M}^{\text{LO}}_{H_iAA})^*\mathcal{M}^{\text{1loop}}_{H_iAA}\right]\\
&= \Gamma^{\text{LO}}\left[1 + \Delta^{\text{virt}}_{H_iAA} + \Delta^{\text{ct}}_{H_iAA}\right],
\end{aligned} \tag{6.17}$$

with

$$\Delta^{\text{virt/ct}}_{H_iAA} \equiv \frac{2\mathcal{M}^{\text{virt/ct}}_{H_iAA}}{g_{H_iAA}} = \frac{2\mathcal{M}^{\text{virt/ct}}_{H_iAA}}{-i\cdot\lambda_{H_iAA}}\,. \tag{6.18}$$

Again we refrain from giving the explicit expressions for the various contributions to Γ^{NLO} as they are quite lengthy.

JHEP12(2017)077

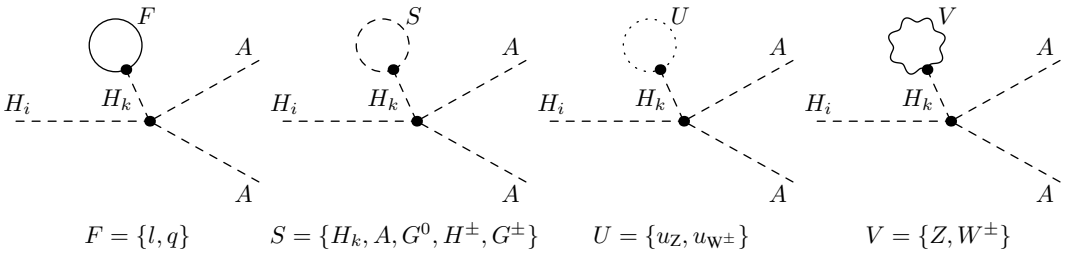

Figure 9. Tadpole contributions to the vertex diagrams to be included in the decay $H_i \to AA$ in the alternative tadpole scheme.

6.3 Electroweak one-loop corrections to $H_j \to H_i H_i$

The LO decay width for the decay of a neutral CP-even Higgs boson into two identical CP-even scalars is given by $(i, j = 1, 2, 3)$

$$\Gamma^{\rm LO}(H_j \to H_i H_i) = \frac{\alpha \left|\lambda_{H_i H_i H_j}\right|^2}{8\, s_W^2\, m_{H_j}} \sqrt{1 - \frac{4m_{H_i}^2}{m_{H_j}^2}}\,, \tag{6.19}$$

with the trilinear Higgs coupling

$$\begin{aligned} g_{H_i H_i H_j} = -i \cdot \lambda_{H_i H_i H_j} = \frac{g}{2m_W} \Bigg\{ -\frac{1}{2} M^2 \Bigg[\left(\frac{R_{i2}}{s_\beta} - \frac{R_{i1}}{c_\beta} \right) \left(6 R_{i2} R_{j2}\, c_\beta^2 - 6 R_{i1} R_{j1}\, s_\beta^2 \right. \\ \left. + \sum_k \epsilon_{ijk}\, R_{k3}\, s_{2\beta} \right) \Bigg] + \frac{2m_{H_i}^2 + m_{H_j}^2}{v_S} \left[R_{i3}^2\, R_{j3}\, v + R_{i2}^2\, R_{j2}\, \frac{v_S}{s_\beta} + R_{i1}^2\, R_{j1}\, \frac{v_S}{c_\beta} \right] \Bigg\}, \end{aligned} \tag{6.20}$$

where ϵ_{ijk} denotes the totally antisymmetric tensor in three dimensions with $\epsilon_{123} = 1$. At variance with the processes discussed so far, Higgs-to-Higgs decays in the CP-even sector are directly sensitive to the singlet VEV v_S at tree level. As discussed in section 4.1, this explicit dependence must be handled with care when the NLO calculations are performed in the alternative tadpole scheme. Here, a non-vanishing UV-divergent singlet VEV shift Δv_S cancels a subset of the UV poles in the NLO Higgs-to-Higgs decay amplitude which genuinely arise in this scheme. To fix Δv_S we proceed along the same lines as for the doublet VEV. First, we identify the singlet VEV input value in this scheme with the (would-be) experimental input, to be extracted eventually through the measurement of an observable Higgs-to-Higgs decay width $\Gamma_{H_i \to H_j H_j}$. When promoted to higher orders, the tree-level relation $v_S^{\rm tree} = f(\Gamma^{\rm tree}_{H_i \to H_j H_j})$ becomes

$$\begin{aligned} v_S^{\rm ren}|_{\rm FJ} = v_S^{\rm tree} = f(\Gamma^{\rm tree}_{H_i \to H_j H_j}) &= f(\Gamma^{\rm ren}_{H_i \to H_j H_j} + \Gamma^{\rm ct}_{H_i \to H_j H_j}) \\ &= \underbrace{\tilde{f}(\Gamma^{\rm ren}_{H_i \to H_j H_j})}_{v_S^{\rm exp.}} + \underbrace{\delta \tilde{f}(\Gamma^{\rm ct}_{H_i \to H_j H_j})}_{\Delta v_S}, \end{aligned} \tag{6.21}$$

in such a way that the (would-be) experimental value $v_S^{\rm exp}$ is properly written in terms of the renormalized (physical) width from which it would be extracted. Notice that the quantity

JHEP12(2017)077

Δv_S is simply a shorthand for the combination of counterterm contributions contained in $\Gamma^{\rm ct}_{H_i\to H_jH_j}$ — the same role that Δv plays in eq. (4.2) for the doublet VEV case. For our sample processes $H_3 \to H_2H_2$ and $H_2 \to H_1H_1$ discussed in the numerical analysis we assume the v_S input values to be extracted from the decay $H_3 \to H_1H_1$.[10] The choice of this process is of course not unique. Therefore, given that the finite parts included in Δv_S are to some degree arbitrary, we could formally resort to $\overline{\rm MS}$-like conditions to fix Δv_S by retaining only the UV-divergent parts contained in $\Gamma^{\rm ct}_{H_i\to H_jH_j}$. In this case the v_S input values could not be extracted directly from the experimental data. The relation to the to be measured $v_S^{\rm exp}$ would be given by a scheme-dependent finite shift. In the process-dependent framework Δv_S can be fixed through the requirement

$$\Gamma^{\rm NLO}_{H_3\to H_1H_1} \stackrel{!}{=} \Gamma^{\rm LO}_{H_3\to H_1H_1}\,. \tag{6.22}$$

Factorising the NLO decay width as

$$\Gamma^{\rm NLO}_{H_3\to H_1H_1} = \Gamma^{\rm LO}_{H_3\to H_1H_1}\Big[1+\Delta^{\rm virt}+\Delta^{\rm ct}(\Delta v_S=0)+\Delta^{\rm ct}(\Delta v_S)\Big] \stackrel{!}{=} \Gamma^{\rm LO}_{H_3\to H_1H_1} \tag{6.23}$$

and isolating the v_S-dependent part of the corresponding self-interaction Lagrangian,

$$\begin{aligned}\mathcal{L}_{H_1H_1H_3} &\supset \frac{1}{v_S}\,(2m^2_{H_1}+m^2_{H_3})\,R^2_{13}\,R_{33}\,, \quad \text{whereby}\\ \delta\mathcal{L}_{H_1H_1H_3} &\supset -\frac{1}{v_S}\,(2m^2_{H_1}+m^2_{H_3})\,R^2_{13}\,R_{33}\,\frac{\Delta\, v_S}{v_S}\,,\end{aligned} \tag{6.24}$$

the condition eq. (6.23) leads to

$$\frac{\Delta v_S}{v_S} = \frac{g_{H_iH_iH_j}\,v_S}{2}\Big[(2m^2_{H_1}+m^2_{H_3})R^2_{13}\,R_{33}\Big]^{-1}\,\Big[\Delta^{\rm virt}+\Delta^{\rm CT}(\Delta v_S=0)\Big]\,. \tag{6.25}$$

The diagrams contributing to the virtual corrections of our process $H_j \to H_iH_i$ are shown in figure 10. The 1PI diagrams contributing to the vertex corrections are depicted in figure 11 and the tadpole diagrams are shown in figure 12. They have to be included in the alternative tadpole scheme. The counterterm is given by the genuine vertex counterterm and the counterterm insertions on the external legs,

$$\delta g_{H_iH_jH_k} = \delta\, g^{\rm field}_{H_iH_jH_k} + \delta\, g^{\rm vertex}_{H_iH_jH_k}\,, \tag{6.26}$$

with

$$\begin{aligned}\delta\, g^{\rm field}_{H_iH_jH_k} = g_{H_iH_jH_k}\Bigg[&\frac{1}{2}\sum_{l=1}^{3}\frac{g_{H_lH_jH_k}}{g_{H_iH_jH_k}}\,\delta Z_{H_lH_i} + \frac{1}{2}\sum_{l=1}^{3}\frac{g_{H_lH_iH_k}}{g_{H_iH_jH_k}}\,\delta Z_{H_lH_j}\\ &+\frac{1}{2}\sum_{l=1}^{3}\frac{g_{H_lH_iH_j}}{g_{H_iH_jH_k}}\,\delta Z_{H_lH_k}\Bigg]\,,\end{aligned} \tag{6.27}$$

[10] The choice of the process relies on the experimental feasibility of measuring it and on its dependence on v_S itself. For some scenarios the parameter configurations can be such that the decay is not measurable or the dependence on Δv_S is almost vanishing, cf. also the discussion in [65] on the renormalization of the NMSSM where similar issues arise.

JHEP12(2017)077

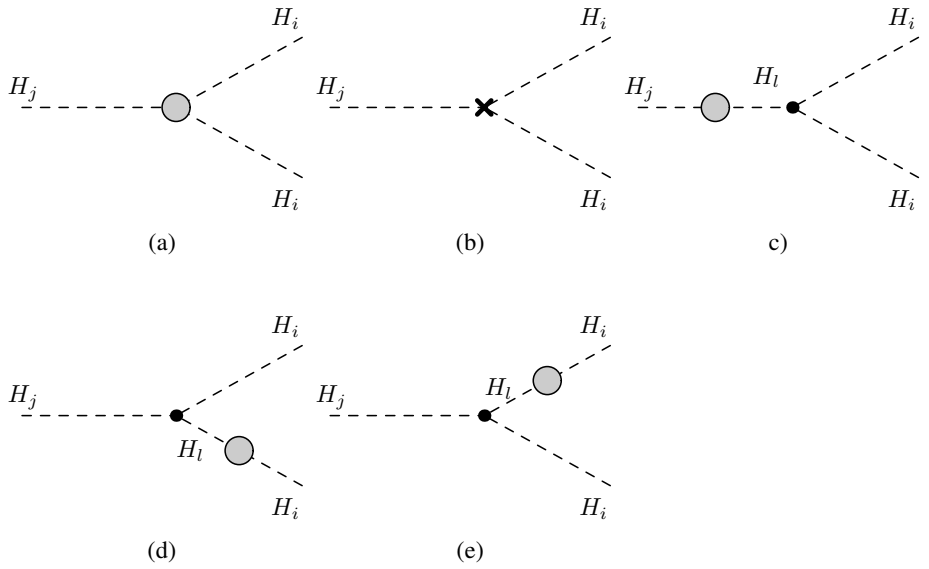

Figure 10. Generic diagrams contributing to the virtual corrections of the decay $H_j \to H_i H_i$: vertex corrections (a) and corrections to the external legs (c)-(e). Diagram (b) displays the corresponding vertex counterterm.

and

$$
\begin{aligned}
\delta g^{\text{vertex}}_{H_i H_j H_k} = & -g_{H_i H_i H_j}\left(\frac{\delta m_W^2}{2m_W^2}-\frac{\delta g}{g}\right)+\frac{1}{v}\left\{-\frac{1}{2}\,\delta M^2\left[\left(\frac{R_{i2}}{s_\beta}-\frac{R_{i1}}{c_\beta}\right)\times\right.\right.\\
&\left.\times\left(6R_{i2}R_{j2}\,c_\beta^2-6R_{i1}R_{j1}\,s_\beta^2+\sum_k \epsilon_{ijk}\,R_{k3}\,s_{2\beta}\right)\right]\\
&-\frac{1}{2}\,M^2\left[\left(\frac{\delta R_{i2}}{s_\beta}-\frac{\delta R_{i1}}{c_\beta}\right)\left(6R_{i2}R_{j2}\,c_\beta^2-6R_{i1}R_{j1}\,s_\beta^2+\sum_k \epsilon_{ijk}\,R_{k3}\,s_{2\beta}\right)\right]\\
&-\frac{1}{2}\,M^2\left[\left(\frac{R_{i1}\,\delta c_\beta}{c_\beta^2}-\frac{R_{i2}\,\delta s_\beta}{s_\beta^2}\right)\left(6R_{i2}R_{j2}\,c_\beta^2-6R_{i1}R_{j1}\,s_\beta^2+\sum_k \epsilon_{ijk}\,R_{k3}\,s_{2\beta}\right)\right]\\
&-\frac{1}{2}\,M^2\left(\frac{R_{i2}}{s_\beta}-\frac{R_{i1}}{c_\beta}\right)\left[6R_{j2}c_\beta^2\delta R_{i2}+6R_{i2}c_\beta^2\delta R_{j2}+12R_{i2}R_{j2}c_\beta\delta c_\beta-6R_{i1}s_\beta^2\delta R_{j1}\right.\\
&\left.-6R_{i1}s_\beta^2\delta R_{j1}-12R_{i1}R_{j1}s_\beta\delta s_\beta+\sum_k \epsilon_{ijk}\left(s_\beta\,\delta R_{k3}+2R_{k3}\left(c_\beta\delta s_\beta+s_\beta\delta c_\beta\right)\right)\right]\\
&+\frac{2\delta m_{H_i}^2+\delta m_{H_j}^2}{v_S}\left[R_{i3}^2\,R_{j3}\,v+R_{i2}^2\,R_{j2}\,\frac{v_S}{s_\beta}+R_{i1}^2\,R_{j1}\,\frac{v_S}{c_\beta}\right]\\
&-\frac{v}{v_S}\left(2m_{H_i}^2+m_{H_j}^2\right)R_{i3}^2\,R_{j3}\,\frac{\Delta\,v_S}{v_S}+\frac{2m_{H_i}^2+m_{H_j}^2}{v_S}\left[2R_{i3}\,R_{j3}\,v\,\delta R_{i3}+R_{i3}^2\,v\,\delta R_{j3}\right.\\
&+R_{i3}^2\,R_{j3}\,\delta v+2R_{i2}\,R_{j2}\,\frac{v_S}{s_\beta}\delta R_{i2}+R_{i2}^2\,\frac{v_S}{s_\beta}\delta R_{j2}-R_{i2}^2\,R_{j2}\,\frac{v_S}{s_\beta^2}\delta s_\beta+2R_{i1}\,R_{j1}\,\frac{v_S}{c_\beta}\delta R_{i1}\\
&\left.\left.+R_{i1}^2\,\frac{v_S}{c_\beta}\delta R_{j1}-R_{i1}^2\,R_{j1}\,\frac{v_S}{c_\beta^2}\,\delta c_\beta\right]\right\}. \qquad (6.28)
\end{aligned}
$$

JHEP12(2017)077

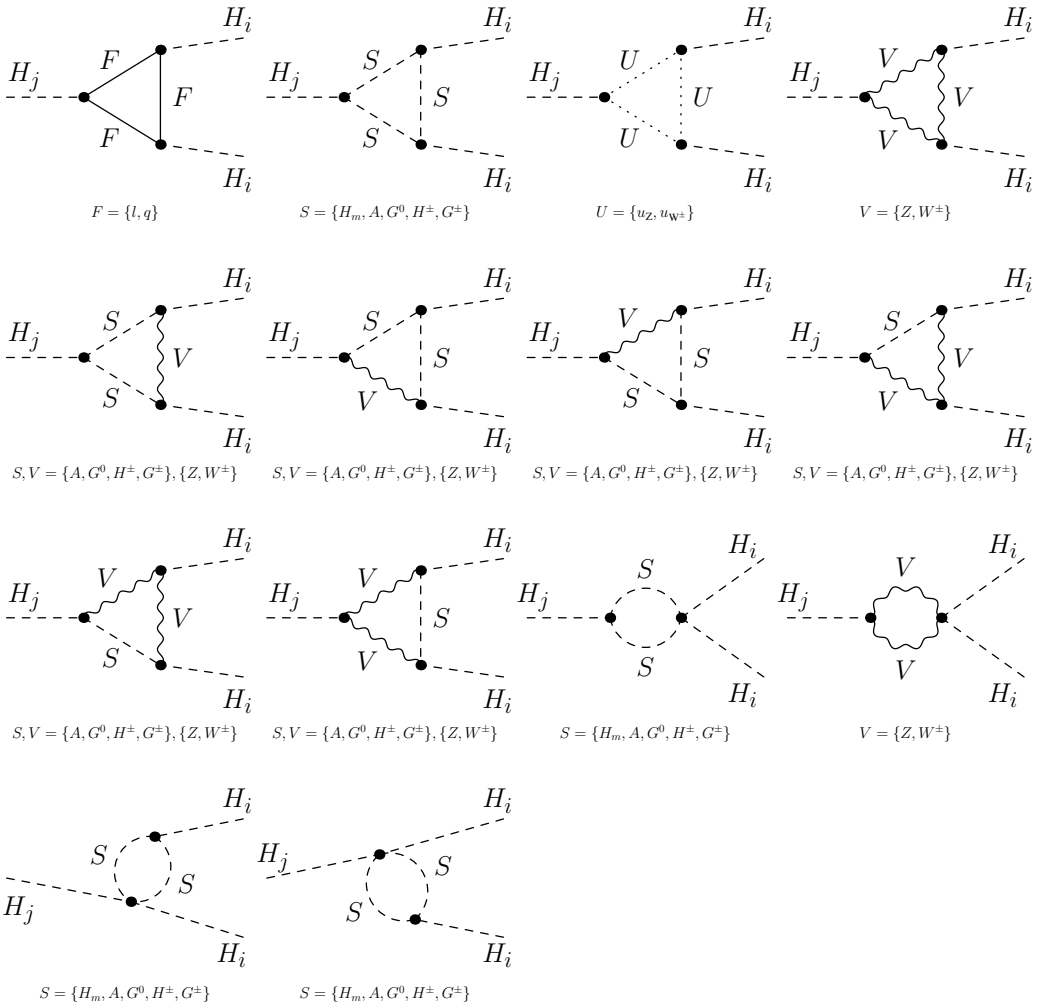

Figure 11. Generic diagrams contributing to the vertex corrections in $H_j \to H_i H_i$.

The NLO corrections factorize so that the loop-corrected decay width can be cast into the form

$$\Gamma^{\rm NLO} = \Gamma^{\rm LO}\left[1 + \Delta^{\rm virt}_{H_iH_jH_k} + \Delta^{\rm ct}_{H_iH_jH_k}\right], \tag{6.29}$$

with

$$\Delta^{\rm virt/ct}_{H_iH_jH_k} \equiv \frac{2\mathcal{M}^{\rm virt/ct}_{H_iH_jH_k}}{g_{H_iH_jH_k}} = \frac{2\mathcal{M}^{\rm virt/ct}_{H_iH_jH_k}}{-i\cdot\lambda_{H_iH_jH_k}} \tag{6.30}$$

in terms of the virtual corrections and counterterm amplitude $\mathcal{M}^{\rm virt}_{H_iH_jH_k}$ and $\mathcal{M}^{\rm ct}_{H_iH_jH_k}$, respectively, where we have included the vertices with the tadpoles in $\mathcal{M}^{\rm ct}_{H_iH_jH_k}$. Due to rather lengthy expressions we refrain from giving the explicit expressions of the various contributions to $\Gamma^{\rm NLO}$.

JHEP12(2017)077

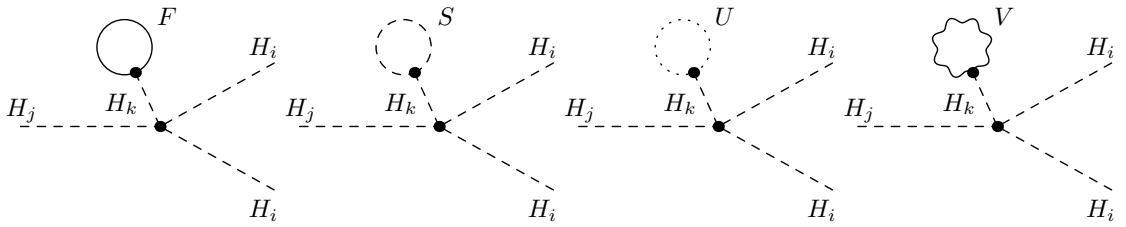

Figure 12. Tadpole contributions to the vertex diagrams to be included in the decay $H_j \to H_i H_i$ in the alternative tadpole scheme.

7 Numerical analysis

For the computation of the NLO EW corrections to the Higgs decays presented in the following the tree-level and one-loop decay amplitudes have been generated with `FeynArts` [66, 67]. The necessary N2HDM Feynman rules have been obtained as UFO [68] and FeynArts [67] model files using FeynRules [69], while all renormalization counterterms have been derived analytically and implemented by hand. The amplitudes have been analytically processed via `FormCalc` [70]. The dimensionally regularized loop form factors have been evaluated in the 't Hooft-Veltman scheme [71, 72] and written in terms of standard loop integrals. These have been further reduced through Passarino-Veltman decomposition and evaluated with the help of `LoopTools` [70].

In the following we give the input parameters for the numerical evaluation. As explained in section 5 we use the fine structure constant α at the Z boson mass scale, given by [73]

$$\alpha(m_Z^2) = \frac{1}{128.962}\,. \tag{7.1}$$

The massive gauge bosons are renormalized OS, and their input masses are chosen as [73, 74]

$$m_W = 80.385\,\text{GeV} \qquad \text{and} \qquad m_Z = 91.1876\ \text{GeV}\,. \tag{7.2}$$

For the lepton masses we take [73, 74]

$$m_e = 0.510998928\,\text{MeV}\,, \quad m_\mu = 105.6583715\,\text{MeV}\,, \quad m_\tau = 1.77682\,\text{GeV}\,. \tag{7.3}$$

These and the light quark masses, which we set [75]

$$m_u = 100\,\text{MeV}\,, \quad m_d = 100\,\text{MeV}\,, \quad m_s = 100\,\text{MeV}\,, \tag{7.4}$$

have only a small impact on our results. Following the recommendation of the LHC Higgs Cross Section Working Group (HXSWG) [74, 76], we use the following OS value for the top quark mass

$$m_t = 172.5\,\text{GeV}\,, \tag{7.5}$$

which is consistent with the ATLAS and CMS analyses. The charm and bottom quark OS masses are set to

$$m_c = 1.51\,\text{GeV} \qquad \text{and} \qquad m_b = 4.92\,\text{GeV}\,, \tag{7.6}$$

JHEP12(2017)077

as recommended by [74]. We consider the CKM matrix to be unity. This approximation has negligible impact on our results. The SM-like Higgs mass value, denoted by m_h, has been set to [27]

$$m_h = 125.09\,\text{GeV}\,. \tag{7.7}$$

Note that, depending on the parameter set, in the N2HDM any of the three neutral CP-even Higgs bosons can be the SM-like Higgs boson.

In the subsequently presented analysis we only used N2HDM parameter sets compatible experimental and theoretical constraints. These data sets have been generated with the tool `ScannerS` [30, 31].[11] The applied theoretical constraints require that the vacuum state found by `ScannerS` is the global minimum, that the N2HDM potential is bounded from below and that tree-level unitarity holds. On the experimental side, compatibility with the EW precision constraints is guaranteed by requiring the oblique parameters S, T and U to be compatible with the SM fit [77] at 2σ, including the full correlations. The constraints from B physics observables [78–82] and the measurement of R_b [79, 83] have been taken into account, as well as the most recent bound of $m_{H^\pm} \gtrsim 580\,\text{GeV}$ for the type II and flipped (N)2HDM [82]. For the compatibility with the LHC Higgs data we require one of the scalar states, denoted by h_{125}, to have a mass of 125.09 GeV and to match the observed LHC signal rates. Furthermore, the remaining Higgs bosons have to be consistent with the exclusion bounds from the collider searches at Tevatron, LEP and LHC. For further details on these checks and the scan procedure, we refer to [22, 23].

Note that in all scenarios presented in the following we stick to the N2HDM type I, with the type II scenarios leading to the same overall results. The only difference between the models comes from the fermion loops. The Yukawa couplings are, in all Yukawa types, well-behaved functions of the α_i and β because extreme values of β are already disallowed by all the constraints imposed on the model. Therefore, this is sufficient for our analysis to illustrate the effects of the EW corrections, without aiming at a full phenomenological analysis of N2HDM Higgs decays.

7.1 Results for $H_{2/3} \to ZZ$

In this section we investigate the relative size of the NLO EW corrections as well as the impact of the different renormalization schemes for the mixing angles on the decay $H_i \to ZZ$. We base our numerical analysis upon a set of representative N2HDM scenarios of phenomenological interest. To this aim we select among the generated parameter points compatible with the theoretical and experimental constraints scenarios that either have a large or a small LO branching fraction (BR) into ZZ. Discarding the SM-like decay of the H_1 fixed to be the 125 GeV Higgs boson, we select hence four scenarios, two for H_2 and H_3, respectively, which we denote by 'BRH2/3high' and 'BRH2/3low' for high and low branching ratio scenarios. The corresponding input parameters are listed in table 6. Note that, if not stated otherwise, the mixing angles are understood to be the angles defined in

[11] We thank Marco Sampaio, one of the authors of `ScannerS`, and Jonas Wittbrodt who kindly provided us with the necessary data sets.

JHEP12(2017)077

	BRH2ZZhigh	BRH3ZZhigh	BRH2ZZlow	BRH3ZZlow
m_{H_1}	125.09	125.09	125.09	125.09
m_{H_2}	673.70	600.76	657.07	283.53
m_{H_3}	692.22	713.74	658.28	751.72
m_A	669.07	743.00	543.62	763.09
$m_{H^\pm}$	679.76	695.73	528.76	733.05
t_β (pOS^c)	6.12	8.39	4.79	3.53
α_1 (pOS)	-1.513	-1.526	-1.489	1.318
α_2 (pOS)	0.098	-0.308	0.225	0.0362
α_3 (pOS)	-0.495	-1.421	-1.001	1.504
m_{12}^2	74518.4	60125.0	87240.8	143579.0
v_s	305.48	854.50	834.33	219.29
Γ_H	2.946	2.241	2.990	2.746
BR	0.327	0.329	0.010	0.010

Table 6. Input parameters for the N2HDM benchmark scenarios used in the numerical analysis of the decay processes $H_{2/3} \to ZZ$. In round brackets we specify the scheme in which α and β are defined. All masses and v_S are given in GeV. The LO total width (also given in GeV) and individual branching fractions in the last two rows correspond to the Higgs state and decay each benchmark is named after, and have been generated with `N2HDECAY`.

the OS tadpole pinched scheme (pOS) with $\delta\beta$ defined via the charged sector, denoted by the superscript 'c'.[12] The branching fractions given in this table have been obtained with the Fortran code `N2HDECAY`.[1] We insured to consider purely OS decays into massive gauge bosons in `N2HDECAY`, as we do not include any gauge boson off-shell effects in the NLO computation. For completeness, a thorough account of the relevant Higgs coupling values for each benchmark is included in appendix A.

High BR scenarios are characterized by i) large Higgs masses; ii) strongly suppressed Yukawas, which explain the dominance of the ZZ decay channel; and iii) a subset of strongly enhanced trilinear couplings. In contrast, the suppressed branching fractions in the BRlow scenarios follow from the small tree-level coupling to ZZ of the decaying Higgs boson. The latter scenarios also involve heavy Higgs spectra, typically with larger relative mass splittings as compared to the BRhigh benchmarks (cf. e.g. the $m_{H_3} - m_{H_2}$ separation in the BRH3ZZlow case).

In table 7 we present for all four benchmark scenarios the results for the LO and the NLO width as well as the relative corrections $\Delta\Gamma$. They are given for four different renormalization schemes. These consist of the $p_\star$ and the pOS tadpole pinched schemes, each of them involving two different momentum scales, and for these additionally the two possibilities to renormalize β, either via the charged sector (denoted by 'c') or the CP-odd sector (denoted by 'o'). The relative corrections are defined as

$$\Delta\Gamma \equiv \frac{\Delta\Gamma^{\rm NLO}}{\Gamma^{\rm LO}} = \frac{\Gamma^{\rm NLO} - \Gamma^{\rm LO}}{\Gamma^{\rm LO}} \,. \tag{7.8}$$

[12] While the scheme choice is not relevant for the LO width alone, it becomes important when the NLO EW corrections are included. The renormalization of the parameters then fixes the scheme of the input parameters at LO.

JHEP12(2017)077

		pOS^c	pOS^o	p$^c_\star$	p$^o_\star$
BRH2ZZhigh	$\Gamma^{\rm LO}(H_2 \to ZZ)$	0.989	0.989	1.008	1.008
	$\Gamma^{\rm NLO}(H_2 \to ZZ)$	1.120	1.122	1.142	1.148
	$\Delta\Gamma^{H_2ZZ}$ [%]	13.2	13.4	13.3	14.0
BRH3ZZhigh	$\Gamma^{\rm LO}(H_3 \to ZZ)$	0.755	0.755	0.782	0.782
	$\Gamma^{\rm NLO}(H_3 \to ZZ)$	0.872	0.867	0.890	0.889
	$\Delta\Gamma^{H_3ZZ}$ [%]	15.6	14.9	13.9	13.7
BRH2ZZlow	$\Gamma^{\rm LO}(H_2 \to ZZ)$	3.130×10^{-2}	3.130×10^{-2}	2.529×10^{-2}	2.533×10^{-2}
	$\Gamma^{\rm NLO}(H_2 \to ZZ)$	3.042×10^{-2}	3.040×10^{-2}	2.840×10^{-2}	2.745×10^{-2}
	$\Delta\Gamma^{H_2ZZ}$ [%]	-2.8	-2.9	12.3	8.4
BRH3ZZlow	$\Gamma^{\rm LO}(H_3 \to ZZ)$	2.870×10^{-2}	2.869×10^{-2}	3.430×10^{-2}	3.418×10^{-2}
	$\Gamma^{\rm NLO}(H_3 \to ZZ)$	2.990×10^{-2}	3.011×10^{-2}	3.593×10^{-2}	3.738×10^{-2}
	$\Delta\Gamma^{H_3ZZ}$ [%]	4.2	5.0	4.8	9.3

Table 7. Higgs decay widths (in GeV) at LO and NLO EW accuracy as well as the relative corrections for the N2HDM benchmarks presented in table 6 and four different renormalization schemes.

When computing the NLO EW corrected decay width $\Gamma^{\rm NLO}$ in a different renormalization scheme b than the one of the input parameters p, scheme a, these parameters first have to be converted to the scheme that is applied. We perform this conversion for the mixing angles α and β through ($p = \alpha, \beta$)

$$p^b = p^a + \delta p^a - \delta p^b \,, \tag{7.9}$$

where δp denotes the counterterm in either scheme a or scheme b. With the thus obtained input parameters in scheme b we compute the quantity $\Delta\Gamma^{\rm NLO}$ and the LO width $\Gamma^{\rm LO}$, to which we normalize the relative correction.[13]

The relative corrections for the scenarios with relatively large branching ratios turn out to be of moderate size with values between 13.2 and 15.6%, and show a mild renormalization scheme dependence of 2% at most, mainly between p_* and pOS-type schemes, which we can interpret as an indication of a relatively small theoretical error due to missing higher order corrections. Nonetheless, we observe that including the one-loop electroweak effects does not visibly reduce the scheme dependence viz. the theoretical uncertainty associated to the NLO predictions with respect to the LO results. We can attribute this behavior to the presence of large Higgs self-couplings, which tend to enhance the loop contributions at NLO and beyond, and thereby to slow down the convergence of the perturbative loop expansion.

[13]Note that the LO widths given in table 7 for the pOS^c scheme slightly differ from the values as obtained from the corresponding BRs and total widths given in table 6, since, in consistency with our NLO computation, we use as input parameters m_W, m_Z and α, while in `N2HDECAY` all decay widths are expressed in terms of the Fermi constant G_F as input value. Including in our LO results the SM correction $\Delta r^{\rm SM}$ [84–86], which relates m_W to G_F, would bring the derived Fermi constant numerically very close to the PDG value $G_F = 1.166 \cdot 10^{-5}\,\text{GeV}^{-1}$ used in `N2HDECAY`.

JHEP12(2017)077

Moderate EW corrections are also obtained in the low BR scenarios. For BRH2ZZlow, the relative corrections at NLO span the range $\Delta\Gamma \sim (-2.9, 12.3)\%$. For BRH3ZZlow, we find relative corrections lying in the ballpark $\Delta\Gamma \sim (4.2, 9.3)\%$. In both cases we observe a larger scheme dependence with respect to the BRZZhigh benchmarks, again arising dominantly between p_* and pOS-type renormalization setups. The respective tree-level couplings, strongly suppressed in this case, vary by $\mathcal{O}(10)\%$ depending on the scheme choice, and give rise to a $\mathcal{O}(20)\%$ variation in the predicted LO decay rates when going from the p_* to the pOS scheme. At NLO, the scheme dependence persists for BRH3ZZlow — while it shrinks down to $\mathcal{O}(10\%)$ for BRH2ZZlow. The fact that the observed pOS versus p_*-type scheme dependence is comparably larger with respect to the BRH2ZZhigh scenarios reflects the more significant Higgs mass splittings of the BRHZZlow setups. The reason is that each class of schemes implies different momentum scale choices at which the self-energies in the angle counterterms are evaluated. As these mass splittings increase, the NLO effects (within both the scheme conversion relations for the mixing angles, and the vertex counterterm themselves) become more responsive to the specific scheme choice. When changing from the charged to the CP-odd based renormalization of β, the change in the relative corrections is rather mild for most of the scenarios. This is because the two different scales, $m_{H^\pm}$ or m_A, involved in these two renormalization schemes of β are close in our scenarios.

7.2 Results for $H_{2/3} \to AA$

Here we study the decay into a pair of pseudoscalars and again concentrate on the decays of the heavier Higgs bosons H_2 and H_3 and choose scenarios where H_1 is the 125 GeV Higgs boson[14] and with low and high branching ratios for $H_{2/3} \to AA$, respectively. The corresponding benchmark scenarios are called 'BRH2/3AAhigh' and 'BRH2/3AAlow', with the input values summarized in table 8 together with the LO total widths and branching ratios computed with `N2HDECAY`. The input mixing angles are given in the pOS scheme and the β renormalization is based on the charged sector. The parameter m_{12}^2 is assumed to be given at the scale $\mu_R = 2m_A$.[15] The corresponding Higgs coupling values are listed in appendix A. High BR scenarios are characterized by i) relatively light Higgs masses, with larger mass splittings for BRH2AAhigh; ii) a considerable mass separation between the charged Higgs and the CP-odd scalar; iii) in general, small to moderate Higgs self-couplings. Low BR scenarios, in turn, are also characterized by sizable mass splittings. In particular, BRH2AAlow entails largely separated charged Higgs and CP-odd scalar masses ($m_{H^\pm} \sim 3m_A$), with a very light CP-odd state $m_A \simeq 70$ GeV, while for BRH3AAlow the largest separation involves the CP-even neutral states $m_{H_3} \sim 4m_{H_2}$. In the BRhigh scenarios, the $H_{2/3} \to AA$ decays are maximized because (*i*) the $H_{2/3}AA$ trilinear couplings are enhanced, (*ii*) the couplings to fermions are suppressed and (*iii*) the decays into massive weak bosons are kinematically closed. The suppressed decay widths in the BRlow scenarios are due to a small trilinear coupling $\lambda_{H_{2/3}AA}$.

[14] We do not consider H_1 decays into AA. They would require m_A to be below about 65 GeV and care would have to be taken to keep the decay $H_1 \to AA$ small enough to still be compatible with the LHC Higgs data.

[15] This choice was shown to yield the most stable results for the 2HDM [37].

JHEP12(2017)077

	BRH2AAhigh	BRH3AAhigh	BRH2AAlow	BRH3AAlow
m_{H_1}	125.09	125.09	125.09	125.09
m_{H_2}	130.48	137.15	294.92	243.70
m_{H_3}	347.65	146.22	503.44	903.07
m_A	58.14	70.27	74.28	429.82
$m_{H^\pm}$	146.93	166.83	278.19	426.18
t_β (pOS^c)	5.89	5.55	6.12	4.01
α_1 (pOS)	-1.535	1.338	-1.457	1.409
α_2 (pOS)	0.369	0.095	-0.117	-0.195
α_3 (pOS)	0.029	-1.28	-0.118	-0.078
m_{12}^2 ($\mu_R = 2m_A$)	864.2	982.9	13036.9	8300.6
v_s	538.37	638.95	1352.51	991.00
Γ_H	2.694	2.005	$4.986 \cdot 10^{-2}$	$26.140 \cdot 10^{-2}$
BR	0.999	0.999	0.010	0.010

Table 8. Input parameters for the N2HDM benchmarks used in the numerical analysis of the decay process $H_{2/3} \to AA$. All masses and v_S are given in GeV. The LO total width (also given in GeV) and individual branching fractions in the last two rows correspond to the Higgs state and decay each benchmark is named after, and have been generated with `N2HDECAY`.

		pOS^c	pOS^o	p$^c_\star$	p$^o_\star$
BRH2AAhigh	$\Gamma^{\rm LO}(H_2 \to AA)$	2.761	2.759	2.761	2.760
	$\Gamma^{\rm NLO}(H_2 \to AA)$	2.454	2.500	2.459	2.500
	$\Delta\Gamma^{H_2AA}$ [%]	-11.1	-9.4	-10.9	-9.4
BRH3AAhigh	$\Gamma^{\rm LO}(H_3 \to AA)$	2.054	2.053	2.042	2.041
	$\Gamma^{\rm NLO}(H_3 \to AA)$	1.840	1.885	1.848	1.886
	$\Delta\Gamma^{H_3AA}$ [%]	-10.4	-8.1	-9.5	-7.6
BRH2AAlow	$\Gamma^{\rm LO}(H_2 \to AA)$	5.097×10^{-2}	5.266×10^{-2}	5.075×10^{-2}	5.208×10^{-2}
	$\Gamma^{\rm NLO}(H_2 \to AA)$	5.408×10^{-2}	-1.013×10^{-2}	4.071×10^{-2}	-9.986×10^{-3}
	$\Delta\Gamma^{H_2AA}$ [%]	6.1	-119.2	-19.8	-119.2
BRH3AAlow	$\Gamma^{\rm LO}(H_3 \to AA)$	0.266	0.266	0.286	0.286
	$\Gamma^{\rm NLO}(H_3 \to AA)$	0.277	0.272	0.270	0.277
	$\Delta\Gamma^{H_3AA}$ [%]	4.4	2.1	-5.5	-3.0

Table 9. Higgs decay widths (in GeV) at LO and NLO EW accuracy as well as the relative corrections for the N2HDM benchmarks presented in table 8 and four different renormalization schemes. The renormalization scale of m_{12}^2 is set to $\mu_R = 2m_A$.

In table 9 we display for all four benchmark scenarios the LO and NLO widths as well as the relative corrections $\Delta\Gamma$. They are given for the four different renormalization schemes, p$^{c/o}_\star$, pOS$^{c/o}$. As can be inferred from the table, for the BRhigh scenarios we obtain moderate corrections of $\mathcal{O}(10)$%, i.e. of the same order as for $H_{2/3} \to ZZ$. The

JHEP12(2017)077

predicted decay rates exhibit a rather tempered renormalization scheme variation of at most 2.8%. The associated theoretical uncertainties are therefore mild. Unlike for the $H \to ZZ$ decays described above, we here observe similar differences between pOS/p_*-based and $(c)/(o)$-type schemes. The reason is that we now have more significant splittings not only among the neutral scalar masses, but also between m_A and $m_{H^\pm}$. The latter explain the more apparent deviations depending on whether the renormalization of the angle β is carried out via the charged Higgs or the CP-odd scalar sectors.

In BRH3AAlow, we find a more remarkable scheme dependence in the LO results, amounting to a $\sim 7.5\%$ variation, mainly between the pOS and p_*-type renormalization setups. Instead, the LO predictions remain unresponsive when switching from (c) to (o)-type conditions, in agreement with the fact that $m_A \sim m_{H^\pm}$, while both fields have at the same time very similar coupling patterns. This explains why the contributions from the charged (CP-odd) Higgs self-energies relevant in the (c)-type ((o)-type) scheme are numerically very similar. Conversely, the sizable mass splittings in the CP-even sector (e.g. $m_{H_2} - m_{H_3}$) amplify the influence of the different momentum scales involved in the pOS versus p_*-based renormalization setups. At the same time, these mass hierarchies give rise to large logarithmic contributions of the form $\sim \log\left(m^2_{H_i}/m^2_{H_j}\right)$, which delay the convergence of the loop expansion — precluding the NLO-corrected width to substantially shrink the theoretical uncertainty with respect to the LO prediction.

The BRH2AAlow scenario exhibits rather peculiar attributes, which deserve a dedicated analysis. First of all, we encounter a remarkably large (o) versus (c)-type scheme dependence, which is already quite apparent in the LO rates. This can be traced back mainly to the top-mediated corrections in the $A - G^0$ resp. $H^\pm - G^\pm$ self-energies. These generate logarithmic contributions of the type $\sim \log(m_t^2/m_A^2)$ resp. $\sim \log(m_t^2/m_{H^\pm}^2)$, the former being enhanced by the very light CP-odd scalar. Similar m_A-dependent contributions to $\delta\beta^{(o)}$ appear through the bosonic loops, giving rise to enlarged logarithmic structures, for instance of the form $\sim \log(m^2_{H_2}/m^2_A)$. These are numerically important as well in the BRH2AAlow scenario due to the mass hierarchy between the H_2 state and the rather light CP-odd scalar. A change from one scheme to the other thus implies large-log differences of the sort $\sim \log(m^2_{H^\pm}/m^2_A)$. Another salient observation is the huge scheme dependence of the one-loop results, which eventually pulls the NLO predictions down to (obviously unphysical) negative values. In first place, this is again due to the above mentioned m_A-enhanced logarithms. The latter contribute differently to the total NLO rates, depending on the chosen renormalization scheme. While the logarithms from the pure vertex corrections $\mathcal{M}^{\text{virt}}_{H_2AA}$ are present regardless of the scheme in use, those linked to the scalar two-point functions within $\mathcal{M}^{\text{CT}}_{H_2AA}$ are only present directly when the mixing angle β is renormalized using (o)-type conditions. At the same time, additional large logarithms $\sim \log(m^2_{H_2}/\mu_R^2)$ arise as well due to the low renormalization scale $\mu_R = 2m_A$ involved in the $\overline{\text{MS}}$ soft-breaking mass term m_{12}^2 renormalization. Overall, these large logarithms lead to a poorer convergence of the corresponding loop expansion — a nice reflect of the connection between the scheme dependence and the theory uncertainties. Another relevant ingredient to understand the sizable scheme dependence of the NLO results is the particularly delicate counterbalance between bosonic and fermionic loops. These two subsets of graphs are

JHEP12(2017)077

separately renormalizable, gauge invariant, and UV-finite, and in the current scenario contribute with different overall signs and quite similar (individually large) sizes. The partial compensation between fermionic and bosonic loops relies on highly non-linear combinations of all mixing angles $\{\beta, \alpha_i\}$ — and hence is very sensitive to the scheme-dependent mixing angle values. It is also illustrative to trace back the origin of the huge negative corrections in the (o)-type schemes. By breaking down the full-fledged contribution to the NLO $H_2 \to AA$ decay width, we single out up to three sources for the m_A-enhanced logarithmic structures alluded to above: i) as already mentioned, the pure virtual vertex corrections $\mathcal{M}^{\rm virt}_{H_2AA}$; ii) the terms in $\mathcal{M}^{\rm CT}_{H_2AA}$ stemming from the $\delta m^2_{H_2}$ piece within the vertex counterterm of eq. (6.15); iii) only for the (o)-type schemes, additional $\sim \log(m_t^2/m_A^2)$ and $\sim \log(m^2_{H_2}/m_A^2)$ terms in $\mathcal{M}^{\rm CT}_{H_2AA}$, predominantly through the (scheme-dependent) δM^2 piece in eq. (6.15). The latter does in fact depend on the renormalization scheme chosen for β through

$$\delta M^2 = \frac{\delta m^2_{12}}{s_\beta\, c_\beta} - m^2_{12}\,\frac{c_{2\beta}}{s^2_\beta\, c^2_\beta}\,\delta\,\beta \stackrel{!}{=} -m^2_{12}\,\frac{c_{2\beta}}{s^2_\beta\, c^2_\beta}\,\delta\,\beta \qquad \text{with} \qquad \delta m^2_{12}|_{\overline{\rm MS}} = 0\,. \tag{7.10}$$

At the same time, the large m^2_{12} and $\tan\beta$ values in the BRH2AAlow benchmark imply as well a sizable prefactor.

The key observation is that these m_A-dependent terms within $\mathcal{M}^{\rm virt}_{H_2AA}$ and $\mathcal{M}^{\rm CT}_{H_2AA}$ turn out to mutually cancel each other in the (c)-type schemes, and thus give rise to the rather moderate EW corrections reported in table 9. At variance, the additional m_A-dependent logarithms from δM^2 in the (o)-type schemes are unmatched to yet-to-be-cancelled counterparts within $\mathcal{M}^{\rm virt}_{H_2AA}$ or the remainder of $\mathcal{M}^{\rm CT}_{H_2AA}$. This leads to an incomplete cancellation of (scheme-dependent) m_A-enhanced finite parts, responsible for the strong negative drift of the total NLO yields.

7.3 Results for $H_3 \to H_2\,H_2$ and $H_2 \to H_1 H_1$

Finally, we consider the decay of a heavy neutral CP-even Higgs boson into a pair of lighter CP-even Higgs bosons. We evaluate the NLO EW corrections for a number of illustrative scenarios, given in table 10. The scenarios have been chosen such that their Higgs mass spectra allow simultaneously for the OS $H_3 \to H_2 H_2$ and $H_2 \to H_1 H_1$ decays. Furthermore, the chosen large m^2_{12} parameter insures these heavy Higgs mass scenarios to be in agreement with the unitarity and vacuum stability constraints. All scenarios feature Higgs-to-Higgs decay branching ratios that are of moderate size. Only HHHIV features a H_2 branching ratio into H_1H_1 that is dominating. All input mixing angles are assumed to be given in the pOS scheme, with charged sector-based renormalization for the angle β, and m^2_{12} is assumed to be defined at the renormalization scale given by the total final state mass, $\mu_R = 2m_{H_i}$. The LO total widths and branching ratios in this table have been obtained from `N2HDECAY`. The Higgs coupling values are reported in table 14 of appendix A. Overall, these scenarios are characterized by i) relatively heavy Higgs spectra; ii) comparably smaller mass splittings with respect to the BRH2AA and BRH3AA benchmarks; iii) a subset of strongly reduced Higgs couplings to fermions, and weak bosons.

JHEP12(2017)077

	HHHI	HHHII	HHHIII	HHHIV
m_{H_1}	125.09	125.09	125.09	125.09
m_{H_2}	304.18	425.61	351.65	298.42
m_{H_3}	630.94	857.27	717.32	743.18
m_A	325.07	547.48	487.07	362.40
$m_{H^\pm}$	265.81	383.85	386.42	306.19
t_β (pOS^c)	6.30	5.17	4.08	6.26
α_1 (pOS)	-1.559	1.495	1.453	1.315
α_2 (pOS)	-0.330	0.082	0.353	-0.148
α_3 (pOS)	-0.077	-0.101	0.340	-0.098
m_{12}^2 ($\mu_R = 2m_{H_{\text{final}}}$)	14312.1	32824.5	35765.3	12707.3
v_s	1327.57	1098.81	630.19	1425.0
Γ_{H_3}	24.160	25.190	43.590	18.750
BR($H_3 \to H_1H_1$)	0.13	0.03	0.08	0.08
BR($H_3 \to H_2H_2$)	0.05	0.10	0.15	0.15
Γ_{H_2}	0.393	0.723	1.558	0.234
BR($H_2 \to H_1H_1$)	0.17	0.47	0.43	0.76

Table 10. Input parameters for the N2HDM benchmarks used in the numerical analysis of the decay processes $H_j \to H_iH_i$. All masses and v_S are given in GeV. In the last five rows the total H_2 and H_3 widths are given in GeV as well as the branching fractions (generated with `N2HDECAY`) of the Higgs-to-Higgs decays $H_3 \to H_1H_1, H_2H_2$ and $H_2 \to H_1H_1$.

In table 11 we summarize the relative NLO corrections for the various decays. Note, that the decay process $H_3 \to H_1H_1$ appears only at LO because we use it for the renormalization of v_S, as explained in detail in section 6.

For most of the decays, the relative NLO corrections are moderate, none of them lying above 21%. The predicted decay rates display a very mild scheme dependence in HHHI already at LO, which is further reduced at NLO. The absence of large logarithms or large self-couplings explains why the inclusion of the NLO corrections in this case is capable to efficiently shrink the theoretical uncertainty. A larger, though yet moderate pOS/p_* scheme dependence is present for HHHII, with LO predictions varying between 0.6% up to 5.8% depending on the chosen scheme. This can be attributed to the comparably larger mass splittings with respect to HHHI, in particular between the CP-even states H_1 and H_3. For HHHIII, we observe a mild scheme dependence (up to 3%) in the LO results, mostly between the pOS and p_* setups. This dependence is tempered even further at NLO for $H_2 \to H_1H_1$, while it remains at the 3% level for $H_3 \to H_2H_2$. In fact, we can identify the renormalization constant $\delta\alpha_3$ to be the most responsive one to a change between schemes. Finally, a very similar picture is encountered for HHHIV — in this case being $H_2 \to H_1H_1$ the process which leads to a more pronounced scheme dependence.

JHEP12(2017)077

		pOS^c	pOS^o	p$^c_\star$	p$^o_\star$
HHHI	$\Gamma(H_3 \to H_1H_1)$	3.206	3.206	3.197	3.197
	$\Gamma^{\rm LO}(H_3 \to H_2H_2)$	1.229	1.229	1.242	1.242
	$\Gamma^{\rm NLO}(H_3 \to H_2H_2)$	1.344	1.343	1.344	1.341
	$\Delta\Gamma^{H_3\to H_2H_2}$ [%]	9.4	9.3	8.2	8.0
	$\Gamma^{\rm LO}(H_2 \to H_1H_1)$	6.699×10^{-2}	6.699×10^{-2}	6.667×10^{-2}	6.667×10^{-2}
	$\Gamma^{\rm NLO}(H_2 \to H_1H_1)$	7.433×10^{-2}	7.429×10^{-2}	7.429×10^{-2}	7.409×10^{-2}
	$\Delta\Gamma^{H_2\to H_1H_1}$ [%]	11.0	10.9	11.4	11.1
HHHII	$\Gamma(H_3 \to H_1H_1)$	0.719	0.719	0.753	0.753
	$\Gamma^{\rm LO}(H_3 \to H_2H_2)$	2.580	2.580	2.730	2.730
	$\Gamma^{\rm NLO}(H_3 \to H_2H_2)$	2.453	2.454	2.493	2.492
	$\Delta\Gamma^{H_3\to H_2H_2}$ [%]	-4.9	-4.9	-8.7	-8.7
	$\Gamma^{\rm LO}(H_2 \to H_1H_1)$	0.345	0.345	0.343	0.343
	$\Gamma^{\rm NLO}(H_2 \to H_1H_1)$	0.398	0.398	0.397	0.397
	$\Delta\Gamma^{H_2\to H_1H_1}$ [%]	15.2	15.2	15.9	15.9
HHHIII	$\Gamma(H_3 \to H_1H_1)$	3.561	3.561	3.565	3.564
	$\Gamma^{\rm LO}(H_3 \to H_2H_2)$	6.662	6.661	6.469	6.466
	$\Gamma^{\rm NLO}(H_3 \to H_2H_2)$	6.071	6.094	6.208	6.264
	$\Delta\Gamma^{H_3\to H_2H_2}$ [%]	-8.9	-8.5	-4.0	-3.1
	$\Gamma^{\rm LO}(H_2 \to H_1H_1)$	0.687	0.687	0.684	0.683
	$\Gamma^{\rm NLO}(H_2 \to H_1H_1)$	0.678	0.679	0.675	0.676
	$\Delta\Gamma^{H_2\to H_1H_1}$ [%]	-1.3	-1.2	-1.3	-1.1
HHHIV	$\Gamma(H_3 \to H_1H_1)$	1.446	1.446	1.422	1.422
	$\Gamma^{\rm LO}(H_3 \to H_2H_2)$	2.873	2.874	2.860	2.859
	$\Gamma^{\rm NLO}(H_3 \to H_2H_2)$	2.793	2.780	2.799	2.820
	$\Delta\Gamma^{H_3\to H_2H_2}$ [%]	-2.8	-3.3	-2.1	-1.4
	$\Gamma^{\rm LO}(H_2 \to H_1H_1)$	0.183	0.183	0.185	0.185
	$\Gamma^{\rm NLO}(H_2 \to H_1H_1)$	0.151	0.144	0.147	0.158
	$\Delta\Gamma^{H_2\to H_1H_1}$ [%]	-17.4	-21.3	-20.6	-14.3

Table 11. Higgs decay width predictions (in GeV) at LO and NLO EW accuracy as well as the relative corrections for the N2HDM benchmarks presented in table 10 and four different renormalization schemes.

8 Conclusions

In this paper we worked out the renormalization of the N2HDM, which is an interesting benchmark model for studying extended Higgs sectors involving Higgs-to-Higgs decays. For the mixing angles, we provided a renormalization scheme that is manifestly gauge

JHEP12(2017)077

independent by applying the alternative tadpole scheme combined with the pinch technique. We explained in great detail the notion of the alternative tadpole scheme in our renormalization framework, and for the first time provided the formulae for the pinched self-energies in the N2HDM. Apart from the additional mixing angles as compared to the 2HDM, in the N2HDM we encounter a singlet VEV that needs to be renormalized as well. We elaborated in detail the implications of the alternative tadpole scheme for the renormalization of the singlet VEV that we renormalize through a physical quantity, given by a Higgs-to-Higgs decay width. The soft $\mathbb{Z}_2$ breaking parameter m_{12}^2, which, like v_S, enters the Higgs self-couplings and hence features in Higgs-to-Higgs decays, is renormalized in the $\overline{\text{MS}}$ scheme. We studied the impact of our renormalization scheme by computing the EW one-loop corrections to various Higgs decay widths, including the Higgs decays into a massive Z-boson pair and into lighter Higgs pairs.

The computation of the EW corrections to our different sample decay widths has shown that the corrections can be sizable and have to be taken into account in order to make reliable predictions for the Higgs observables. It has also illustrated the importance of comparing different renormalization schemes. For a broad range of phenomenologically representative scenarios we find a rather weak renormalization scheme dependence, indicative of a rather small theoretical error due to missing higher order corrections. In several instances, we observe that the inclusion of the one-loop EW corrections does not visibly reduce the scheme dependence of the NLO prediction with respect to the LO result. This may be attributed to certain dynamical features (e.g. large scalar self-couplings, sizable mass hierarchies) which tend to enhance the higher-order radiative corrections and, thereby, to slow down the convergence of the perturbative loop expansion.

With this paper, we have provided an important contribution to the renormalization of extended Higgs sectors involving singlet fields. This is crucial input for the computation of the EW corrections to the Higgs bosons of such models and therefore indispensable for the correct prediction and interpretation of Higgs observables at the LHC.

Acknowledgments

The authors acknowledge financial support from the DFG project "Precision Calculations in the Higgs Sector — Paving the Way to the New Physics Landscape" (ID: MU 3138/1-1). We would like to thank Marco Sampaio, Michael Spira and Jonas Wittbrodt for useful discussions.

A N2HDM benchmarks

In this appendix we provide a thorough characterization of the Higgs coupling patterns in the different N2HDM benchmark scenarios used in our analysis. In tables 12, 13 and 14 we list the values of all N2HDM Higgs couplings to fermions and gauge bosons, as well as a representative subset of trilinear Higgs self-couplings. The values of the underlying parameters of the scalar potential, i.e. the mass terms and quartic self-couplings in eq. (2.3), are displayed in the lowest rows of each table. All coupling values in each benchmark are

JHEP12(2017)077

	BRH2ZZhigh	BRH3ZZhigh	BRH2ZZlow	BRH3ZZlow
κ_{H_1VV}	-0.9713	-0.9403	-0.9348	0.9991
κ_{H_2VV}	0.1465	0.3198	-0.0271	-0.0377
κ_{H_3VV}	0.1872	0.1166	0.3542	0.0209
$\tilde{\kappa}_{H_1VH}$	-0.2168	-0.1555	-0.2765	0.0234
$\tilde{\kappa}_{H_2VH}$	-0.8691	-0.0984	-0.5703	0.0655
$\tilde{\kappa}_{H_3VH}$	-0.4446	-0.9829	-0.7735	-0.9976
κ_{Aff}	-0.1635	-0.1192	-0.2087	-0.2831
$\kappa_{H^\pm ff}$	0.1635	0.1192	0.2087	0.2831
κ_{H_1ff}	-1.0068	-0.9588	-0.9925	1.0057
κ_{H_2ff}	0.0044	0.3081	-0.1462	-0.0191
κ_{H_3ff}	0.1145	-0.0005	0.1928	-0.2614
$\hat{g}_{H_1H_1H_1}$	-0.0754	-0.4064	0.3528	0.9621
$\hat{g}_{H_2H_2H_2}$	-2.8501	-4.8025	-4.9322	5.6839
$\hat{g}_{H_3H_3H_3}$	18.1437	2.5606	7.8003	4.3542
$\hat{g}_{H_1H_1H_2}$	0.0815	1.9609	-1.3620	-0.1459
$\hat{g}_{H_1H_1H_3}$	1.2430	-0.0047	1.5036	0.7230
$\hat{g}_{H_1H_2H_2}$	-9.8646	-2.9288	-3.0089	0.0840
$\hat{g}_{H_1H_3H_3}$	-1.9330	-13.7739	-8.8389	1.8755
$\hat{g}_{H_2H_2H_3}$	6.4419	1.0246	3.3931	0.8193
$\hat{g}_{H_2H_3H_3}$	-6.5823	-0.1195	0.4235	1.9800
$\hat{g}_{H_1H_2H_3}$	-6.1122	-2.0460	-5.5180	0.5181
$\hat{g}_{H_1AA}$	-11.9181	-15.5153	-6.0623	2.6592
$\hat{g}_{H_2AA}$	-0.2621	0.3922	-0.3366	1.9990
$\hat{g}_{H_3AA}$	2.3815	1.0683	0.9277	1.4698
$\hat{g}_{H_1H^+H^-}$	-12.5149	-12.7907	-5.4275	0.7464
$\hat{g}_{H_2H^+H^-}$	-0.1721	-0.5344	-0.3182	2.0712
$\hat{g}_{H_3H^+H^-}$	2.4965	0.7303	0.6872	1.4297
m_{11}^2	-1.8480×10^5	1.8141×10^5	-1.8480×10^5	4.2831×10^5
m_{22}^2	1.5853×10^5	-1.6297×10^5	1.5853×10^5	3.9148×10^4
m_S^2	-1.5249×10^5	-2.1843×10^5	-1.5249×10^5	-4.0292×10^4
λ_1	1.4496	1.4759	4.9322	4.7876
λ_2	0.1631	0.6997	0.3677	0.1789
λ_3	10.5046	9.7457	4.8262	0.3034
λ_4	-0.1445	1.6185	2.9189	0.9382
λ_5	0.3433	-0.6821	2.3798	-0.5819
λ_6	5.0271	0.4550	0.5911	1.7143
λ_7	0.6629	1.0337	-0.1617	2.0958
λ_8	0.6137	-0.4826	0.4547	-0.2017

Table 12. Higgs couplings to gauge bosons, fermions, and an illustrative subset of trilinear self-interactions, for the different benchmark scenarios used in the analysis of the decay modes $H_{2,3} \to ZZ$ in section 7. The lowest rows display the values of the mass terms squared (in GeV^2) and quartic couplings in the Higgs potential eq. (2.3). The corresponding input parameters are given in table 6.

JHEP12(2017)077

	BRH2AAhigh	BRH3AAhigh	BRH2AAlow	BRH3AAlow
κ_{H_1VV}	-0.9134	0.9940	-0.9555	0.9778
κ_{H_2VV}	0.2131	0.1068	0.2840	-0.0972
κ_{H_3VV}	0.3469	0.0240	-0.0797	0.1859
$\tilde{\kappa}_{H_1VH}$	-0.1892	-0.05372	-0.2708	0.0808
$\tilde{\kappa}_{H_2VH}$	-0.9766	0.2853	-0.9517	0.9923
$\tilde{\kappa}_{H_3VH}$	0.1019	0.9569	-0.1447	0.0938
κ_{Aff}	-0.1698	-0.1802	-0.1635	-0.2493
$\kappa_{H^\pm ff}$	0.1697	0.1802	0.1635	0.2493
κ_{H_1ff}	-0.9455	0.9843	-0.9998	0.9979
κ_{H_2ff}	0.0047	0.1582	0.1285	0.1502
κ_{H_3ff}	0.3642	0.1964	-0.1033	0.2093
$\hat{g}_{H_1H_1H_1}$	0.7913	0.9895	-0.8501	0.9258
$\hat{g}_{H_2H_2H_2}$	4.5527	-0.4737	3.3928	-6.3034
$\hat{g}_{H_3H_3H_3}$	3.1861	-4.6479	2.9196	12.3941
$\hat{g}_{H_1H_1H_2}$	0.0576	0.0810	-0.0180	-0.1064
$\hat{g}_{H_1H_1H_3}$	1.1984	-0.0737	-0.5819	3.5969
$\hat{g}_{H_1H_2H_2}$	0.0413	0.1379	-2.4521	1.1302
$\hat{g}_{H_1H_3H_3}$	0.1111	1.1497	-0.2966	-0.1129
$\hat{g}_{H_2H_2H_3}$	-0.7074	-0.1878	3.0177	-3.0344
$\hat{g}_{H_2H_3H_3}$	0.1475	-1.2555	0.4978	-0.7138
$\hat{g}_{H_1H_2H_3}$	-0.0636	0.3085	0.1271	1.0972
$\hat{g}_{H_1AA}$	0.0078	0.3635	0.5150	6.6765
$\hat{g}_{H_2AA}$	1.4634	-0.3903	0.2167	-2.6515
$\hat{g}_{H_3AA}$	-0.5695	-1.7132	2.9769	-1.4536
$\hat{g}_{H_1H^+H^-}$	-0.7008	1.333	-2.4108	6.5464
$\hat{g}_{H_2H^+H^-}$	1.6287	-0.2862	1.0864	-2.6385
$\hat{g}_{H_3H^+H^-}$	-0.3004	-1.6899	2.7330	-1.4782
m_{11}^2	2.8243×10^4	3.9147×10^3	-3.6627×10^5	3.0674×10^5
m_{22}^2	-5.3878×10^4	-7.4886×10^3	6.2391×10^4	-3.5363×10^5
m_S^2	-6.1241×10^4	-9.4445×10^3	-1.2208×10^5	-4.0844×10^5
λ_1	7.3165	8.3056	5.9259	7.6888
λ_2	0.5058	0.2752	0.2976	0.8532
λ_3	0.4843	0.7331	1.8445	4.5533
λ_4	-0.5845	-0.7627	-1.1396	-2.4210
λ_5	0.0314	0.0117	1.2916	-2.5266
λ_6	0.3695	0.0465	0.1355	0.7954
λ_7	-0.1879	-0.0278	0.4198	-0.5616
λ_8	0.2729	-0.0010	-0.0769	0.6774

Table 13. Higgs couplings to gauge bosons, fermions, and an illustrative subset of trilinear self-interactions, for the different benchmark scenarios used in the analysis of the decay modes $H_{2,3} \to AA$ in section 7. The lowest rows display the values of the mass terms squared (in GeV^2) and quartic couplings in the Higgs potential eq. (2.3). The corresponding input parameters are given in table 8.

JHEP12(2017)077

	HHHI	HHHII	HHHIII	HHHIV
κ_{H_1VV}	-0.9372	0.9900	0.9311	0.9845
κ_{H_2VV}	0.1925	-0.1060	-0.2414	0.0821
κ_{H_3VV}	-0.3050	-0.0927	-0.2735	0.1552
$\tilde{\kappa}_{H_1VH}$	-0.1593	0.1145	0.1152	-0.0958
$\tilde{\kappa}_{H_2VH}$	-0.9786	0.9892	0.9059	0.9919
$\tilde{\kappa}_{H_3VH}$	-0.1304	0.0911	-0.4075	0.0831
κ_{Aff}	-0.1586	-0.1936	-0.2452	-0.1599
$\kappa_{H^\pm ff}$	0.1586	0.1936	0.2452	0.1599
κ_{H_1ff}	-0.9580	1.0122	0.9593	0.9691
κ_{H_2ff}	0.0373	0.0855	-0.0193	0.2407
κ_{H_3ff}	-0.3257	-0.0751	-0.3734	0.1685
$\hat{g}_{H_1H_1H_1}$	-0.7307	0.7941	0.6681	0.8639
$\hat{g}_{H_2H_2H_2}$	1.1414	-2.8917	4.8702	-2.3250
$\hat{g}_{H_3H_3H_3}$	3.1216	9.8683	10.1021	5.8741
$\hat{g}_{H_1H_1H_2}$	0.3116	-0.6998	-0.9627	0.5195
$\hat{g}_{H_1H_1H_3}$	-2.4379	-1.3180	-2.7114	1.7543
$\hat{g}_{H_1H_2H_2}$	-1.9620	2.3943	1.2415	0.0282
$\hat{g}_{H_1H_3H_3}$	-2.6046	0.8897	5.7246	0.1491
$\hat{g}_{H_2H_2H_3}$	2.8081	-7.0922	8.0938	-3.1091
$\hat{g}_{H_2H_3H_3}$	0.3277	-2.2661	-3.4942	-0.6264
$\hat{g}_{H_1H_2H_3}$	0.1311	0.6743	-0.5699	1.3242
$\hat{g}_{H_1AA}$	-2.4375	7.4960	4.8950	1.5980
$\hat{g}_{H_2AA}$	0.4906	-1.5151	0.8029	-0.6405
$\hat{g}_{H_3AA}$	2.4602	-7.3335	8.0143	-2.9253
$\hat{g}_{H_1H^+H^-}$	-1.0462	1.0679	0.8686	0.0218
$\hat{g}_{H_2H^+H^-}$	0.2034	-0.8267	1.8469	-0.7720
$\hat{g}_{H_3H^+H^-}$	2.9153	-6.7314	9.1970	-3.1739
m_{11}^2	-3.4641×10^5	8.0817×10^5	-4.0889×10^5	5.4249×10^5
m_{22}^2	2.9654×10^5	1.2101×10^5	1.8651×10^5	-2.6940×10^5
m_S^2	-1.6803×10^5	-3.5510×10^5	-1.7904×10^5	-2.7513×10^5
λ_1	2.9570	7.9450	5.7400	4.4204
λ_2	0.9200	0.2521	1.3008	0.5659
λ_3	0.0444	1.2754	-2.2594	-0.5947
λ_4	0.9616	3.0610	2.0359	0.4287
λ_5	-0.2227	-2.0941	-1.3976	-0.8426
λ_6	0.2022	0.6000	1.0260	0.2641
λ_7	0.4674	-1.1777	2.9728	-0.4306
λ_8	-0.3647	-0.2058	-1.0641	0.2520

Table 14. Higgs couplings to gauge bosons, fermions, and an illustrative subset of trilinear self-interactions, for the different benchmark scenarios used in the analysis of the decay modes $H_3 \to H_2H_2$ and $H_2 \to H_1H_1$ in section 7. The lowest rows display the values of the mass terms squared (in GeV^2) and quartic couplings in the Higgs potential eq. (2.3). The corresponding input parameters are given in table 10.

JHEP12(2017)077

obtained from the input parameters which define each of these benchmarks, as given in tables 6, 8 and 10, and evaluated via tree-level relations. As indicated in these tables, we assume the input mixing angles to be defined in the pOS scheme, and β in the pOS^c scheme. These couplings are fully consistent with the ScannerS framework from which our benchmarks are derived — ensuring their compatibility with all constraints on the model.

For the Higgs couplings to the fermions and gauge bosons we give the values of the rescaling factors $\kappa_{H_iVV}, \tilde{\kappa}_{H_iVH}$ and κ_{H_iff} respectively, as defined in tables 1, 5 and 3. We normalize the trilinear Higgs self-couplings to the strength of the trilinear Higgs self-coupling in the SM, i.e. $\hat{g}_{H_iH_jH_k} \equiv g_{H_iH_jH_k}/g^{\rm SM}_{HHH}$, where $g^{\rm SM}_{HHH} = -3\frac{m_H^2}{v} = -190.823\,\text{GeV}$.

B The pinch technique in the N2HDM

In this section, we present the explicit gauge dependences appearing in the scalar-scalar and scalar-vector self-energies in the N2HDM. Additionally, we present the application of the pinch technique in the N2HDM for the first time, as well as the cancellation of all gauge dependences by the generation of pinched self-energies.

B.1 Gauge dependence of the self-energies

We begin by setting the notation used in the explicit expressions of the gauge dependences. Following the notation of ref. [59], we define the functions

$$f_{\Phi_i\Phi_j}(p^2) = p^2 - \frac{m^2_{\Phi_i} + m^2_{\Phi_j}}{2} \tag{B.1}$$

$$g_{\Phi_i\Phi_j}(p^2, m^2) = 2\left(p^2 - m^2\right)\left(p^2 - \frac{m^2_{\Phi_i} + m^2_{\Phi_j}}{2}\right) - \left(p^2 - m^2_{\Phi_i}\right)\left(p^2 - m^2_{\Phi_j}\right), \tag{B.2}$$

where Φ stands for an arbitrary neutral or charged scalar particle and $m_{\Phi_{i,j}} = 0$ in case $\Phi_{i,j}$ is a Goldstone boson. We introduce the one-loop integrals

$$\alpha_V = \frac{1}{(1-\xi_V)\,m_V^2}\left[A_0\left(m_V^2\right) - A_0\left(\xi_V m_V^2\right)\right] = B_0\left(0; m_V^2, \xi_V m_V^2\right) \tag{B.3}$$

$$\begin{aligned}\beta_{V\Phi_i}(p^2) &= \frac{1}{(1-\xi_V)\,m_V^2}\left[B_0\left(p^2; m_V^2, m^2_{\Phi_i}\right) - B_0\left(p^2; \xi_V m_V^2, m^2_{\Phi_i}\right)\right] \\ &= C_0\left(0, p^2, p^2; m_V^2, \xi_V m_V^2, m^2_{\Phi_i}\right)\end{aligned} \tag{B.4}$$

$$\begin{aligned}\beta_{V\xi V}(p^2) &= \frac{1}{(1-\xi_V)\,m_V^2}\left[B_0\left(p^2; m_V^2, \xi_V m_V^2\right) - B_0\left(p^2; \xi_V m_V^2, \xi_V m_V^2\right)\right] \\ &= C_0\left(0, p^2, p^2; \xi_V m_V^2, \xi_V m_V^2, m^2_{\Phi_i}\right)\end{aligned} \tag{B.5}$$

$$C_2^{V\Phi_i}(p^2) = C_2\left(0, p^2, p^2; m_V^2, \xi_V m_V^2, m^2_{\Phi_i}\right), \tag{B.6}$$

where A_0, B_0 and C_0 denote the usual scalar one-, two- and three-point integrals and C_2 denotes the coefficient integral of the tensor integral C_μ, which can be expressed solely through A_0 and B_0 integrals, cf. refs. [49, 61]. The index V denotes a vector boson $V \in \{W^\pm, Z, \gamma\}$.

In what follows, we extract the gauge dependences of all self-energies via the definition

$$i\Sigma^{\rm tad}(p^2) = i\Sigma^{\rm tad}(p^2)\Big|_{\xi_V=1} + i\Sigma(p^2)\Big|_{\rm g.d.}\,, \tag{B.7}$$

JHEP12(2017)077

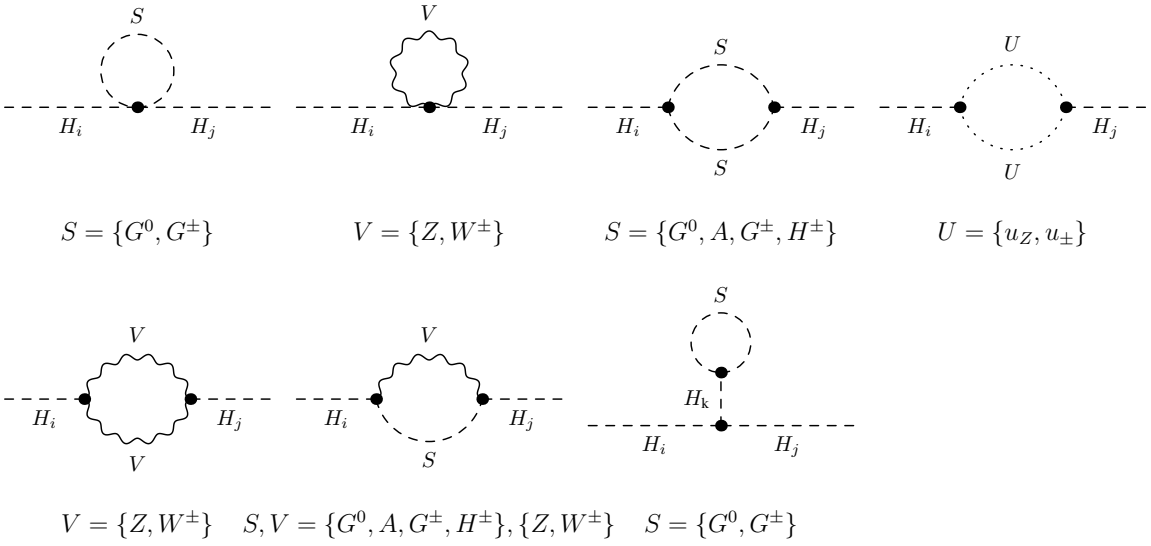

Figure 13. All Feynman diagrams contributing to the gauge dependence of the CP-even self-energies $\Sigma^{\text{tad}}_{H_iH_j}(p^2)$. For the tadpole diagram, a sum over intermediate Higgs states H_k $(k = 1, 2, 3)$ is assumed. Note that the ghost and vector boson contributions in the tadpole diagrams precisely cancel against each other, so that these are not shown.

where $i\Sigma^{\text{tad}}(p^2)$ is the fully gauge-dependent modified self-energy with tadpole contributions included, cf. figure 3, $i\Sigma(p^2)\big|_{\text{g.d.}}$ represents the truly gauge-dependent part of the self-energy and $i\Sigma(p^2)\big|_{\xi_V=1}$ denotes the evaluation of the self-energy in the 't-Hooft Feynman gauge. The inclusion of tadpole contributions for the analysis of the self-energies with respect to gauge dependence is necessary for a consistent application of the pinch technique [52]. While the extraction of the gauge dependence via eq. (B.7) is not unique, we show in the following by applying the pinch technique that $i\Sigma(p^2)\big|_{\text{g.d.}}$ is considered to be the truly gauge-dependent part of the self-energies, since it is precisely these terms which are cancelled by the pinch contributions.

B.1.1 Gauge dependence of the CP-even scalar self-energies

First, we consider the gauge dependence of the CP-even scalar self-energies, i.e. the self-energies of all possible combinations of H_i and H_j $(i, j = 1, 2, 3)$. All Feynman diagrams contributing gauge-dependent terms are shown in figure 13. The evaluation of eq. (B.7) for the CP-even scalars of the N2HDM sector yields

$$\begin{aligned}
i\Sigma^{\text{tad}}_{H_iH_j}(p^2) = i\Sigma^{\text{tad}}_{H_iH_j}(p^2)\Big|_{\xi_V=1} \\
+ \frac{ig^2\,(1-\xi_Z)}{64\pi^2\cos\Theta_W}\Big[g_{H_iH_j}(p^2, m_A^2)\mathcal{O}^{(1)}_{H_iH_j}\beta_{ZA}(p^2) - f_{H_iH_j}(p^2)\mathcal{O}^{(4)}_{H_iH_j}\alpha_Z \\
+ \frac{1}{2}g_{H_iH_j}(p^2, 0)\mathcal{O}^{(2)}_{H_iH_j}\left(\beta_{ZZ}(p^2) + \beta_{Z\xi Z}(p^2)\right)\Big] \\
+ \frac{ig^2\,(1-\xi_W)}{32\pi^2}\Big[g_{H_iH_j}(p^2, m_{H^\pm}^2)\mathcal{O}^{(1)}_{H_iH_j}\beta_{WH^\pm}(p^2) - f_{H_iH_j}(p^2)\mathcal{O}^{(4)}_{H_iH_j}\alpha_W \\
+ \frac{1}{2}g_{H_iH_j}(p^2, 0)\mathcal{O}^{(2)}_{H_iH_j}\left(\beta_{WW}(p^2) + \beta_{W\xi W}(p^2)\right)\Big],
\end{aligned} \tag{B.8}$$

JHEP12(2017)077

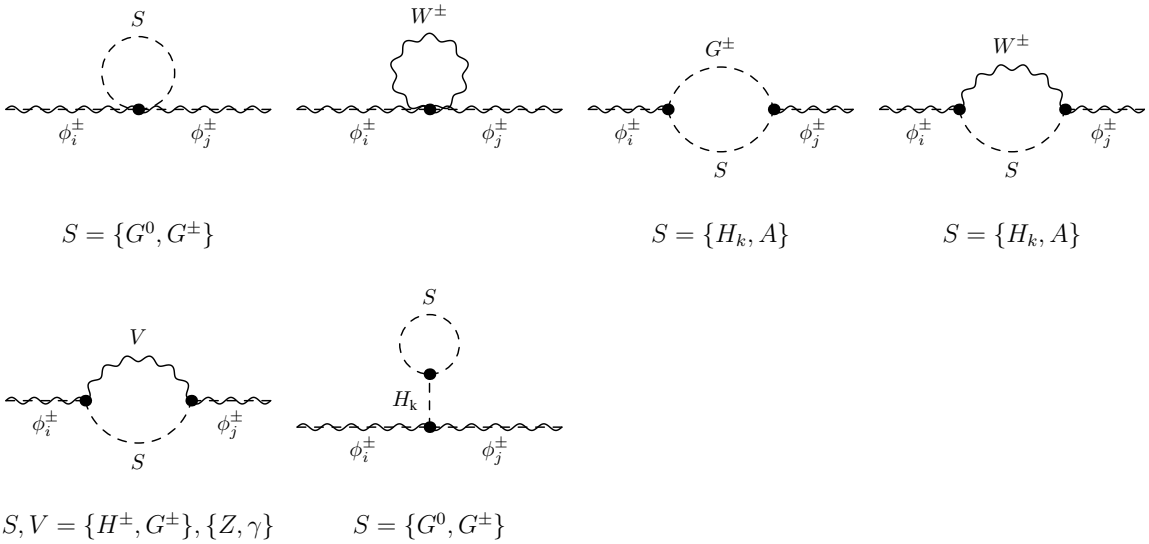

Figure 14. All Feynman diagrams contributing to the gauge-dependence of the charged self-energies $\Sigma^{\text{tad}}_{\phi_i^\pm \phi_j^\pm}(p^2)$ where $\phi^\pm_{i,j} \in \{W, G^\pm, H^\pm\}$. A sum over intermediate Higgs states H_k is assumed wherever they appear. Overlapping dashed and twiggled lines denote a scalar or a gauge boson, respectively, depending on the chosen particles. Note that we only consider contributions to the extended scalar sector of the N2HDM. Depending on the particles $\phi^\pm_{i,j}$ chosen, some of the diagrams shown may not exist in the N2HDM.

where the combinations $\mathcal{O}^{(1)}_{H_iH_j}$, $\mathcal{O}^{(2)}_{H_iH_j}$ and $\mathcal{O}^{(4)}_{H_iH_j}$ have been defined in eq. (5.30). We note that when evaluating these combinations in the 2HDM limit, i.e. by applying eq. (2.35), where $\mathcal{O}^{(4)}_{H_iH_j}$ reduces to the Kronecker delta $\delta_{H_iH_j}$, the result in eq. (B.8) coincides with the results presented in refs. [40, 60] for the 2HDM as well as with the result presented in ref. [59] for the MSSM, since the structure of the gauge-dependence of the CP-even scalar self-energies does not differ between the MSSM and the 2HDM.

B.1.2 Gauge dependence of the charged scalar and vector self-energies

Next, we consider the charged sector. Due to the mixing of the charged particles of the N2HDM, we have to consider not only all possible self-energy combinations of the scalar particles $H^\pm$ and $G^\pm$, but additionally their mixing with the charged vector bosons $W^\pm$. In the SM, where only one Higgs boson exists, it was shown that the Higgs contributions to the gauge dependence of the charged sector form a gauge-dependent subset which is cancelled by a corresponding subset of pinch contributions [56]. In the N2HDM we follow the same approach, i.e. we focus only on gauge-dependent contributions stemming from the enriched scalar sector of the N2HDM, which form a subset with respect to gauge dependence as well.

We first consider the gauge dependence of the self-energies of all combinations of $W^\pm$ and $G^\pm$. The relevant contributions from the Higgs sector are given by the Feynman diagrams in figure 14 for all possible self-energies. Note that since we consider only the subset where the scalars of the N2HDM appear in the loops, only terms containing the

JHEP12(2017)077

gauge-fixing parameter ξ_W contribute to these self-energies. They explicitly read[16]

$$i\Sigma^{\text{tad}}_{WW,\mu\nu}(p^2) = i\Sigma^{\text{tad}}_{WW,\mu\nu}(p^2)\Big|_{\xi_V=1} - (1-\xi_W)\frac{ig^2 m_W^2}{64\pi^2} p_\mu p_\nu \sum_{H_i} \mathcal{O}^{(2)}_{H_i H_i} \left\{\beta_{WH_i}(p^2) + 4C_2^{WH_i}(p^2)\right\} \tag{B.9}$$

$$i\Sigma^{\text{tad}}_{WG^\pm,\mu}(p^2) = i\Sigma^{\text{tad}}_{WG^\pm,\mu}(p^2)\Big|_{\xi_V=1} + (1-\xi_W)\frac{ig^2 m_W}{64\pi^2} p_\mu \left\{\alpha_W + \sum_{H_i} \mathcal{O}^{(2)}_{H_i H_i} \left[m^2_{H_i}\beta_{WH_i}(p^2) + 2p^2 C_2^{WH_i}(p^2)\right]\right\} \tag{B.10}$$

$$i\Sigma^{\text{tad}}_{G^\pm G^\pm}(p^2) = i\Sigma^{\text{tad}}_{G^\pm G^\pm}(p^2)\Big|_{\xi_V=1} + (1-\xi_W)\frac{ig^2}{64\pi^2}\left\{-2 f_{G^\pm G^\pm}(p^2)\alpha_W + \sum_{H_i} \mathcal{O}^{(2)}_{H_i H_i} g_{G^\pm G^\pm}(p^2, m^2_{H_i})\beta_{WH_i}(p^2)\right\}. \tag{B.11}$$

Next, the gauge dependence of the self-energies of all combinations of $H^\pm$ and $G^\pm$ or $W^\pm$ is given by the relevant contributions from the Higgs sector as given by the Feynman diagrams in figure 14 as well. In the case of the self-energy for two $H^\pm$ particles, additional dependences on ξ_Z and ξ_γ appear even when focusing on the extended scalar sector of the N2HDM only, while for the other self-energies only the dependence on ξ_W is relevant. The self-energies explicitly read

$$\begin{aligned} i\Sigma^{\text{tad}}_{H^\pm H^\pm}(p^2) = {} & i\Sigma^{\text{tad}}_{H^\pm H^\pm}(p^2)\Big|_{\xi_V=1} \\ & + (1-\xi_W)\frac{ig^2}{64\pi^2}\Big\{ -2 f_{H^\pm H^\pm}(p^2)\alpha_W + g_{H^\pm H^\pm}(p^2, m_A^2)\beta_{WA} \\ & + \sum_{H_i} \mathcal{O}^{(2)}_{H_i H_i} g_{H^\pm H^\pm}(p^2, m^2_{H_i})\beta_{WH_i}\Big\} \\ & + (1-\xi_Z)\frac{ig^2(\cos^2\Theta_W - \sin^2\Theta_W)^2}{64\pi^2\cos^2\Theta_W} \\ & \times \left\{g_{H^\pm H^\pm}(p^2, m^2_{H^+})\beta_{ZH^\pm}(p^2) - f_{H^\pm H^\pm}(p^2)\alpha_Z\right\} \\ & + (1-\xi_\gamma)\frac{ie^2}{16\pi^2}\left\{-f_{H^\pm H^\pm}(p^2)\alpha_\gamma + g_{H^\pm H^\pm}(p^2, m^2_{H^+})\beta_{\gamma H^\pm}(p^2)\right\} \end{aligned} \tag{B.12}$$

$$\begin{aligned} i\Sigma^{\text{tad}}_{H^\pm G^\pm}(p^2) = {} & i\Sigma^{\text{tad}}_{H^\pm G^\pm}(p^2)\Big|_{\xi_V=1} \\ & + (1-\xi_W)\frac{ig^2}{64\pi^2}\sum_{H_i} \mathcal{O}^{(3)}_{H_i H_i} g_{H^\pm G^\pm}(p^2, m^2_{H_i})\beta_{WH_i}(p^2) \end{aligned} \tag{B.13}$$

$$\begin{aligned} i\Sigma^{\text{tad}}_{WH^\pm,\mu}(p^2) = {} & i\Sigma^{\text{tad}}_{WH^\pm,\mu}(p^2)\Big|_{\xi_V=1} - (1-\xi_W)\frac{ig^2 m_W}{64\pi^2} p_\mu \\ & \times \sum_{H_i} \mathcal{O}^{(3)}_{H_i H_i}\left\{f_{H^\pm H^\pm}(m^2_{H_i})\beta_{WH_i}(p^2) + 2 f_{H^\pm H^\pm}(p^2) C_2^{WH_i}(p^2)\right\} \end{aligned} \tag{B.14}$$

[16] Note that in the case of the self-energy $\Sigma^{\text{tad}}_{G^\pm G^\pm}$ we subtracted an additional term of $f_{G^\pm G^\pm}(p^2)\alpha_W$ with respect to the diagrams shown in figure 14. This term stems from other gauge-dependent subsets of the gauge-dependence of the self-energy, which we do not present explicitly here. This is in line with [56], where these additional terms are simply dropped since they cancel elsewhere.

JHEP12(2017)077

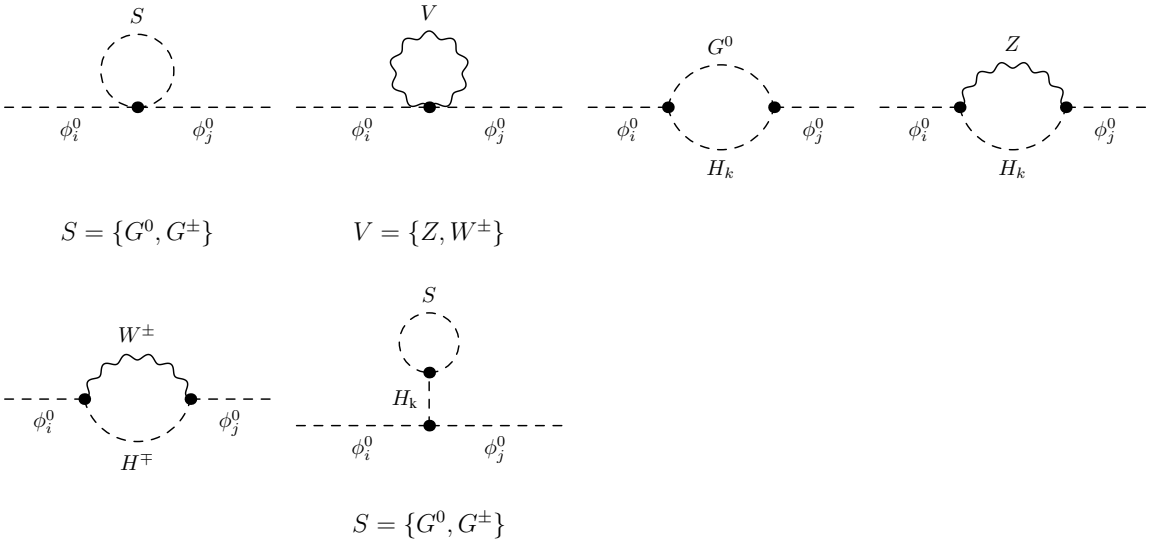

Figure 15. All Feynman diagrams contributing to the gauge-dependence of the CP-odd self-energies $\Sigma^{\text{tad}}_{\phi^0_i\phi^0_j}(p^2)$ where $\phi^0_{i,j} \in \{A, G^0\}$. A sum over intermediate Higgs states H_k is assumed wherever they appear. Note that we only consider contributions to the extended scalar sector of the N2HDM. Depending on the particles $\phi^0_{i,j}$ chosen, some of the diagrams shown may not exist in the N2HDM.

Note that when the former two equations are evaluated in the 2HDM-limit, cf. eq. (2.35), these reproduce the formulae given in ref. [40] for the 2HDM.

B.1.3 Gauge dependence of the CP-odd scalar and vector self-energies

In the neutral CP-odd sector the calculation of the gauge dependences and of the pinch contributions is even more involved than in the charged sector, since one has to take into account not only the mixing of the Z boson with G^0 and A, but additionally the mixing of the photon γ with all other possible contributions. It is only the coherent sum of all these mixing contributions which gives the correct gauge dependences and pinch results. Due to these additional complications, we restrict the presentation to the self-energies of two A and the mixing between A and G^0. As in the charged sector, we focus on the N2HDM Higgs contributions to the self-energies and pinch terms only, since they form a gauge-independent subset on their own. The relevant contributions are given by the Feynman diagrams in figure 15. In total, the self-energies of this subset read

$$\begin{aligned} i\Sigma^{\text{tad}}_{AA}(p^2) &= i\Sigma^{\text{tad}}_{AA}(p^2)\Big|_{\xi_V=1} \\ &\quad + (1-\xi_Z)\frac{ig^2}{64\pi^2\cos^2\Theta_W}\left\{-f_{AA}(p^2)\alpha_Z + \sum_{H_i}\mathcal{O}^{(1)}_{H_iH_i}g_{AA}(p^2,m^2_{H_i})\beta_{ZH_i}(p^2)\right\} \\ &\quad + (1-\xi_W)\frac{ig^2}{32\pi^2}\left\{-f_{H^\pm H^\pm}(p^2)\alpha_W + g_{AA}(p^2,m^2_{H^\pm})\beta_{WH^\pm}(p^2)\right\} \end{aligned} \tag{B.15}$$

$$\begin{aligned} i\Sigma^{\text{tad}}_{AG^0}(p^2) &= i\Sigma^{\text{tad}}_{AG^0}(p^2)\Big|_{\xi_V=1} \\ &\quad + (1-\xi_Z)\frac{ig^2}{64\pi^2\cos^2\Theta_W}\sum_{H_i}\mathcal{O}^{(3)}_{H_iH_i}g_{AG^0}(p^2,m^2_{H_i})\beta_{ZH_i}(p^2)\,. \end{aligned} \tag{B.16}$$

JHEP12(2017)077

As in the charged sector, these results, evaluated in the 2HDM limit, reproduce the ones presented in ref. [40] for the 2HDM.

B.2 Pinch contributions for the N2HDM

The intricate gauge dependence of the scalar self-energies of the N2HDM makes a gauge-independent definition of the counterterms of the scalar mixing angles complicated. If one considers instead an S-matrix element, e.g. a scattering process of a pair of fermions, where these self-energies may appear as intermediate states, the whole S-matrix element is gauge independent by construction. Consequently, the gauge dependences cancel in an intricate way between the self-energies and other contributions from vertex and box corrections within the S-matrix element.

The main idea of the pinch technique (cf. refs. [51–58] for a detailed exposition) is to isolate the gauge dependences of an arbitrary toy scattering process, which features the to-be pinched self-energies in a unique way. This is achieved by applying the elementary Ward identities

$$\begin{aligned} \not{k}\, P_{L/R} &= S_1^{-1}(p+k)P_{L/R} - P_{R/L}S_2^{-1}(p) + m_1 P_{L/R} - m_2 P_{R/L} \\ P_{L/R}\not{k} &= P_{L/R}S_1^{-1}(p+k) - S_2^{-1}(p)P_{R/L} + m_1 P_{L/R} - m_2 P_{R/L}\,, \end{aligned} \tag{B.17}$$

where k denotes the loop momentum, m_1 and m_2 the masses of the external fermions of the considered toy process and $S(p)$ the fermion propagator

$$iS_k(p) = \frac{i(\not{p}+m_k)}{p^2-m_k^2} = \frac{i}{\not{p}-m_k}\,. \tag{B.18}$$

It turns out that the gauge dependences are all similar in structure, i.e. they are always self-energy-like, independently of their origin within the scattering process. The isolation of all pinch contributions from the toy scattering process then allows for a manifestly gauge-independent definition of *pinched self-energies*. Since these self-energies are considered to be independent from the toy process chosen, cf. [52], the pinched self-energies are unique.

B.2.1 Pinch contributions for the CP-even sector

The full derivation of all pinch contributions for the N2HDM is beyond the scope of this paper. We nevertheless present the derivation of the pinch contributions for a few selected diagrams since we hope it is instructive to the reader and since it demonstrates how the pinch technique is applied. As the toy process for extracting the gauge dependences for the CP-even sector we choose the process $\mu^+\mu^- \to \bar{b}b$. All Feynman diagrams yielding contributions for the CP-even pinched self-energies are depicted in figure 16. It can be shown that all pinch contributions stemming from these diagrams can be brought into the form

$$\Gamma^{H_i bb}\frac{i}{p^2-m_{H_i}^2}i\Sigma^{\mathrm{PT}}_{H_iH_j}(p^2)\frac{i}{p^2-m_{H_j}^2}\Gamma^{H_j\mu\mu}\,, \tag{B.19}$$

where $i\Sigma^{\mathrm{PT}}_{H_iH_j}(p^2)$ is a relevant self-energy-like pinch contribution for the CP-even Higgs bosons H_i and H_j. Additionally, we define the contracted vertices of a CP-even Higgs

JHEP12(2017)077

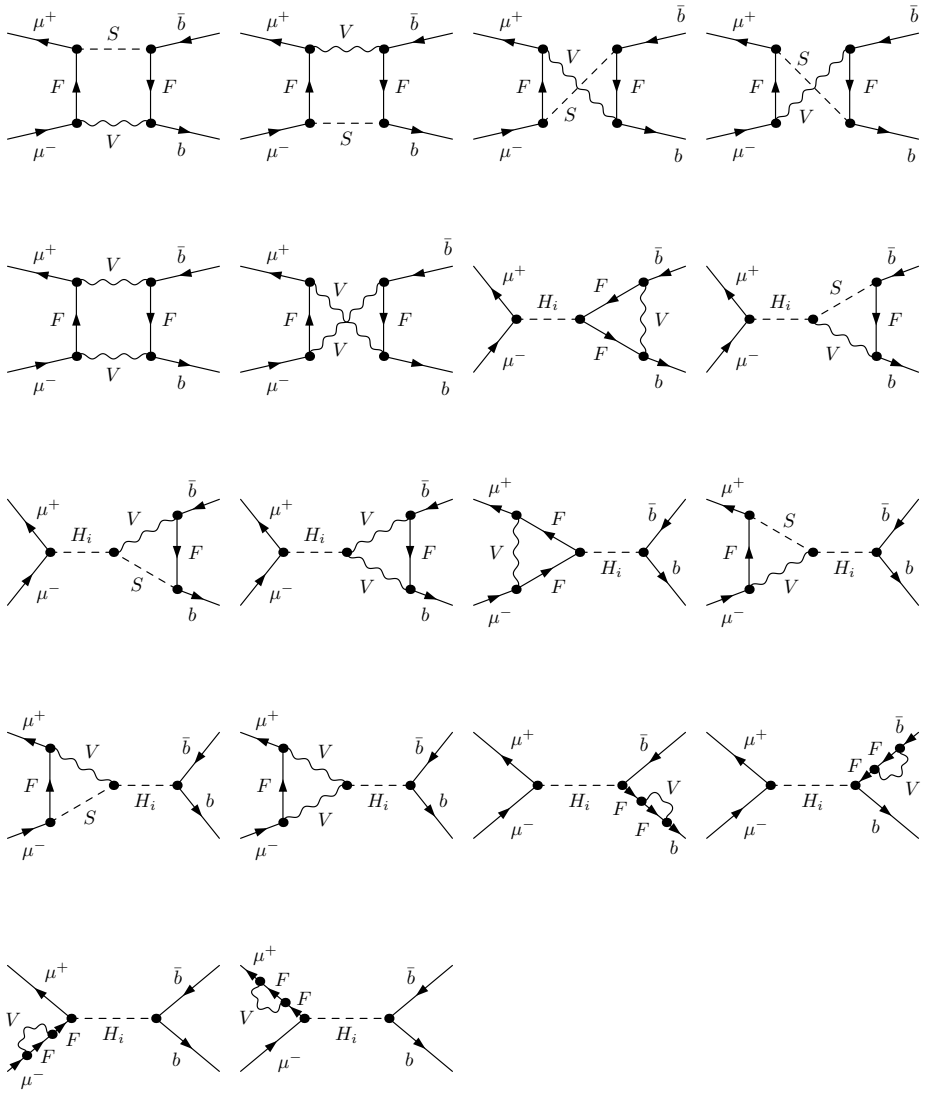

Figure 16. All generic Feynman diagrams contributing to the CP-even pinched self-energies.

boson with a pair of external bottom quarks or a pair of external muons as

$$\Gamma^{H_i bb} = \bar{u}(r_1)\frac{-igm_b\kappa_{H_i bb}}{2m_W}v(r_2) \qquad \text{and} \qquad \Gamma^{H_i\mu\mu} = \bar{v}(p_2)\frac{-igm_\mu\kappa_{H_i\mu\mu}}{2m_W}u(p_1)\,, \tag{B.20}$$

where $u(p_1)$ and $v(r_2)$ and $\bar{u}(r_1)$ and $\bar{v}(p_2)$ are the (adjoint) spinors of the external on-shell fermions with their respective momenta.

In order to derive the pinch contributions, we apply the elementary Ward identities, cf. eq. (B.17), and insert additional CP-even Higgs boson propagators into the amplitude via

$$1 = -\frac{i}{p^2 - m_{H_i}^2} i(p^2 - m_{H_i}^2)\,. \tag{B.21}$$

Additionally, we make use of the sum rules of the N2HDM as given in eq. (5.31) as well as of the coupling relation

$$\kappa_{H_i ff} = \kappa_{H_i VV} - \tilde{\kappa}_{H_i VH}\kappa_{Aff}\,. \tag{B.22}$$

JHEP12(2017)077

The application of these formulae to fermion-fermion-Higgs couplings enables the projection of the pinch contributions onto the desired CP-even Higgs couplings to the fermions,

$$\tilde{\kappa}\kappa_{All} = \sum_{H_j} \tilde{\kappa}\kappa_{H_jVV}\kappa_{All}\kappa_{H_jll} = -\sum_{H_j} \mathcal{O}^{(1)}_{H_iH_j}\kappa_{H_jll} + \dots \tag{B.23}$$

where "..." contains pinch contributions for other than the CP-even Higgs self-energies. Consequently, we can neglect them for the CP-even self-energies.

We consider the two contributions depicted in the Feynman diagrams in figure 17. The momenta are as defined in the diagrams. With the definitions given above, the sum of both diagrams reads[17]

$$\begin{aligned}
&\sum_{H_i} \Gamma^{H_ibb} \frac{i}{p^2-m^2_{H_i}} \frac{g^2}{32\pi^2} \int \frac{\mathrm{d}^4k}{i\pi^2} \frac{1}{\left[k^2-m^2_W\right]\left[(k+p)^2-m^2_{H^\pm}\right]} \\
&\quad \cdot \Big\{ \bar{v}(p_2)\left[P_L S_{\mu_\nu}(k+p_1)(\not{k}+2\not{p})P_L + P_R(-\not{k}-2\not{p})S_{\mu_\nu}(-k-p_2)P_R\right] \frac{igm_\mu}{2m_W}\kappa_{All}\tilde{\kappa}_{H_iVH}u(p_1) \\
&\quad -(1-\xi_W)\bar{v}(p_2)\left[P_L S_{\mu_\nu}(k+p_2)\not{k}P_L + P_R(-\not{k})S_{\mu_\nu}(-k-p_2)P_R\right] \frac{igm_\mu}{2m_W}\kappa_{All}\tilde{\kappa}_{H_iVH}u(p_1) \Big\} \\
&\overset{(B.17)}{=} \sum_{H_i} \Gamma^{H_ibb} \frac{i}{p^2-m^2_{H_i}} \frac{g^2}{32\pi^2} \bar{v}(p_2) \frac{igm_\mu}{2m_W}\kappa_{All}\tilde{\kappa}_{H_iVH}u(p_1) \Big\{ B_0(p^2;m^2_W,m^2_{H^\pm}) \\
&\quad -(1-\xi_W)\left[\alpha_W - f_{H^\pm H^\pm}(p^2)\beta_{WH^\pm}\right] \Big\} + \dots \\
&\overset{(B.23)}{=} \sum_{H_i,H_j} \Gamma^{H_ibb} \frac{i}{p^2-m^2_{H_i}} \frac{-g^2}{32\pi^2} \mathcal{O}^{(1)}_{H_iH_j} \Big\{ B_0(p^2;m^2_W,m^2_{H^\pm}) \\
&\quad -(1-\xi_W)\left[\alpha_W - f_{H^\pm H^\pm}(p^2)\beta_{WH^\pm}\right] \Big\} \Gamma^{H_j\mu\mu} + \dots \\
&\overset{(B.21)}{=} \sum_{H_i,H_j} \Gamma^{H_ibb} \frac{i}{p^2-m^2_{H_i}} \frac{-ig^2}{16\pi^2} \left(\frac{p^2}{2} - \frac{m^2_{H_j}}{2}\right) \mathcal{O}^{(1)}_{H_iH_j} \Big\{ B_0(p^2;m^2_W,m^2_{H^\pm}) \\
&\quad -(1-\xi_W)\left[\alpha_W - f_{H^\pm H^\pm}(p^2)\beta_{WH^\pm}\right] \Big\} \frac{i}{p^2-m^2_{H_j}} \Gamma^{H_j\mu\mu} + \dots \\
&= \sum_{H_i,H_j} \Gamma^{H_ibb} \frac{i}{p^2-m^2_{H_i}} i\Sigma^{\mathrm{PT}}_{H_iH_j}(p^2) \frac{i}{p^2-m^2_{H_j}} \Gamma^{H_j\mu\mu} + \dots
\end{aligned} \tag{B.24}$$

The first term of the right-hand side of the Ward identities in eq. (B.17) removes the internal fermion propagators from the loops, i.e. the fermions are *pinched out*, while the second term of the Ward identities vanishes due to the Dirac equation. The third and fourth terms produce pinch contributions to pinched vertices, but not to pinched self-energies. Consequently, these terms are collected in "...", since they are of no interest for the generation of a pinched self-energy. The application of the sum rule in eq. (B.23) produces additional pinch contributions to other self-energies than the CP-even ones due to different fermion-Higgs couplings. Consequently, these other terms are collected in "..." as well.

[17] Note that the shift from four to D dimensions as well as the $+i\epsilon$ terms in the propagators are not explicitly stated here, but implicitly assumed to be set.

JHEP12(2017)077

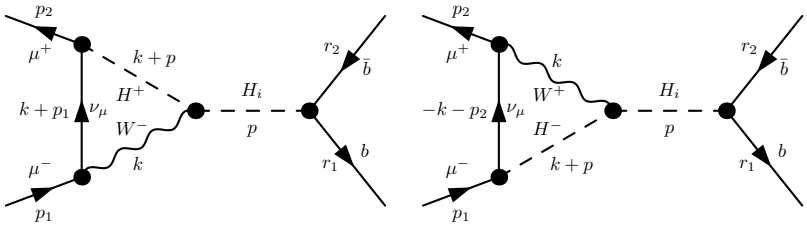

Figure 17. Two Feynman diagrams for the toy process $\mu^+\mu^- \to \bar{b}b$ involving scalar-scalar-vector vertices which give rise to gauge-dependent as well as additional gauge-independent pinch contributions for the CP-even self-energies. The momenta p_1 and p_2 are taken as incoming and the momenta r_1 and r_2 as outgoing, and $p = p_1 + p_2$.

As mentioned before, the pinch contributions take the form of a self-energy and here they explicitly read

$$i\Sigma^{\text{PT}}_{H_iH_j}(p^2) = \frac{-ig^2}{16\pi^2}\left(\frac{p^2}{2} - \frac{m^2_{H_j}}{2}\right)\mathcal{O}^{(1)}_{H_iH_j}\Big\{B_0(p^2;m^2_W,m^2_{H^\pm}) \\ -(1-\xi_W)\left[\alpha_W + (m^2_{H^\pm} - p^2)\beta_{WH^\pm}\right]\Big\}. \tag{B.25}$$

The terms proportional to $(1-\xi_W)$ are gauge-dependent pinch contributions which cancel against parts of the gauge dependence of the CP-even self-energies. The other term which remains for $\xi_W = 1$ is an additional gauge-independent pinch contribution which is specific to scalar-scalar-vector vertices in the vertex corrections [52, 59]. Repeating the calculation for the vertex corrections of the bottom quarks containing $H^\pm$ and $W^\pm$ bosons in the loop yields the same result as in eq. (B.25), but with $m^2_{H_j}$ replaced by $m^2_{H_i}$. The combination of these results yields the first term in the second line of eq. (5.27).

All Feynman diagrams contributing to the pinch terms for the CP-even sector are depicted in figure 16. Repeating the calculation as demonstrated above and combining all results leads to the pinch contributions to the CP-even sector,

$$\begin{aligned} i\Sigma^{\text{PT}}_{H_iH_j}(p^2) = {} & i\Sigma^{\text{add}}_{H_iH_j}(p^2) \\ & - \frac{ig^2(1-\xi_Z)}{64\pi^2\cos\Theta_W}\Big[g_{H_iH_j}(p^2,m^2_A)\mathcal{O}^{(1)}_{H_iH_j}\beta_{ZA}(p^2) - f_{H_iH_j}(p^2)\mathcal{O}^{(4)}_{H_iH_j}\alpha_Z \\ & \qquad + \frac{1}{2}g_{H_iH_j}(p^2,0)\mathcal{O}^{(2)}_{H_iH_j}\left(\beta_{ZZ}(p^2) + \beta_{Z\xi Z}(p^2)\right)\Big] \\ & - \frac{ig^2(1-\xi_W)}{32\pi^2}\Big[g_{H_iH_j}(p^2,m^2_{H^\pm})\mathcal{O}^{(1)}_{H_iH_j}\beta_{ZH^\pm}(p^2) - f_{H_iH_j}(p^2)\mathcal{O}^{(4)}_{H_iH_j}\alpha_W \\ & \qquad + \frac{1}{2}g_{H_iH_j}(p^2,0)\mathcal{O}^{(2)}_{H_iH_j}\left(\beta_{WW}(p^2) + \beta_{W\xi W}(p^2)\right)\Big]. \end{aligned} \tag{B.26}$$

By comparing this result with eq. (B.8), we realize that in the sum of the pinch contributions with the CP-even self-energies all gauge-dependent terms proportional to $(1-\xi_W)$ and $(1-\xi_Z)$ precisely cancel, leading to

$$\overline{\Sigma}_{H_iH_j}(p^2) = \Sigma^{\text{tad}}_{H_iH_j}(p^2) + \Sigma^{\text{PT}}_{H_iH_j}(p^2) = \Sigma^{\text{tad}}_{H_iH_j}(p^2)\Big|_{\xi_V=1} + \Sigma^{\text{add}}_{H_iH_j}(p^2). \tag{B.27}$$

JHEP12(2017)077

Due to the cancellation of all gauge-dependent terms, the pinched self-energy $\overline{\Sigma}_{H_iH_j}(p^2)$ is gauge independent by construction and equivalent to the self-energy evaluated in the Feynman gauge, together with the sum of all additional terms stemming from diagrams with internal scalar-scalar-vector vertices, as given in eq. (5.27).

B.2.2 Pinch contributions for the charged sector

For the derivation of the pinch contributions of the charged sector we use the toy process $\nu_e e^+ \to \nu_e e^+$. The calculation is analogous to the CP-even sector, i.e. we apply the elementary Ward identities from eq. (B.17) and use the N2HDM sum rules to identify the correct couplings between the external fermions and the scalar or vector particles of interest. In the case of the self-energies involving the $H^\pm$ particles, we again insert the corresponding propagator by

$$1 = -\frac{i}{p^2 - m_{H^\pm}^2} i(p^2 - m_{H^\pm}^2)\,. \tag{B.28}$$

For the self-energies involving $G^\pm$ or $W^\pm$, the corresponding propagators

$$\Delta_{\mu\nu}(p) \equiv \frac{-i}{p^2 - m_W^2}\left[g_{\mu\nu} - (1-\xi_W)\frac{p_\mu p_\nu}{p^2 - \xi_W m_W^2}\right] \quad \text{and} \quad D(p) \equiv \frac{i}{p^2 - \xi_W m_W^2} \tag{B.29}$$

are included into the pinch contributions by applying the identities [56]

$$g_{\nu\alpha} = i\left\{\Delta_{\nu\mu}(p)\left[(p^2 - m_W^2)g_\alpha^\mu - p^\mu p_\alpha\right] - p_\nu p_\alpha D(p)\right\} \tag{B.30}$$

$$ip_\mu = p^2 D(p^2) p_\mu + m_W^2 p^\nu \Delta_{\nu\mu}\,. \tag{B.31}$$

Due to these identities, the pinch contributions of the charged sector have to be correctly assigned to all possible self-energy combinations of $H^\pm$, $G^\pm$ and $W^\pm$. Consequently, the analysis of the charged sector is significantly more involved than the one of the CP-even sector. Taking into account all Feynman diagrams contributing to the pinched self-energies of the charged sector,[18] the collocation of all pinch contributions for the various combinations of $W^\pm$ and $G^\pm$ yields

$$i\Sigma^{\mathrm{PT}}_{WW,\mu\nu}(p^2) = (1-\xi_W)\frac{ig^2 m_W^2}{64\pi^2} p_\mu p_\nu \sum_{H_i} \mathcal{O}^{(2)}_{H_iH_i}\left\{\beta_{WH_i}(p^2) + 4C_2^{WH_i}(p^2)\right\} \tag{B.32}$$

$$i\Sigma^{\mathrm{PT}}_{WG^\pm,\mu}(p^2) = -(1-\xi_W)\frac{ig^2 m_W}{64\pi^2} p_\mu \left\{\alpha_W + \sum_{H_i} \mathcal{O}^{(2)}_{H_iH_i}\left[m_{H_i}^2 \beta_{WH_i}(p^2) + 2p^2 C_2^{WH_i}(p^2)\right]\right\} \tag{B.33}$$

$$i\Sigma^{\mathrm{PT}}_{G^\pm G^\pm}(p^2) = i\Sigma^{\mathrm{add}}_{G^\pm G^\pm}(p^2) \tag{B.34}$$
$$-(1-\xi_W)\frac{ig^2}{64\pi^2}\left\{-2 f_{G^\pm G^\pm}(p^2)\alpha_W + \sum_{H_i} \mathcal{O}^{(2)}_{H_iH_i} g_{G^\pm G^\pm}(p^2, m_{H_i}^2)\beta_{WH_i}(p^2)\right\}$$

[18] These diagrams are obtained analogously to the CP-even case. Since they are numerous, we show exemplary only those for the CP-even sector.

JHEP12(2017)077

and for the combinations of $H^\pm$ and $G^\pm$ or $W^\pm$ results in

$$
\begin{aligned}
i\Sigma^{\text{PT}}_{H^\pm H^\pm}(p^2) = {} & i\Sigma^{\text{add}}_{H^\pm H^\pm}(p^2) \\
& - (1-\xi_W)\frac{ig^2}{64\pi^2}\Big\{ -2 f_{H^\pm H^\pm}(p^2)\alpha_W + g_{H^\pm H^\pm}(p^2, m_A^2)\beta_{WA} \\
& + \sum_{H_i} \mathcal{O}^{(2)}_{H_i H_i} g_{H^\pm H^\pm}(p^2, m_{H_i}^2)\beta_{WH_i}\Big\} \\
& - (1-\xi_Z)\frac{ig^2(\cos^2\Theta_W - \sin^2\Theta_W)^2}{64\pi^2\cos^2\Theta_W} \\
& \times \left\{ -f_{H^\pm H^\pm}(p^2)\alpha_Z + g_{H^\pm H^\pm}(p^2, m_{H^+}^2)\beta_{ZH^\pm}(p^2)\right\} \\
& - (1-\xi_\gamma)\frac{ie^2}{16\pi^2}\left\{ -f_{H^\pm H^\pm}(p^2)\alpha_\gamma + g_{H^\pm H^\pm}(p^2, m_{H^+}^2)\beta_{\gamma H^\pm}(p^2)\right\}
\end{aligned} \tag{B.35}
$$

$$
\begin{aligned}
i\Sigma^{\text{PT}}_{H^\pm G^\pm}(p^2) = {} & i\Sigma^{\text{add}}_{H^\pm G^\pm}(p^2) \\
& - (1-\xi_W)\frac{ig^2}{64\pi^2}\sum_{H_i} \mathcal{O}^{(3)}_{H_i H_i} g_{H^\pm G^\pm}(p^2, m_{H_i}^2)\beta_{WH_i}(p^2)
\end{aligned} \tag{B.36}
$$

$$
\begin{aligned}
i\Sigma^{\text{PT}}_{H^\pm W^\pm,\mu}(p^2) = {} & (1-\xi_W)\frac{ig^2 m_W}{64\pi^2} p_\mu \sum_{H_i} \mathcal{O}^{(3)}_{H_i H_i}\Big\{ f_{H^\pm H^\pm}(m_{H_i}^2)\beta_{WH_i}(p^2) \\
& + 2 f_{H^\pm H^\pm}(p^2) C_2^{WH_i}(p^2)\Big\} \,.
\end{aligned} \tag{B.37}
$$

By adding the pinch contributions to the gauge-dependent charged self-energies, the pinched self-energies of the charged sector read

$$\overline{\Sigma}_{WW,\mu\nu}(p^2) = \Sigma^{\text{tad}}_{WW,\mu\nu}(p^2)\Big|_{\xi_V=1} \tag{B.38}$$

$$\overline{\Sigma}_{WG^\pm,\mu}(p^2) = \Sigma^{\text{tad}}_{WG^\pm,\mu}(p^2)\Big|_{\xi_V=1} \tag{B.39}$$

$$\overline{\Sigma}_{G^\pm G^\pm}(p^2) = \Sigma^{\text{tad}}_{G^\pm G^\pm}(p^2)\Big|_{\xi_V=1} + \Sigma^{\text{add}}_{G^\pm G^\pm}(p^2) \tag{B.40}$$

$$\overline{\Sigma}_{H^\pm H^\pm}(p^2) = \Sigma^{\text{tad}}_{H^\pm H^\pm}(p^2)\Big|_{\xi_V=1} + \Sigma^{\text{add}}_{H^\pm H^\pm}(p^2) \tag{B.41}$$

$$\overline{\Sigma}_{H^\pm G^\pm}(p^2) = \Sigma^{\text{tad}}_{H^\pm G^\pm}(p^2)\Big|_{\xi_V=1} + \Sigma^{\text{add}}_{H^\pm G^\pm}(p^2) \tag{B.42}$$

$$\overline{\Sigma}_{WH^\pm,\mu}(p^2) = \Sigma^{\text{tad}}_{WH^\pm,\mu}(p^2)\Big|_{\xi_V=1} \,. \tag{B.43}$$

The additional gauge-independent pinch contributions for $\Sigma^{\text{tad}}_{H^\pm G^\pm}(p^2)$ are stated[19] in eq. (5.29). The remaining additional contributions are analogously derived from Feynman

[19] For the derivation of all additional pinch contributions we took into account all possible diagrams, not only the ones containing only the extended scalar sector of the N2HDM. This is consistent since the gauge dependence is cancelled already in the pinched self-energies.

JHEP12(2017)077

diagrams involving internal scalar-scalar-vector vertices and explicitly read

$$\Sigma^{\text{add}}_{G^\pm G^\pm}(p^2) = \frac{-g^2}{32\pi^2} p^2 \Bigg\{ B_0(p^2; m_W^2, m_W^2) + \sum_{H_i} \mathcal{O}^{(2)}_{H_i H_i} B_0(p^2; m_{H_i}^2, m_W^2) + \frac{(\cos^2\Theta_W - \sin^2\Theta_W)^2}{\cos^2\Theta_W} B_0(p^2; m_W^2, m_Z^2) + 4\sin^2\Theta_W B_0(p^2; 0, m_{H^\pm}^2) \Bigg\} \tag{B.44}$$

$$\Sigma^{\text{add}}_{H^\pm H^\pm}(p^2) = \frac{-g^2}{32\pi^2} (p^2 - m_{H^\pm}^2) \Bigg\{ B_0(p^2; m_A^2, m_W^2) + \sum_{H_i} \mathcal{O}^{(1)}_{H_i H_i} B_0(p^2; m_{H_i}^2, m_W^2) + \frac{(\cos^2\Theta_W - \sin^2\Theta_W)^2}{\cos^2\Theta_W} B_0(p^2; m_{H^\pm}^2, m_Z^2) + 4\sin^2\Theta_W B_0(p^2; 0, m_{H^\pm}^2) \Bigg\} . \tag{B.45}$$

Note that self-energies involving the gauge boson $W^\pm$ as an external particle do not receive additional gauge-independent pinch contributions.

B.2.3 Pinch contributions for the CP-odd sector

For pinching the CP-odd sector we choose the same process as for the CP-even sector, i.e. the process $\mu^+\mu^- \to \bar{b}b$. The derivation of the pinch contributions is exactly analogous to the CP-even neutral and to the charged sector. By inserting the propagators and applying the elementary identities eq. (B.17) and eqs. (B.28)–(B.31), we isolate all pinch contributions from the Feynman diagrams for the corresponding CP-odd self-energies. In total, the pinch contributions read

$$i\Sigma^{\text{tad}}_{AA}(p^2) = i\Sigma^{\text{add}}_{AA}(p^2)\Big|_{\xi_V=1} - \frac{ig^2}{64\pi^2\cos^2\Theta_W}(1-\xi_Z) \left\{ -f_{AA}(p^2)\alpha_Z + \sum_{H_i} \mathcal{O}^{(1)}_{H_i H_i} g_{AA}(p^2, m_{H_i}^2)\beta_{ZH_i}(p^2) \right\} \tag{B.46}$$

$$i\Sigma^{\text{tad}}_{AG^0}(p^2) = i\Sigma^{\text{add}}_{AG^0}(p^2)\Big|_{\xi_V=1} - \frac{ig^2}{64\pi^2\cos^2\Theta_W}(1-\xi_Z) \sum_{H_i} \mathcal{O}^{(3)}_{H_i H_i} g_{AG^0}(p^2, m_{H_i}^2)\beta_{ZH_i}(p^2) . \tag{B.47}$$

Adding the pinch contributions to the gauge-dependent self-energies allows for the generation of the pinched self-energies of the CP-odd sector:

$$\overline{\Sigma}_{AA}(p^2) = \Sigma^{\text{tad}}_{AA}(p^2)\Big|_{\xi_V=1} + \Sigma^{\text{add}}_{AA}(p^2) \tag{B.48}$$

$$\overline{\Sigma}_{AG^0}(p^2) = \Sigma^{\text{tad}}_{AG^0}(p^2)\Big|_{\xi_V=1} + \Sigma^{\text{add}}_{AG^0}(p^2) . \tag{B.49}$$

The additional pinch contribution for the self-energy $\Sigma^{\text{tad}}_{AG^0}(p^2)$ is given in eq. (5.28), and the remaining additional gauge-independent pinch contribution explicitly reads

$$\Sigma^{\text{add}}_{AA}(p^2) = \frac{-g^2}{32\pi^2\cos^2\Theta_W}(p^2 - m_A^2) \times \left\{ 2\cos^2\Theta_W B_0(p^2; m_W^2, m_{H^\pm}^2) + \sum_{H_i} \mathcal{O}^{(1)}_{H_i H_i} B_0(p^2; m_{H_i}^2, m_Z^2) \right\} \tag{B.50}$$

JHEP12(2017)077

References

[1] ATLAS collaboration, *Observation of a new particle in the search for the Standard Model Higgs boson with the ATLAS detector at the LHC*, *Phys. Lett.* **B 716** (2012) 1 [arXiv:1207.7214] [INSPIRE].

[2] CMS collaboration, *Observation of a new boson at a mass of 125 GeV with the CMS experiment at the LHC*, *Phys. Lett.* **B 716** (2012) 30 [arXiv:1207.7235] [INSPIRE].

[3] J.F. Gunion, H.E. Haber, G.L. Kane and S. Dawson, *The Higgs Hunter's Guide*, *Front. Phys.* **80** (2000) 1 [INSPIRE].

[4] T.D. Lee, *A Theory of Spontaneous T Violation*, *Phys. Rev.* **D 8** (1973) 1226 [INSPIRE].

[5] G.C. Branco, P.M. Ferreira, L. Lavoura, M.N. Rebelo, M. Sher and J.P. Silva, *Theory and phenomenology of two-Higgs-doublet models*, *Phys. Rept.* **516** (2012) 1 [arXiv:1106.0034] [INSPIRE].

[6] X.-G. He, T. Li, X.-Q. Li, J. Tandean and H.-C. Tsai, *Constraints on Scalar Dark Matter from Direct Experimental Searches*, *Phys. Rev.* **D 79** (2009) 023521 [arXiv:0811.0658] [INSPIRE].

[7] B. Grzadkowski and P. Osland, *Tempered Two-Higgs-Doublet Model*, *Phys. Rev.* **D 82** (2010) 125026 [arXiv:0910.4068] [INSPIRE].

[8] H.E. Logan, *Dark matter annihilation through a lepton-specific Higgs boson*, *Phys. Rev.* **D 83** (2011) 035022 [arXiv:1010.4214] [INSPIRE].

[9] M.S. Boucenna and S. Profumo, *Direct and Indirect Singlet Scalar Dark Matter Detection in the Lepton-Specific two-Higgs-doublet Model*, *Phys. Rev.* **D 84** (2011) 055011 [arXiv:1106.3368] [INSPIRE].

[10] X.-G. He, B. Ren and J. Tandean, *Hints of Standard Model Higgs Boson at the LHC and Light Dark Matter Searches*, *Phys. Rev.* **D 85** (2012) 093019 [arXiv:1112.6364] [INSPIRE].

[11] Y. Bai, V. Barger, L.L. Everett and G. Shaughnessy, *Two-Higgs-doublet-portal dark-matter model: LHC data and Fermi-LAT* 135 *GeV line*, *Phys. Rev.* **D 88** (2013) 015008 [arXiv:1212.5604] [INSPIRE].

[12] X.-G. He and J. Tandean, *Low-Mass Dark-Matter Hint from CDMS II, Higgs Boson at the LHC and Darkon Models*, *Phys. Rev.* **D 88** (2013) 013020 [arXiv:1304.6058] [INSPIRE].

[13] Y. Cai and T. Li, *Singlet dark matter in a type-II two Higgs doublet model*, *Phys. Rev.* **D 88** (2013) 115004 [arXiv:1308.5346] [INSPIRE].

[14] J. Guo and Z. Kang, *Higgs Naturalness and Dark Matter Stability by Scale Invariance*, *Nucl. Phys.* **B 898** (2015) 415 [arXiv:1401.5609] [INSPIRE].

[15] L. Wang and X.-F. Han, *A simplified 2HDM with a scalar dark matter and the galactic center gamma-ray excess*, *Phys. Lett.* **B 739** (2014) 416 [arXiv:1406.3598] [INSPIRE].

[16] A. Drozd, B. Grzadkowski, J.F. Gunion and Y. Jiang, *Extending two-Higgs-doublet models by a singlet scalar field - the Case for Dark Matter*, *JHEP* **11** (2014) 105 [arXiv:1408.2106] [INSPIRE].

JHEP12(2017)077

[17] R. Campbell, S. Godfrey, H.E. Logan, A.D. Peterson and A. Poulin, *Implications of the observation of dark matter self-interactions for singlet scalar dark matter*, *Phys. Rev.* **D 92** (2015) 055031 [arXiv:1505.01793] [INSPIRE].

[18] A. Drozd, B. Grzadkowski, J.F. Gunion and Y. Jiang, *Isospin-violating dark-matter-nucleon scattering via two-Higgs-doublet-model portals*, *JCAP* **10** (2016) 040 [arXiv:1510.07053] [INSPIRE].

[19] S. von Buddenbrock et al., *Phenomenological signatures of additional scalar bosons at the LHC*, *Eur. Phys. J.* **C 76** (2016) 580 [arXiv:1606.01674] [INSPIRE].

[20] T. Alanne, K. Kainulainen, K. Tuominen and V. Vaskonen, *Baryogenesis in the two doublet and inert singlet extension of the Standard Model*, *JCAP* **08** (2016) 057 [arXiv:1607.03303] [INSPIRE].

[21] C.-Y. Chen, M. Freid and M. Sher, *Next-to-minimal two Higgs doublet model*, *Phys. Rev.* **D 89** (2014) 075009 [arXiv:1312.3949] [INSPIRE].

[22] M. Muhlleitner, M.O.P. Sampaio, R. Santos and J. Wittbrodt, *The N2HDM under Theoretical and Experimental Scrutiny*, *JHEP* **03** (2017) 094 [arXiv:1612.01309] [INSPIRE].

[23] M. Mühlleitner, M.O.P. Sampaio, R. Santos and J. Wittbrodt, *Phenomenological Comparison of Models with Extended Higgs Sectors*, *JHEP* **08** (2017) 132 [arXiv:1703.07750] [INSPIRE].

[24] A. Djouadi, W. Kilian, M. Muhlleitner and P.M. Zerwas, *Testing Higgs selfcouplings at e^+e^- linear colliders*, *Eur. Phys. J.* **C 10** (1999) 27 [hep-ph/9903229] [INSPIRE].

[25] A. Djouadi, W. Kilian, M. Muhlleitner and P.M. Zerwas, *Production of neutral Higgs boson pairs at LHC*, *Eur. Phys. J.* **C 10** (1999) 45 [hep-ph/9904287] [INSPIRE].

[26] M.M. Muhlleitner, *Higgs particles in the standard model and supersymmetric theories*, hep-ph/0008127 [INSPIRE].

[27] ATLAS, CMS collaborations, *Combined Measurement of the Higgs Boson Mass in pp Collisions at $\sqrt{s} = 7$ and 8 TeV with the ATLAS and CMS Experiments*, *Phys. Rev. Lett.* **114** (2015) 191803 [arXiv:1503.07589] [INSPIRE].

[28] A. Djouadi, J. Kalinowski and M. Spira, *HDECAY: A program for Higgs boson decays in the standard model and its supersymmetric extension*, *Comput. Phys. Commun.* **108** (1998) 56 [hep-ph/9704448] [INSPIRE].

[29] J.M. Butterworth et al., *The Tools and Monte Carlo Working Group Summary Report from the Les Houches 2009 Workshop on TeV Colliders*, arXiv:1003.1643 [INSPIRE].

[30] R. Coimbra, M.O.P. Sampaio and R. Santos, *ScannerS: Constraining the phase diagram of a complex scalar singlet at the LHC*, *Eur. Phys. J.* **C 73** (2013) 2428 [arXiv:1301.2599] [INSPIRE].

[31] R. Costa, R. Guedes, M.O.P. Sampaio and R. Santos, SCANNERS *project*, http://scanners.hepforge.org (2014).

[32] CMS collaboration, *Constraints on the spin-parity and anomalous HVV couplings of the Higgs boson in proton collisions at 7 and 8 TeV*, *Phys. Rev.* **D 92** (2015) 012004 [arXiv:1411.3441] [INSPIRE].

[33] ATLAS collaboration, *Study of the spin and parity of the Higgs boson in diboson decays with the ATLAS detector*, *Eur. Phys. J.* **C 75** (2015) 476 [arXiv:1506.05669] [INSPIRE].

JHEP12(2017)077

[34] CMS collaboration, *Precise determination of the mass of the Higgs boson and tests of compatibility of its couplings with the standard model predictions using proton collisions at 7 and 8 TeV*, *Eur. Phys. J.* **C 75** (2015) 212 [arXiv:1412.8662] [INSPIRE].

[35] ATLAS collaboration, *Measurements of the Higgs boson production and decay rates and coupling strengths using pp collision data at $\sqrt{s} = 7$ and 8 TeV in the ATLAS experiment*, *Eur. Phys. J.* **C 76** (2016) 6 [arXiv:1507.04548] [INSPIRE].

[36] M. Krause, R. Lorenz, M. Muhlleitner, R. Santos and H. Ziesche, *Gauge-independent Renormalization of the 2-Higgs-Doublet Model*, *JHEP* **09** (2016) 143 [arXiv:1605.04853] [INSPIRE].

[37] M. Krause, M. Muhlleitner, R. Santos and H. Ziesche, *Higgs-to-Higgs boson decays in a 2HDM at next-to-leading order*, *Phys. Rev.* **D 95** (2017) 075019 [arXiv:1609.04185] [INSPIRE].

[38] A. Denner, L. Jenniches, J.-N. Lang and C. Sturm, *Gauge-independent $\overline{MS}$ renormalization in the 2HDM*, *JHEP* **09** (2016) 115 [arXiv:1607.07352] [INSPIRE].

[39] L. Altenkamp, S. Dittmaier and H. Rzehak, *Renormalization schemes for the Two-Higgs-Doublet Model and applications to $h \to WW/ZZ \to 4$ fermions*, *JHEP* **09** (2017) 134 [arXiv:1704.02645] [INSPIRE].

[40] S. Kanemura, M. Kikuchi, K. Sakurai and K. Yagyu, *Gauge invariant one-loop corrections to Higgs boson couplings in non-minimal Higgs models*, *Phys. Rev.* **D 96** (2017) 035014 [arXiv:1705.05399] [INSPIRE].

[41] M. Fox, W. Grimus and M. Löschner, *Renormalization and radiative corrections to masses in a general Yukawa model*, arXiv:1705.09589 [INSPIRE].

[42] F. Bojarski, G. Chalons, D. Lopez-Val and T. Robens, *Heavy to light Higgs boson decays at NLO in the Singlet Extension of the Standard Model*, *JHEP* **02** (2016) 147 [arXiv:1511.08120] [INSPIRE].

[43] D.A. Ross and J.C. Taylor, *Renormalization of a unified theory of weak and electromagnetic interactions*, *Nucl. Phys.* **B 51** (1973) 125 [*Erratum ibid.* **B 58** (1973) 643] [INSPIRE].

[44] L. Baulieu, *Perturbative Gauge Theories*, *Phys. Rept.* **129** (1985) 1 [INSPIRE].

[45] R. Santos and A. Barroso, *On the renormalization of two Higgs doublet models*, *Phys. Rev.* **D 56** (1997) 5366 [hep-ph/9701257] [INSPIRE].

[46] J. Fleischer and F. Jegerlehner, *Radiative Corrections to Higgs Decays in the Extended Weinberg-Salam Model*, *Phys. Rev.* **D 23** (1981) 2001 [INSPIRE].

[47] M. Sperling, D. Stöckinger and A. Voigt, *Renormalization of vacuum expectation values in spontaneously broken gauge theories*, *JHEP* **07** (2013) 132 [arXiv:1305.1548] [INSPIRE].

[48] P. Gambino and P.A. Grassi, *The Nielsen identities of the SM and the definition of mass*, *Phys. Rev.* **D 62** (2000) 076002 [hep-ph/9907254] [INSPIRE].

[49] A. Denner, *Techniques for calculation of electroweak radiative corrections at the one loop level and results for W physics at LEP-200*, *Fortsch. Phys.* **41** (1993) 307 [arXiv:0709.1075] [INSPIRE].

[50] A. Pilaftsis, *Resonant CP-violation induced by particle mixing in transition amplitudes*, *Nucl. Phys.* **B 504** (1997) 61 [hep-ph/9702393] [INSPIRE].

JHEP12(2017)077

[51] D. Binosi, *Electroweak pinch technique to all orders*, *J. Phys.* **G 30** (2004) 1021 [hep-ph/0401182] [INSPIRE].

[52] D. Binosi and J. Papavassiliou, *Pinch Technique: Theory and Applications*, *Phys. Rept.* **479** (2009) 1 [arXiv:0909.2536] [INSPIRE].

[53] J.M. Cornwall and J. Papavassiliou, *Gauge Invariant Three Gluon Vertex in QCD*, *Phys. Rev.* **D 40** (1989) 3474 [INSPIRE].

[54] J. Papavassiliou, *Gauge Invariant Proper Selfenergies and Vertices in Gauge Theories with Broken Symmetry*, *Phys. Rev.* **D 41** (1990) 3179 [INSPIRE].

[55] G. Degrassi and A. Sirlin, *Gauge invariant selfenergies and vertex parts of the Standard Model in the pinch technique framework*, *Phys. Rev.* **D 46** (1992) 3104 [INSPIRE].

[56] J. Papavassiliou, *Gauge independent transverse and longitudinal self energies and vertices via the pinch technique*, *Phys. Rev.* **D 50** (1994) 5958 [hep-ph/9406258] [INSPIRE].

[57] N.J. Watson, *Universality of the pinch technique gauge boson selfenergies*, *Phys. Lett.* **B 349** (1995) 155 [hep-ph/9412319] [INSPIRE].

[58] J. Papavassiliou and A. Pilaftsis, *Gauge invariance and unstable particles*, *Phys. Rev. Lett.* **75** (1995) 3060 [hep-ph/9506417] [INSPIRE].

[59] J.R. Espinosa and Y. Yamada, *Scale independent and gauge independent mixing angles for scalar particles*, *Phys. Rev.* **D 67** (2003) 036003 [hep-ph/0207351] [INSPIRE].

[60] M. Krause, *On the Renormalization of the Two-Higgs-Doublet Model*, MSc Thesis, Karlsruhe Institute of Technology (2016) [INSPIRE].

[61] G. 't Hooft and M.J.G. Veltman, *Scalar One Loop Integrals*, *Nucl. Phys.* **B 153** (1979) 365 [INSPIRE].

[62] G. Passarino and M.J.G. Veltman, *One Loop Corrections for e^+e^- Annihilation Into $\mu^+\mu^-$ in the Weinberg Model*, *Nucl. Phys.* **B 160** (1979) 151 [INSPIRE].

[63] J.R. Espinosa and I. Navarro, *Scale independent mixing angles*, *Phys. Rev.* **D 66** (2002) 016004 [hep-ph/0109126] [INSPIRE].

[64] K.E. Williams, H. Rzehak and G. Weiglein, *Higher order corrections to Higgs boson decays in the MSSM with complex parameters*, *Eur. Phys. J.* **C 71** (2011) 1669 [arXiv:1103.1335] [INSPIRE].

[65] G. Bélanger, V. Bizouard, F. Boudjema and G. Chalons, *One-loop renormalization of the NMSSM in SloopS: The neutralino-chargino and sfermion sectors*, *Phys. Rev.* **D 93** (2016) 115031 [arXiv:1602.05495] [INSPIRE].

[66] J. Kublbeck, M. Böhm and A. Denner, *Feyn Arts: Computer Algebraic Generation of Feynman Graphs and Amplitudes*, *Comput. Phys. Commun.* **60** (1990) 165 [INSPIRE].

[67] T. Hahn, *Generating Feynman diagrams and amplitudes with FeynArts 3*, *Comput. Phys. Commun.* **140** (2001) 418 [hep-ph/0012260] [INSPIRE].

[68] C. Degrande, C. Duhr, B. Fuks, D. Grellscheid, O. Mattelaer and T. Reiter, *UFO — The Universal FeynRules Output*, *Comput. Phys. Commun.* **183** (2012) 1201 [arXiv:1108.2040] [INSPIRE].

[69] A. Alloul, N.D. Christensen, C. Degrande, C. Duhr and B. Fuks, *FeynRules 2.0 — A complete toolbox for tree-level phenomenology*, *Comput. Phys. Commun.* **185** (2014) 2250 [arXiv:1310.1921] [INSPIRE].

JHEP12(2017)077

[70] T. Hahn and M. Pérez-Victoria, *Automatized one loop calculations in four-dimensions and D-dimensions*, *Comput. Phys. Commun.* **118** (1999) 153 [hep-ph/9807565] [INSPIRE].

[71] G. 't Hooft and M.J.G. Veltman, *Regularization and Renormalization of Gauge Fields*, *Nucl. Phys.* **B 44** (1972) 189 [INSPIRE].

[72] C.G. Bollini and J.J. Giambiagi, *Dimensional Renormalization: The Number of Dimensions as a Regularizing Parameter*, *Nuovo Cim.* **B 12** (1972) 20 [INSPIRE].

[73] Particle Data Group collaboration, K.A. Olive et al., *Review of Particle Physics*, *Chin. Phys.* **C 38** (2014) 090001 [INSPIRE].

[74] A. Denner et al., *Standard Model input parameters for Higgs physics*, LHCHXSWG-INT-2015-006.

[75] LHC Higgs Cross Section Working Group, https://twiki.cern.ch/twiki/bin/view/LHCPhysics/ LHCHXSWG.

[76] LHC Higgs Cross Section Working Group collaboration, S. Dittmaier et al., *Handbook of LHC Higgs Cross Sections: 1. Inclusive Observables*, arXiv:1101.0593 [INSPIRE].

[77] Gfitter Group collaboration, M. Baak et al., *The global electroweak fit at NNLO and prospects for the LHC and ILC*, *Eur. Phys. J.* **C 74** (2014) 3046 [arXiv:1407.3792] [INSPIRE].

[78] F. Mahmoudi and O. Stal, *Flavor constraints on the two-Higgs-doublet model with general Yukawa couplings*, *Phys. Rev.* **D 81** (2010) 035016 [arXiv:0907.1791] [INSPIRE].

[79] O. Deschamps, S. Descotes-Genon, S. Monteil, V. Niess, S. T'Jampens and V. Tisserand, *The Two Higgs Doublet of Type II facing flavour physics data*, *Phys. Rev.* **D 82** (2010) 073012 [arXiv:0907.5135] [INSPIRE].

[80] T. Hermann, M. Misiak and M. Steinhauser, $\bar{B} \to X_s\gamma$ *in the Two Higgs Doublet Model up to Next-to-Next-to-Leading Order in QCD*, *JHEP* **11** (2012) 036 [arXiv:1208.2788] [INSPIRE].

[81] M. Misiak et al., *Updated NNLO QCD predictions for the weak radiative B-meson decays*, *Phys. Rev. Lett.* **114** (2015) 221801 [arXiv:1503.01789] [INSPIRE].

[82] M. Misiak and M. Steinhauser, *Weak radiative decays of the B meson and bounds on* $M_{H^\pm}$ *in the Two-Higgs-Doublet Model*, *Eur. Phys. J.* **C 77** (2017) 201 [arXiv:1702.04571] [INSPIRE].

[83] H.E. Haber and H.E. Logan, *Radiative corrections to the* $Zb\bar{b}$ *vertex and constraints on extended Higgs sectors*, *Phys. Rev.* **D 62** (2000) 015011 [hep-ph/9909335] [INSPIRE].

[84] D.C. Kennedy and B.W. Lynn, *Electroweak Radiative Corrections with an Effective Lagrangian: Four Fermion Processes*, *Nucl. Phys.* **B 322** (1989) 1 [INSPIRE].

[85] W.F.L. Hollik, *Radiative Corrections in the Standard Model and their Role for Precision Tests of the Electroweak Theory*, *Fortsch. Phys.* **38** (1990) 165 [INSPIRE].

[86] M. Awramik, M. Czakon, A. Freitas and G. Weiglein, *Precise prediction for the W boson mass in the standard model*, *Phys. Rev.* **D 69** (2004) 053006 [hep-ph/0311148] [INSPIRE].

JHEP12(2017)077